TEMPERATURE EFFECTS
IN
ALLUVIAL STREAMS

Thesis by

Brent Dalton Taylor

In Partial Fulfillment of the Requirements

For the Degree of

Doctor of Philosophy

California Institute of Technology

Pasadena, California

1972

(Submitted August 2, 1971)

ACKNOWLEDGMENTS

The writer would like to express deep appreciation to his advisor Professor Vito A. Vanoni for kind guidance, encouragement, and generous assistance during this investigation.

The writer would also like to thank Professor Norman H. Brooks for initially interesting him in graduate study at Caltech; and he and Professor Fredric Raichlen for their helpful interest in the temperature-effects study.

During the experimental investigation and thesis preparation skillful and considerate assistance was given by Mrs. Arvilla F. Krugh, Mrs. Patricia A. Rankin, Mr. Elton F. Daly, Mr. Robert L. Greenway, Mr. Carl A. Green, Jr., Mr. Ronald G. Patterson, and Mr. Carl T. Eastvedt. To each of these people the writer offers his sincere thanks.

The writer wishes also to thank the Civil Engineering Department at the California Institute of Technology for making possible four years of graduate study in an atmosphere of creativity and excellence.

This research was supported by the National Science Foundation, Grant No. GK 3910.

ABSTRACT

A laboratory investigation was conducted to determine the effects of water temperature on sediment discharge close to the bed (bed-load discharge), and on bed roughness and geometry in alluvial, open-channel flows.

Three types of experiments were made: 1) Low-transport, flat-bed experiments in which all of the sediment discharged moved as bed load; 2) high-transport, flat-bed experiments with fine sands wherein there was considerable suspended sediment discharge; and 3) a series of experiments where the discharge was kept constant and the velocity varied to produce ripple, dune, and flat-bed configurations. The experiments were made in pairs. In each pair the velocity and depth were the same or nearly the same, but in one experiment the water temperature was from 15°C to 20°C higher than in the other.

It was found that in low-transport, flat-bed flows where particle transport is by rolling and sliding along the bed, a 15°C to 20°C increase in water temperature can produce a relatively large change in sediment discharge. The nature of this change depends on the flow condition at the bed. With hydrodynamically smooth flow there is an increase in sediment discharge with increase in water temperature; whereas in transition from smooth to rough an increase in water temperature effects a reduction in sediment discharge. With fully-rough flow which obtains at boundary Reynolds numbers larger than approximately 200, sediment discharge does not depend on water

temperature. A phenomenological explanation has been presented for these observed temperature effects on sediment discharge.

In high-transport, flat-bed flows with suspended sediment transport, it was observed that the temperature effects on bed-load discharge are qualitatively the same as those which obtain in low-transport, flat-bed flows of approximately the same boundary Reynolds numbers.

It was also found that under certain flow conditions a change in water temperature alone can cause a change in bed form. The nature of this change in bed form seems to be related to the boundary Reynolds numbers R'_{*b} of the flows. For R'_{*b} less than a value near 8 bed form transitions were accomplished at lower velocities in a warm water flow than in a cold water flow at the same discharge; whereas for larger values of R'_{*b} contrary temperature effects on bed form transitions have been observed.

TABLE OF CONTENTS

TABLE OF CONTENTS (continued)

TABLE OF CONTENTS (continued)

TABLE OF CONTENTS (continued)

LIST OF FIGURES

LIST OF FIGURES (continued)

LIST OF FIGURES (continued)

LIST OF FIGURES (continued)

LIST OF FIGURES (continued)

LIST OF TABLES

CHAPTER 1

INTRODUCTION

Water flowing over a bed of loose sediment produces forces on the sediment particles. If these fluid forces are sufficiently large particles will be dislodged and transported. Under certain flow conditions this particle transport will form complex bed waves which significantly alter the hydraulic roughness of the bed. It is also through particle transport and deposition that a stream is able to change its planform and slope.

The practical signifigance of this phenomenon is clear. To design loose-boundary conveyance channels successfully, or alter the flow conditions in a natural stream for navigation, flood control, etc., it is important that the engineer understand the mechanics of sediment transport in order to predict the streams' response to different alterations. Unfortunately present knowledge of this phenomenon is limited. After more than 50 years of related research the mechanisms which produce transport and boundary deformation are still not well understood.

Field data and laboratory studies indicate that water temperature can have a significant effect on sediment transport and bed geometry. Large changes in sediment discharge and bed roughness have been observed with temperature changes of 15°C to 30°C in streams at constant discharge.

With a 1°C increase in water temperature over the range 5°C to 50°C there is a 2% decrease in kinematic viscosity. In a turbulent shear flow this change in viscosity may alter particle fall velocity, and the flow conditions in a thin layer near the bed, called the viscous sublayer. Each of these changes affects the hydrodynamic forces on the sediment particles, and thus may also affect particle transport and bed geometry.

The purpose of this study has been to investigate the mechanisms through which temperature may influence sediment discharge and boundary roughness. Variable-temperature experiments were made in two laboratory flumes with bed materials ranging from fine, naturally-worn, silica sand to coarse, artificial clay-aggregate particles approximately 18.5 mm in diameter. The experiments included flows wherein the bed was flat, rippled, and covered with dunes; where all the sediment discharged moved by rolling and sliding along the bed, and flows carrying large amounts of suspended material.

In Chapter 2 a brief review is given of temperature effects on sediment discharge, bed configuration and roughness that have been reported; and of Rouse's suspended distribution theory and Einstein's bed-load function wherein explicit attempts have been made to incorporate the effect of water temperature on the relative distribution of suspended sediment, and sediment discharge near the bed.

The 40-ft and 60-ft recirculating flumes and associated apparatus used in the experiments of this study are described in Chapter 3; and in Chapter 4 the experimental procedure is outlined for each of the three types of experiments that were made.

The experimental results are presented and briefly discussed in Chapter 5.

In Chapter 6 the experimental results are discussed further, and a phenomenological explanation is advanced for the observed temperature effects on sediment discharge in low-transport, flat-bed flows. In the last section of the chapter an attempt is made to relate the results obtained in this study with the temperature effects that have been observed in natural streams.

A summary of conclusions is given in Chapter 7.

The symbols used are defined where they first appear in the text, and also in Appendix A. In Appendix B a fall-velocity separation process used to obtain well-sorted size fractions of fine sand is described. Appendices D, E, and F contain copies of literature discussions written during the course of the study, each of which deals with the problems of sediment discharge and bed roughness in an alluvial channel.

CHAPTER 2

LITERATURE REVIEW

Over the past four decades there have been few contributions to the literature on sedimentation regarding the effects of water temperature. The contributions are primarily expositions of field and laboratory observations, but there have also been two noteworthy analytical contributions – the relative suspended concentration theory developed by Rouse (1937), and Einstein's (1950) bed-load function.

A review of this literature is given in the following sections.

2.1 FIELD OBSERVATIONS

In 1949 Lane et al.(1949) reported that data collected on the Lower Colorado River from 1943 to 1947 indicate that "for a given discharge the [suspended] sediment [discharge] ... may be as much as 2-1/2 times as great in winter [water temperature $T \sim 55^{\circ}F$] as in summer [$T \sim 85^{\circ}F$]". The sediment discharge along this reach is composed almost entirely of fine-sand bed material, and the discharge is maintained fairly constant by upstream dams.

Lane et al. suggest that the reduction in particle fall velocity at the lower water temperatures is not sufficient to explain the measured increases in suspended sediment discharge, and thus conclude that "most of the effect of temperature observed in the Colorado River ... is due to the rate of picking up of material from the stream bed".

Colby and Scott (1965) have measured the temperature effect on suspended sediment discharge in the Middle Loup River at Dunning, Nebraska, the Niobrara River near Cody, Nebraska; and the Mississippi River at St. Louis, Missouri, by correlating water temperature with observed changes in the coefficient A in the sediment discharge equation $Q_{ss} = AU^b$, where Q_{ss} is the measured suspended sediment discharge, U is the mean velocity of the stream, and A and b are empirical factors. (Colby (1964) has shown elsewhere that strong correlation exists between suspended sediment discharge and velocity.) In each of the three rivers the mean changes in A indicated that the suspended discharge of bed material is approximately 1.4 times larger at $40^{\circ}F$ than at $80^{\circ}F$.

By measuring bed profiles with a sonic sounder in the Middle Loup River, Colby and Scott also observed changes in bed configuration with water temperature. On June 25, 1959 with a discharge of 350 cfs and water temperature of $83^{\circ}F$ the bed was covered with large dune-like bed waves (see Fig. 2.1); whereas on December 5, 1959 with a discharge of 360 cfs but a water temperature of $39^{\circ}F$ the bed was nearly flat. With this flattening of the bed there was a significant reduction in bed roughness and increase in velocity.

Carey (1963) and Burke (1965) after analyzing bed profiles along a 200-mile reach of the Lower Mississippi River upstream from New Orleans, Louisiana, and stage-discharge measurements have observed that with a reduction in water temperature the heights of river crossings and amplitudes of bed waves are reduced, and that these changes in bed

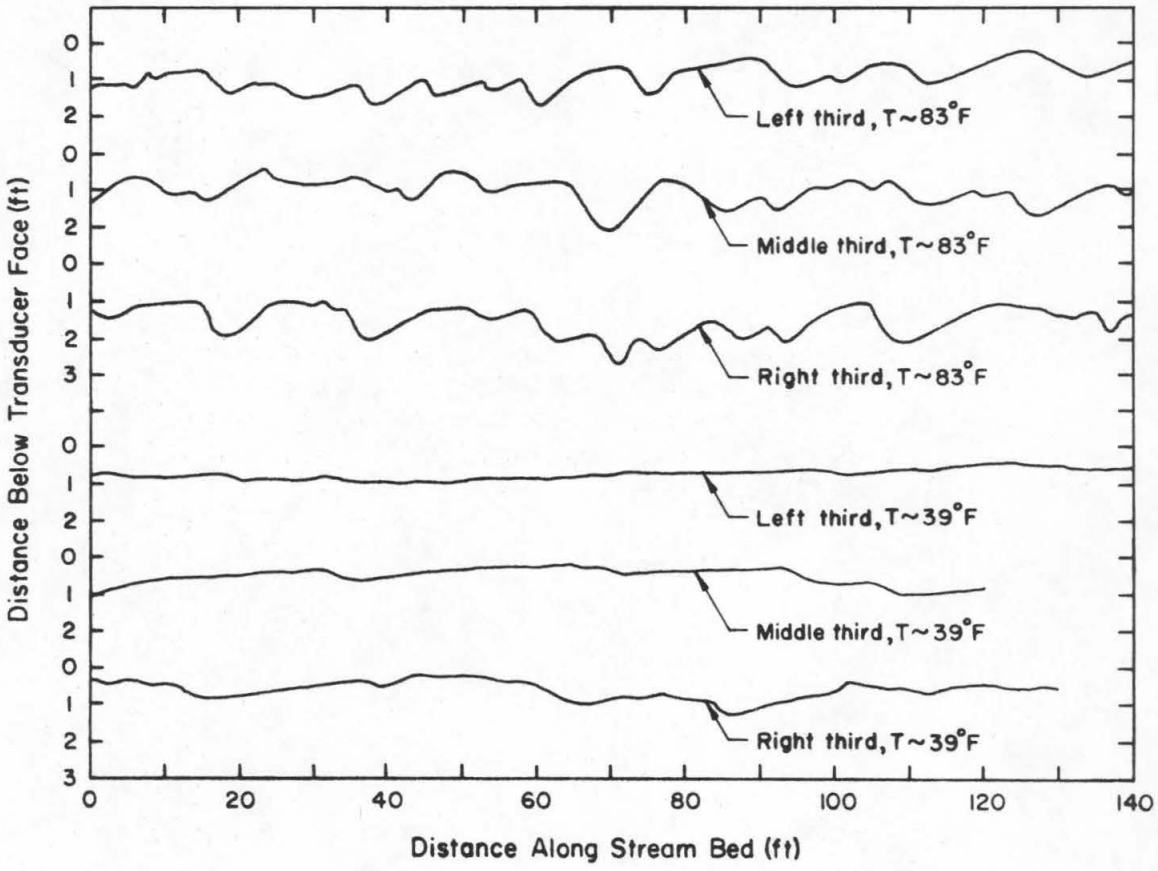

Fig. 2.1. Longitudinal profiles along stream bed at different water temperatures, Middle Loup River at Dunning, Nebraska. Upper set of profiles was measured June 25, 1959 (discharge 350 cfs; temperature, 83°F); and lower set was measured on December 5, 1959 (discharge, 360 cfs; temperature, 39°F). Flow is from left to right. (After Colby and Scott (1965)).

configuration reduce the channel roughness. Thus at a given stage low-temperature flows have a larger discharge than high-temperature flows.

Comprehensive data compiled as part of a continuing investigation on a seven-mile reach of the Missouri River at Omaha, Nebraska, by the U. S. Army Corps of Engineers (1969) provide a fairly complete description of the temperature related phenomena. The river discharge along this reach is maintained at 30,000 to 35,000 cfs for navigational purposes from April to November, and the bed material is predominantly fine sand.

Bed profiles measured during August, September, October, and November show that as the water temperature drops from 80°F to 45°F large bed waves present in August are washed out and replaced by a relatively flat bed in November. This change in bed form reduces roughness and thereby produces an increase in velocity and a reduction in depth. Increases of 50% in suspended sediment discharge have been measured with this reduction in water temperature and change in bed form.

2.2 OBSERVATIONS IN LABORATORY FLUMES

Ho (1939) in a series of experiments designed to measure the effect of a change in water temperature on sediment discharge close to the bed observed that at approximately the same velocity and depth with an increase in water temperature over the range 2°C to 45°C there was a relatively large increase in sediment discharge, and an increase in bed roughness. In these experiments the bed material was coarse

sand (geometric mean size D_g = 1.40 mm, geometric standard deviation of sizes σ_g = 1.29); and the bed shear stresses were near the values necessary to produce incipient particle movement, thus sediment transport was accomplished primarily by rolling and sliding along the bed. In each of Ho's experiments there was considerable bed wave development.

Mostafa (1949) made two series of low-transport experiments in a feed-type flume; the water temperature was approximately 65°F in one series and 130°F in the other. The bed material was medium sand (D_g = 0.675 mm, σ_g = 1.13). In each experiment the discharge and sediment feed rate were set and after equilibrium flow conditions obtained mean depth and friction slope were measured as dependent variables. Bed waves formed on the bed in each experiment.

Mostafa's data do not indicate a temperature effect on either mean velocity or friction slope for given discharge and sediment discharge.

Vanoni and Brooks (1957) made two experiment-pairs in a recirculating flume with fine sand (D_g = 0.145 mm, σ_g = 1.30). In each experiment-pair the velocity and depth were nearly the same but in one experiment the water temperature was 15°C, and in the other the temperature was near 37°C. The bed forms in the two pairs were ripples and flat, respectively. In the flat-bed experiments the transport rate was high and there was considerable suspended transport.

In the ripple pair when the water temperature was increased to 36°C the measured sediment discharge decreased 64% and the computed Darcy-Weisbach friction factor of the bed was reduced 22%. The observed temperature effects in the flat-bed pair were similar. At 38°C the sediment discharge was 51% of that at 15°C, and the flat-bed friction factor was reduced 8% in the warm water flow.

Straub, et al. (1958) conducted a series of variable-temperature experiments in a recirculating flume using bed material from the Missouri River (D_g = 0.163 mm, σ_g = 1.36). In these high-transport experiments the bed configuration approached a flat-bed and there was considerable suspended sediment discharge. As the water temperature was raised from 35°F to 86°F the sediment discharge decreased 71% and the bed friction factor was reduced 16%. In these experiments the discharge was held constant but the mean velocity in the low temperature experiment was 10% larger than in the high temperature experiment.

Straub, et al. measured sediment concentration profiles along the flume centerline during their experiments. These measurements indicate that at 86°F the suspended sediment concentrations above 0.035 ft from the bed were significantly smaller than those at 35°F.

Hubbel and Ali (1961) made experiments in a recirculating flume using as bed material sand taken from the bed of the Elkhorn River near Waterloo, Nebraska (D_g = 0.131 mm, σ_g = 1.5). The experimental temperatures ranged from 7°C to 35°C and the bed forms included ripples, dunes, flat-bed and antidunes. However in

the results presented by the authors the observed temperature effects on sediment discharge concentration and bed roughness are not consistent and it is not possible to clearly interpret these results without additional hydraulic data.

Franco (1968) has presented data from a series of experiments in a feed-type flume with fine sand (D_g = 0.23 mm, σ_g = 1.32) wherein the water temperature was varied from 40°F to 80°F. In all experiments the bed was covered with ripples. Franco's data indicate (see Appendix D) that at a given velocity and depth sediment discharge and bed roughness are significantly larger at a water temperature of 40°F than at 80°F.

2.3 FORMULAS FOR TEMPERATURE EFFECT ON SEDIMENT TRANSPORT

Phenomenological differences between particle transport close to the bed and transport away from the bed, have led to separate analytic treatments of these two modes of transport. In two of these formulas the effect of a change in water temperature on sediment transport are considered explicitly. These formulas and their development are reviewed in Sections 2.3.1 and 2.3.2, respectively.

2.3.1 Rouse's Suspended Sediment Distribution Equation

The mean concentration of sediment particles of given size, shape, and density in a steady, uniform, open-channel flow is constant at each elevation. This condition can be expressed by the following equation

$$C(y)\omega + \epsilon_s \frac{dC(y)}{dy} = 0 \qquad (2.1)$$

where C(y) is the mean concentration of sediment particles of given size, shape, and density at elevation y above the bed, ω is the particle fall velocity, and ϵ_s is the diffusion coefficient for sediment.

In turbulent flows, if it is assumed that ϵ_s is related to ϵ_m, the turbulent diffusion coefficient for momentum by the equation

$$\epsilon_s = \beta \epsilon_m \qquad (2.2)$$

where β is constant over the flow depth; and that ω does not vary with y Eq. (2.1) can be integrated using von Karman's velocity distribution equation to give,

$$\frac{C(y)}{C(a)} = \left(\frac{H-y}{y}\frac{a}{H-a}\right)^Z \qquad (2.3)$$

where C(a) is the mean concentration at y = a, and H is the flow depth. The value of Z is defined by

$$Z = \frac{\omega}{\beta K U_{*b}} \qquad (2.4)$$

where K is the von Karman constant, equal to 0.4 for clear water, $U_{*b} = \sqrt{\tau_{ob}/\rho}$, called bed shear velocity, τ_{ob} is the mean bed shear stress, and ρ is the fluid density.

Eq. (2.3) was first presented by Rouse (1937).

Data collected by Vanoni (1946) and others indicate that Eq. (2.3) approximates the relative sediment distribution in the upper flow region where the assumptions made in its development are valid.

According to Eq. (2.3) a change in water temperature can alter the relative sediment distribution by causing a change in particle fall

velocity. With a reduction in ω Eq. (2.3) predicts that sediment concentration will become more nearly uniform over the flow depth. Still-water fall velocities of fine and medium silica sand grains increase with increase in water temperature (ASCE Task Committee on Preparation of Sedimentation Manual (1962)); thus according to Eq. (2.3) in flows where there is a suspended transport of fine and medium sands it is to be expected that with a change in temperature there will also be a change in the relative distribution of suspended sediment.

2.3.2 Einstein Bed-Load Function

Einstein (1950) has proposed a set of relations for computing sediment discharge close to the bed (bed-load discharge). With these relations the temperature effect on the bed-load discharge of different size particles may be computed.

Einstein's development begins by assuming steady, uniform flow conditions and equating the number of particles of a given size and density deposited in a unit area of the bed per second to the number of particles eroded from a unit area of the bed per second,

$$\frac{g_B i_B}{A_L D A_2 D^3 \rho_s g} = \frac{i_b P_s}{A_1 D^3} \qquad (2.5)$$

where g_B is the bed-load discharge per unit width, i_B is the fraction by weight of bed-load discharge of a particular size, D is the characteristic particle diameter, A_L is the ratio of the mean particle travel distance between erosion and deposition to D, (taken by Einstein to depend only on D), A_2 is the ratio of particle volume to D^3, ρ_s is particle density, g is the gravitational constant, i_b is the fraction

by weight of bed sediment of size D, P_s is the probability of a particle of size D being eroded per unit time, and A_1 is the ratio of the bed area a particle occupies to D^2.

Einstein replaces P_s with P/t_1, where t_1 is the exchange time, or the time necessary to replace a bed particle by a similar one. Thus P is the total exchange time per unit time. Assuming that t_1 is proportional to the time it takes for a particle to fall a distance equal to its own diameter Eq. (2.5) becomes

$$\frac{i_B g_B}{\rho_s A_2 A_L g D^4} = \frac{i_b P}{A_3 A_1 D^2} \sqrt{\frac{g(\rho_s - \rho)}{D\rho}} \qquad (2.6)$$

where $A_3 = t_1 \omega_s / D$ and ω_s = still-water particle fall velocity, assumed by Einstein to be given by the relation $\sqrt{\frac{gD(\rho_s - \rho)}{\rho}}$.

A_L is actually a function of P, for after a particle has travelled the mean path length defined by the limiting condition $P \to 0$ there is a probability P that at its destination the hydrodynamic forces will be large enough to transport it an additional path length. The mean path length under these circumstances is given by

$$A_L D = \frac{A_{L0} D}{1 - P}$$

where A_{L0} is the value of A_L for the limiting condition $P \to 0$.

Einstein assumes that the conditions for incipient particle movement obtain when the hydrodynamic lift on the particle is equal to its submerged weight, and that the mean fluid velocity near

the bed particles may be obtained from the velocity distribution equation proposed for open channel flows by Keulegan (1938).

Einstein and El-Samni (1949) found that with hydrodynamically rough conditions and uniform bed material the particle lift coefficient has a value near 0.178, and that the velocity (u) used to calculate lift must be measured at y = 0.35 D.

For non-uniform bed particles u is computed at y = 0.35X, where

$$X = \frac{0.77K_s}{\chi} \qquad \text{for } \frac{K_s}{\chi\delta'} > 1.80 \tag{2.7a}$$

and

$$X = 1.39\,\delta' \qquad \text{for } \frac{K_s}{\chi\delta'} < 1.80 \tag{2.7b}$$

where K_s = bed roughness length; for uniform material K_s = D, for non-uniform material $K_s = D_{65}$ where D_{65} is the particle size for which 65% by weight are finer. χ is a correction faction in Keulegan's logarithmic velocity equation which is an empirical function of the boundary Reynolds number $R_{*b} = U_{*b}K_s/\nu$, where ν is the dynamic viscosity of the fluid, and $\delta' = 11.6\,\nu/U_{*b}$.

In addition Einstein applies a lift correction factor Y for non-uniform bed materials. Y is an empirical function of K_s/δ'. For particles smaller than 1.5 X a general lift correction factor ξ is defined to correct for sheltering by other larger particles or the viscous sublayer.

With some experimental verification (Einstein and El-Samni (1949) Einstein takes the variation in particle lift force to be distributed according to the normal error law, with a normalized standard deviation of 0.5.

Using these relations P is evaluated by integrating the error function to determine the time fraction over which the instantaneous lift force at the bed exceeds the buoyant particle weight. Two constants present in the solution were solved for empirically using data from experiments with uniform bed material. The bed-load discharge function is plotted in Fig. 2.2 as

$$\Phi_* = \varphi(\Psi_*) \tag{2.8}$$

where

$$\Psi_* = \xi Y \frac{\log_{10}^2(10.6)}{\log_{10}^2\left(\frac{10.6X\chi}{K_s}\right)} \left(\frac{(\rho_s-\rho)}{\rho}\right)\frac{gD}{U_*'^2}$$

$$\Phi_* = \left(\frac{i_B}{i_b}\right)\frac{g_B}{\rho_s g}\left(\frac{\rho}{(\rho_s-\rho)gD^3}\right)^{\frac{1}{2}}$$

and $U'_{*b} = \sqrt{\tau'_{ob}/\rho}$ where τ'_{ob} is the bed shear stress due to grain roughness.

According to Eq. (2.8) a change in water temperature can effect the bed-load discharge of uniform bed materials by affecting the viscous sheltering (ξ) of the bed particles, and the mean lift velocity.

For boundary Reynolds numbers based on grain roughness ($R'_{*b} = U'_{*b}K_s/\nu$) less than a value near 15 (ξ and χ can be expressed as functions of R'_*) the change in Ψ_* with increase in water temperature

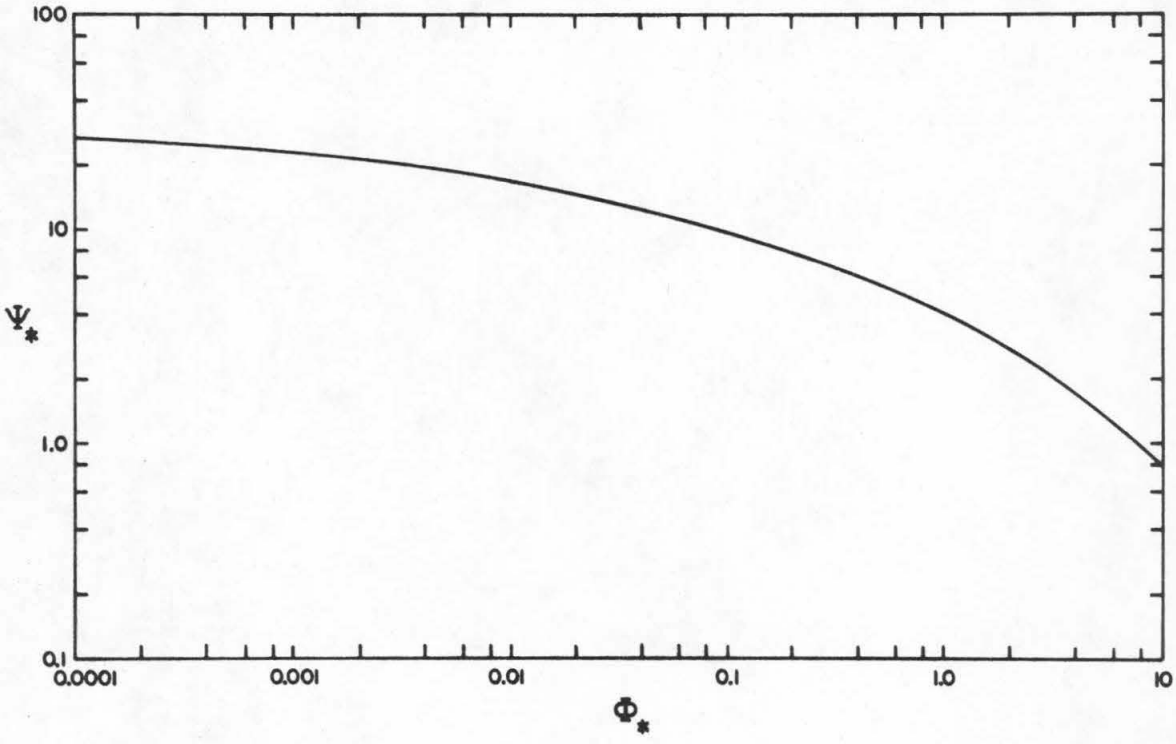

Fig. 2.2. Einstein Bed-Load Function, Ψ_* versus Φ_*.

is negative due primarily to the reduction in the lift parameter ξ. This reduction in Ψ_* indicates an increase in bed-load discharge according to the relation defined in Fig. 2.2.

For boundary Reynolds numbers larger than a value near 15 but less than 100 the temperature related change in Ψ_* is accomplished primarily by the temperature effect on the lift velocity, and an increase in temperature results in an increase in Ψ_*, there is a reduction in bed-load discharge.

For R'_{*b} larger than 100 hydrodynamically rough conditions obtain and Ψ_* does not vary with water temperature.

Therefore according to Einstein's bed-load function for uniform bed material, and R'_{*b} less than approximately 15 an increase in water temperature effects an increase in bed-load discharge; for R'_{*b} larger than a value near 15 but less than 100 a temperature increase causes a reduction in bed-load discharge; and for R'_{*b} larger than 100 bed-load discharge is not affected by a change in water temperature.

CHAPTER 3

EXPERIMENTAL APPARATUS

The experiments described in Chapter 4 were made in two straight flumes of uniform rectangular cross section. The flumes are located in the W. M. Keck Laboratory of Hydraulics and Water Resources at the California Institute of Technology, Pasadena, California. Both are of the recirculating type – the discharge is caught in a small outlet basin and pumped back to the inlet through a circular pipe. The experiments in Series B, C, D, G, and H were made in the 40-ft flume, and those in Series E and F in the 60-ft flume. A description of the 40-ft and 60-ft flumes and their associated apparatus are given in Sections 3.1 and 3.2, respectively.

In Section 3.3 the equipment used to determine the weight, size distribution and specific gravity of the sediment samples is described; and in Section 3.4 a description is given of the nine bed materials that were used.

3.1 THE 40-FT FLUME

The 40-ft flume is 10.5 in. wide and has a working length of 40-ft. A schematic diagram of the flume is given in Fig. 3.1. An axial-flow pump connected to a two-speed electric motor through a variable-drive reducer recirculates the flume discharge (sediment and water) to the inlet section through a 4 in. return line located in the support structure below the flume.

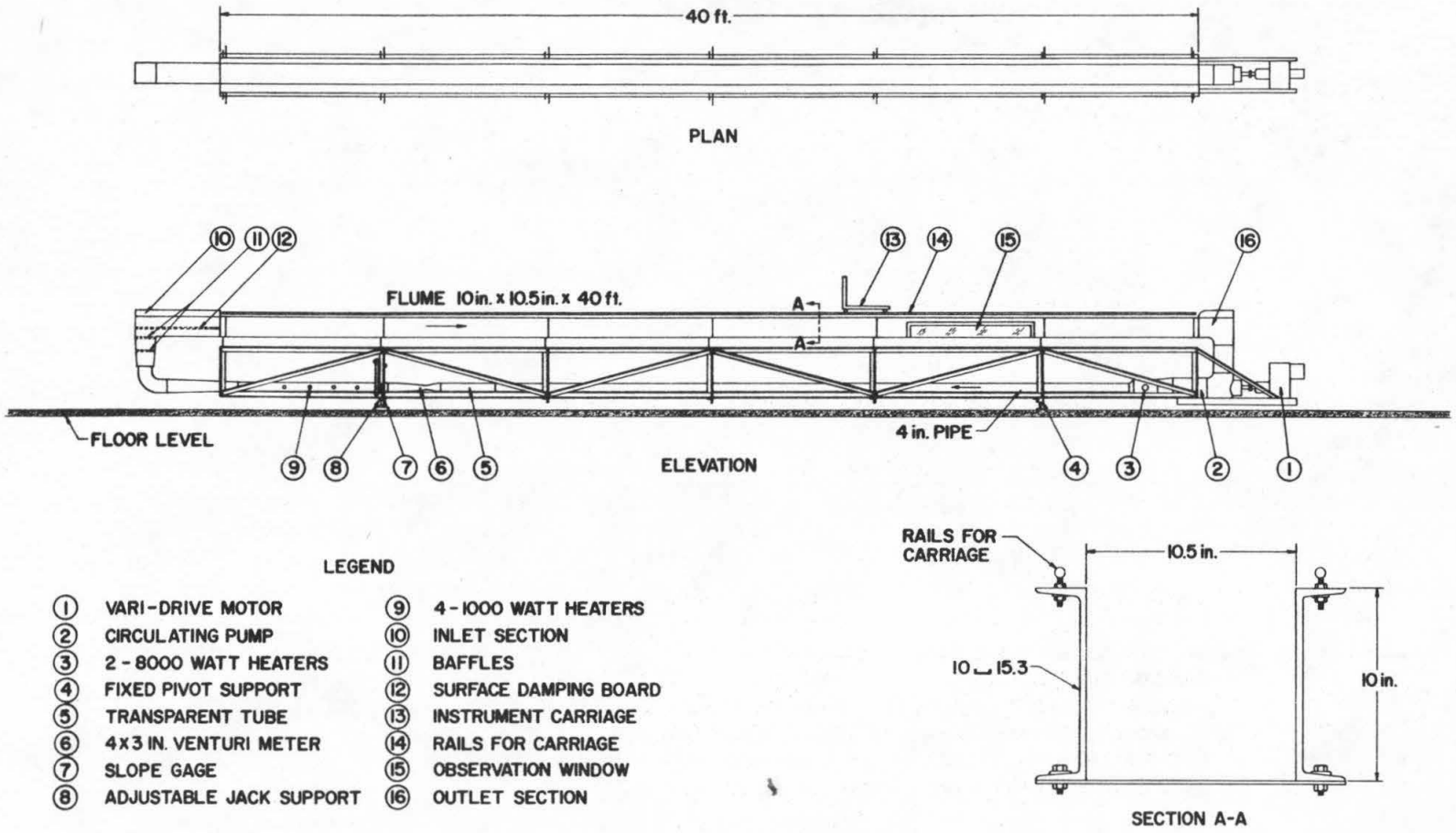

Fig. 3.1. Schematic diagram of 40-ft flume.

The flume, pump assembly, and return line are mounted on a truss which is supported by a pivot near the downstream end and a manually operated, screw-type jack near the upstream end. This allows the flume slope to be varied continuously over the range -0.01 to +0.038. Flume slope can be read directly from a scale located near the jack.

There are four 1000-watt immersion heaters located in the return pipe near the upstream end. Three of the heaters are wired so they can be operated on 110 volts at 250 watts or on 220 volts at 1000 watts. With these four heaters water temperature in the flume could be raised from 20°C ambient to approximately 38°C. This temperature differential was sufficient for the experiments of Series B, C, and D. But in Series G and H larger temperature differentials were desired. In order to maintain water temperatures approaching 70°C two additional 8460-watt immersion heaters were installed in an 8 in. I. D. section of pipe placed just downstream from the pump housing. One of the 8460-watt heaters was wired to a variable-inductance powerstat which afforded continuous control of the heater's output from 0% to 83% maximum rated power.

A venturi tube (D_1 = 4.04 in., D_2 = 2.99 in.) connected to a vertical, air-water differential manometer which can be read to the nearest 0.0005 ft is located in the return pipe near the upstream end to measure discharge. The venturi tube had been calibrated prior to this investigation using clear water and a direct volumetric discharge procedure. This prior calibration was used in computing flume discharge.

A 4 in. I. D. lucite section, 57 in. long located in the return line near the venturi tube provided a means of checking flow conditions in the pipe. The primary concern was sediment deposition which may alter the venturi calibration. However in experiments G-9 and G-10 where the sediment discharged through the flume was recirculated, the mean velocity in the pipe was 151 cm/sec, and visual observations indicated that there was no deposition.

In the vertical throat of the inlet section there are two baffles made from lucite strips glued together in a rectangular grid. The baffles are spaced 8.5 in. apart. Their purpose is to damp the large scale turbulence and secondary currents created in the return line. In experiments G-9 and G-10 it was also necessary to float a plywood board (0.2 in. thick x 10 in. wide x 27 in. long) above the baffles to damp surface disturbances produced by the inlet condition.

The flume itself consists of two 10 in. steel channel beams bolted to a 0.25 in. thick bed plate. In the lower reach glass observation windows 58 in. long by 8 in. high have been installed in each wall of the flume. Except for the glass windows the inside walls and bed of the flume are covered with a bitumastic paint which has a nearly hydrodynamically-smooth finish.

Steel rods (1 in. O. D.) mounted on the top flange of the 10 in. channels which form the side walls act as rails for a metal instrument carriage. These rails extend the entire length of the flume.

To measure water surface and bed elevations in the flume a brass rod with a conical point on one end (point gage) can be clamped to a mounting plate on the instrument carriage, and with gear mechanisms on the instrument carriage this point gage can be positioned both laterally and vertically to within 0.05 mm.

The brass rod point gage can be interchanged easily with a point sediment sampler (Section 3.1.2) or a Pitot tube (Section 3.1.3), and by locating each of these instruments in the same relative position with respect to the mounting plate all three have the same location for the same reading on the scales.

Using the point gage and a still water surface in the flume the variation in the carriage rails and flume bed, and the calibration of the slope scale were checked. This was done by plotting measured water surface and bed elevations at different stations along the flume and fitting straight lines to these points. The differences between the straight-line elevations and the measured elevations were taken to be the variation in the carriage rails and flume bed. The slope of the straight line fitted to the carriage rail elevations, which was parallel with the straight line fitted to the bed elevations, was used to check the calibration of the flume slope scale. It was found that a flume slope of zero corresponded to a scale reading of -0.00032 and that the variation in the carriage rails and flume bed did not exceed ±0.5 mm.

The flume has a second carriage, shown in Fig. 3.2, which can be used to level loose material on the bed. The carriage consists of a welded frame supported on the flume rails by four small, hard-rubber

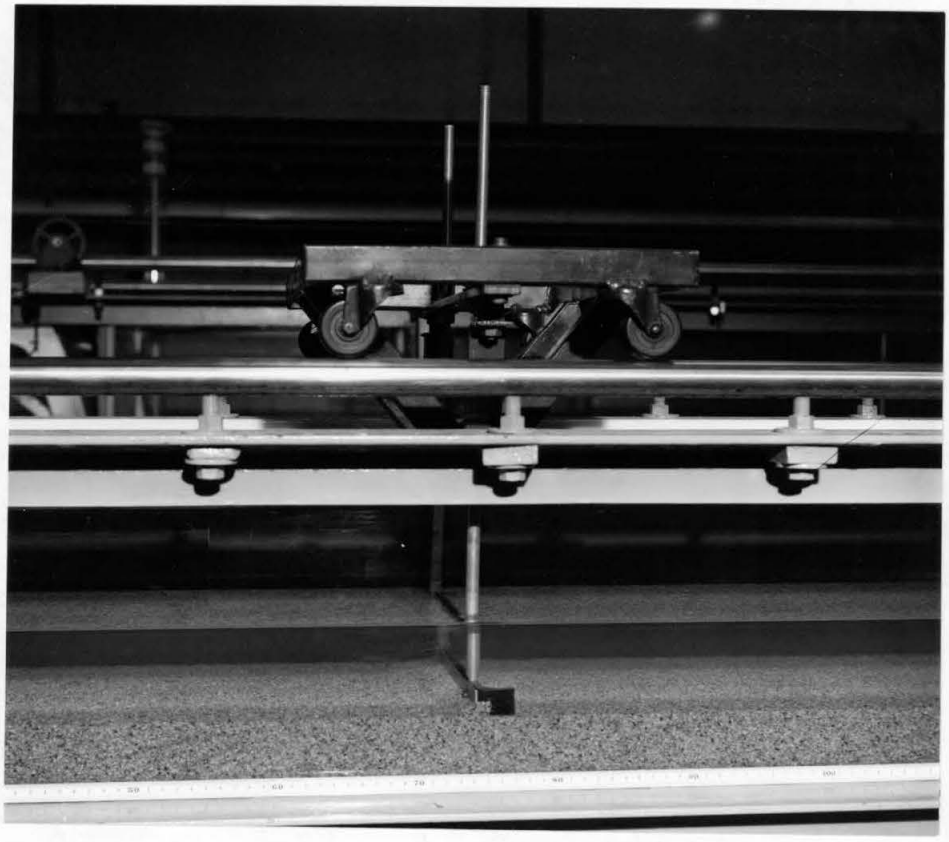

Fig. 3.2 Bed Leveling Carriage for 40-ft Flume Used in Series B, C, and H, and Experiments G-1, G-4, and G-5. (Photograph taken during Series H, Photo No. 11205)

wheels. Two aluminum rods threaded on one end extend down from the carriage, and aluminum strips are bolted horizontally to the lower ends of the rods. The lower edges of these strips act as leveling guides. Elevation of the guides is set by adjusting wing-nuts on the upper ends of the support rods.

3.1.1 Sediment Discharge Sampling Apparatus

In the low-transport experiments of Series B, C, D, and H, and experiments G-1, G-4, and G-5 the sediment load was trapped in a slot near the downstream end of the flume as illustrated in Fig. 3.3. The load material in Series D (D_g = 18.5 mm) was removed from the sampling slot one particle at a time with a large pair of tweezers. In the other experiments the load samples were removed by siphoning a water-sediment mixture out of the slot and into a conical-shaped filter paper placed in a large metal funnel. The sediment sample remained in the filter paper and the water drained into a glass container below.

In experiments G-9 and G-10 considerable sediment was transported in suspension and the load could not be trapped. Therefore in these experiments a sediment discharge sampling procedure similar to that employed by Vanoni and Brooks (1957) was used (see Fig. 3.4). The sampling tube was made from a 41 in. length of 0.25 in. I.D. cold-drawn copper tubing. It had a 180° bend in one end, and a circular sampling tip that had been turned to a thin edge. To sample sediment discharge the tube was suspended vertically in the throad of the outlet box. The upper end was connected to the inlet nozzle of a sampling

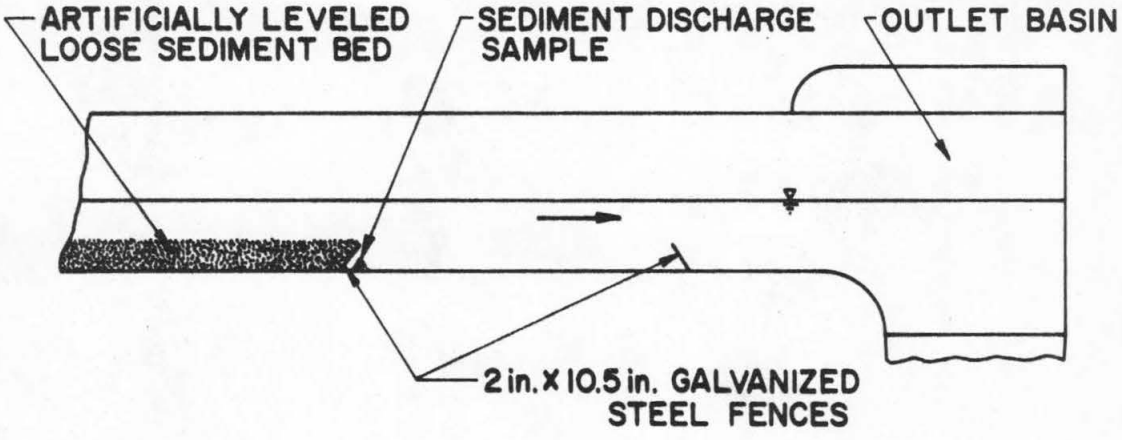

Fig. 3.3. Longitudinal section of 40-ft flume near downstream end, showing slot used to trap load in Series B, C, D, and H, and in experiments G-1, G-4, and G-5.

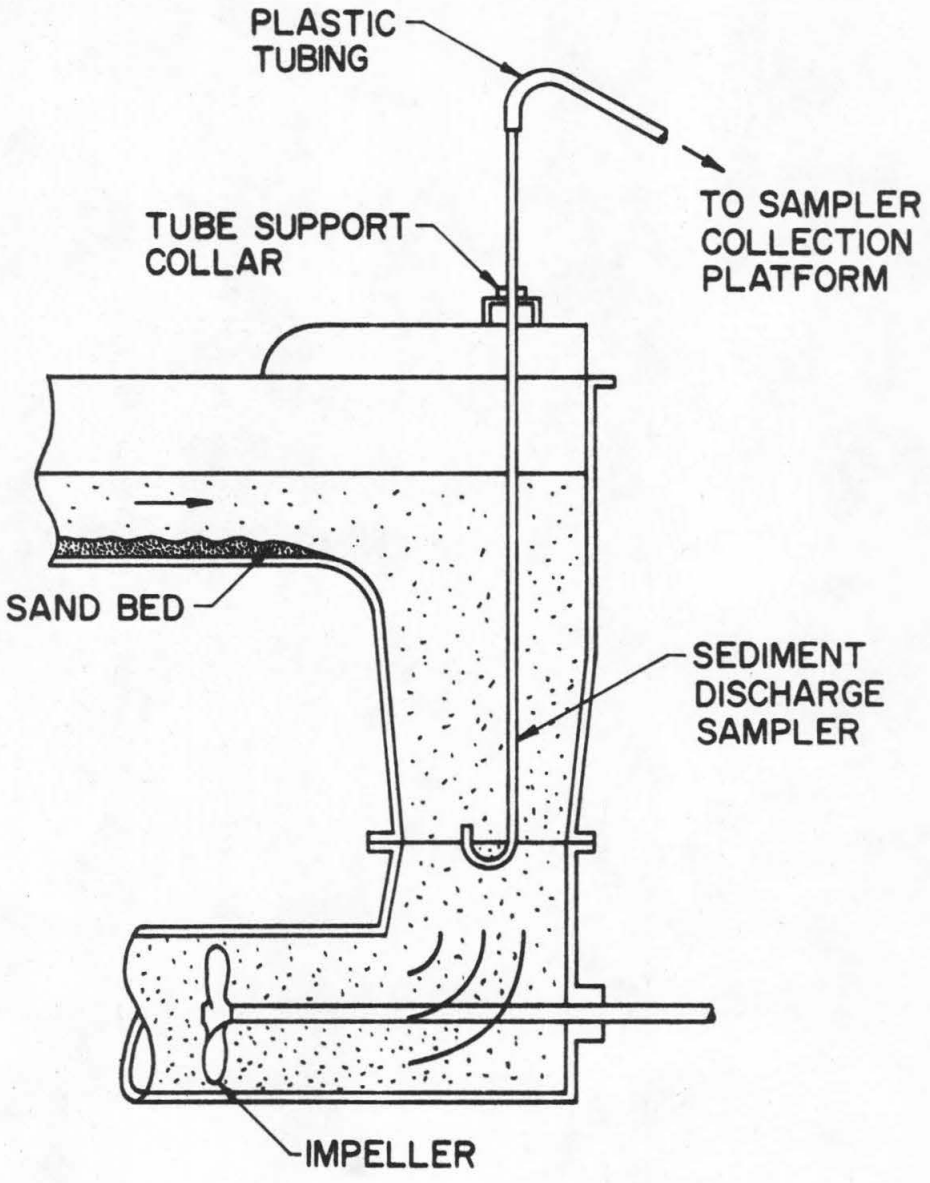

Fig. 3.4. Longitudinal section of 40-ft flume at downstream end showing sediment discharge sampler used in experiments G-9 and G-10.

platform by a 5 ft length of 0.25 in. I. D. plastic hose. The sampling platform can be raised or lowered to provide the head difference necessary to match sampling velocity with the mean velocity in the outlet throat. The sampling velocity was determined from the rate of flow in the sampler which was obtained by measuring the volume of the sample and the time to collect it.

3.1.2 Point Sediment Sampler

In runs G-9 and G-10 a point sampler made from an 0.188 in. I. D. brass tube was used to measure suspended concentrations at different elevations in the flume. The sampling tip had been flattened to give a vertical opening of 0.040 in. and a horizontal opening of 0.217 in. (see Fig. 3.5). This tip design provides a relatively narrow vertical sampling section which is particularly important in sampling near the bed where the non-linear velocity and sediment concentration gradients are large, but offers a fairly large sampling area so that sampling times need not be inordinately long.

3.1.3 Point Velocity Measurements

A 0.250 in. O. D. Prandtl-type Pitot tube with a 0.075 in. tip hole was used to measure local mean velocities in the flume. The Pitot tube was connected to an air-water vertical differential manometer that could be read to the nearest 0.005 ft.

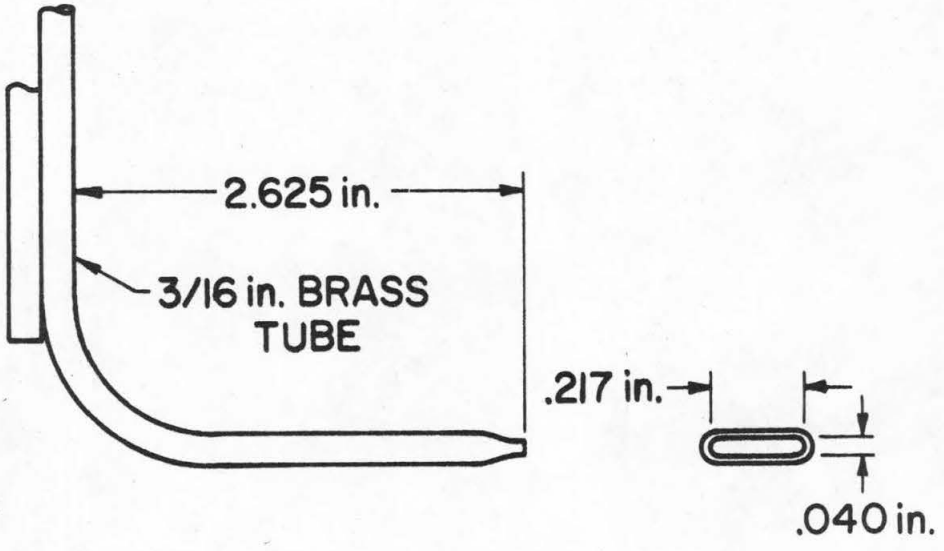

Fig. 3.5. Point sampler used in measuring suspended sediment concentrations in 40-ft, and 60-ft flumes.

3.2 THE 60-FT FLUME

The 60-ft flume is shown schematically in Fig. 3.6. It is 33.5 in. wide and has a working length of 60-ft. The discharge is caught in an inverted, pyramidal outlet basin, fed into a 10 in. I. D. suction of the pump and returned to the inlet box at the upstream end of the flume through an 8 in. I. D. pipe. The bottom section of the outlet basin, the pump-electric motor assembly, and the return line of the flume are permanently bolted to the floor of the laboratory. The bottom section of the outlet basin is connected to the top section by a flexible rubber diaphragm; and the upstream end of the return line is connected to the bottom of the inlet box by a 8.5 ft length of 8 in. I. D. reinforced rubber hose. The inlet box, flume, and top section of the outlet basin are mounted on a truss which is supported by a pivot near its lower end and a power-driven, screw-type jack at the upper end. With this mounting the flume can be set to any slope in the range 0.0 to 0.033. A scale which can be used to measure flume slope is located near the jack.

The axial-flow pump located in the return line near the downstream end of the flume is driven by a two-speed electric motor. The pump and motor are connected through a variable-drive reducer which is itself power operated. A gate valve near the pump provides an additional control of flume discharge.

In order to obtain water temperatures 20°C above ambient three 220-volt, 8460-watt immersion heaters were installed in a short dog-leg section of the return pipe just downstream from the gate valve.

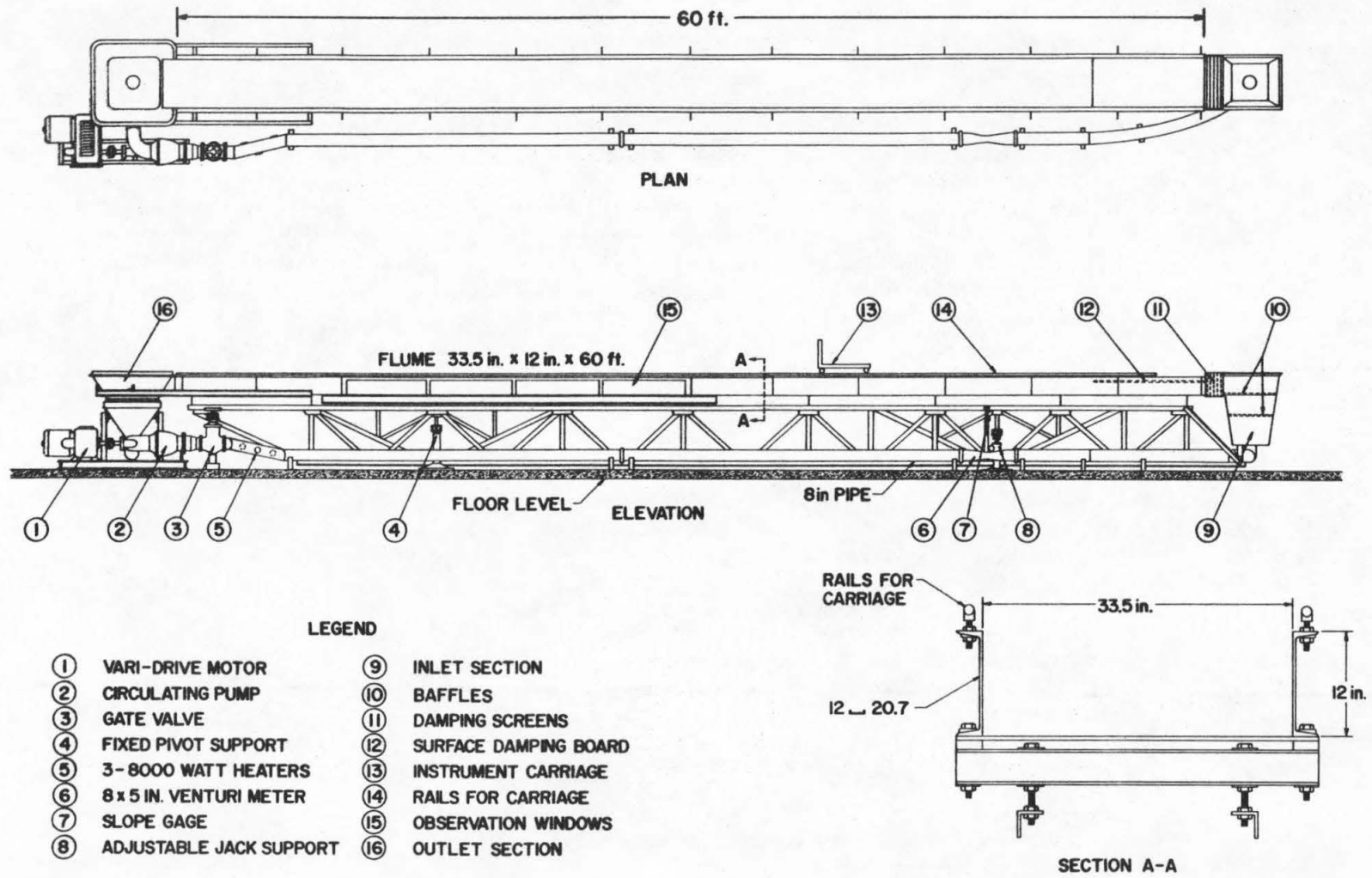

Fig. 3.6. Schematic diagram of 60-ft flume.

The heaters have independent On-Off controls; and one of them was wired through a variable-inductance powerstat to obtain continuous control from 0% to 83% maximum power on this heater.

A venturi tube (D_1 = 8.08 in., D_2 = 5.00 in.) located near the upstream end in the return line is used to measure flume discharge. The venturi tube was connected to a water-mercury vertical differential manometer which can be read to the nearest 0.0005 ft. A clear-water calibration of the venturi tube made prior to this investigation was used to compute flume discharge.

In the inlet box two baffles similar in design to those in the inlet throat of the 40-ft flume are spaced 9.5 in. apart. The baffles are constructed of wood strips 0.88 in. thick and 2 in. wide.

Between the inlet box and the upstream end of the flume there is a wide, metal slot in the side walls and bed where fine-mesh screens can be placed to further damp the large scale turbulence present in the inlet box.

In some of the runs of Series E and F a 0.6 in. thick plywood sheet, 8 ft long and 33 in. wide was floated on the water surface just downstream from the inlet screens to damp surface disturbances produced by the screens. This plywood sheet was coated with a glass epoxy resin to prevent it from absorbing water and warping.

The flume itself is constructed of two 12 in. steel channel beams bolted to a 0.312 in. thick bed plate. One flume wall has a section of four glass windows 58 in. long and 10 in. high. The other

wall has a single window 29 in. long and 8 in. high. Except for the glass windows the walls and bed of the flume are covered with a bitumastic paint.

Steel rods (1.125 in. O.D.) mounted on the top flange of the 12-in. channel beams that form the side walls serve as carriage rails. These rails extend from 31 in. below the beginning of the flume to its downstream end. A metal instrument carriage rides on the rails. An aluminum point gage, and the point sediment sampler and Pitot tube used in the 40-ft flume, can be mounted on adjustable gages which in turn may be clamped to a slotted, 4 in. aluminum channel mounted horizontally on the instrument carriage. This instrument mounting affords an accuracy in vertical positioning of ±0.05 mm, and in lateral positioning of ±0.5 mm.

The flume slope scale was calibrated and the carriage rail and bed variations checked using the same procedure employed in the 40-ft flume. The measured carriage rail and bed variations of the flume were less than ±0.6 mm.

There is also a leveling carriage for the 60-ft flume. It has the same basic construction as its counterpart for the 40-ft flume, and the support rods and leveling guides are virtually identical (see Fig. 3.2). This carriage was used to level the fine gravel bed material in Series E.

A special leveling guide was attached to the carriage (see Fig. 3.7) for the ripple and dune bed experiments of Series F. This guide consisted of a 0.188 in. thick steel plate 33.3 in. long and 6 in. wide.

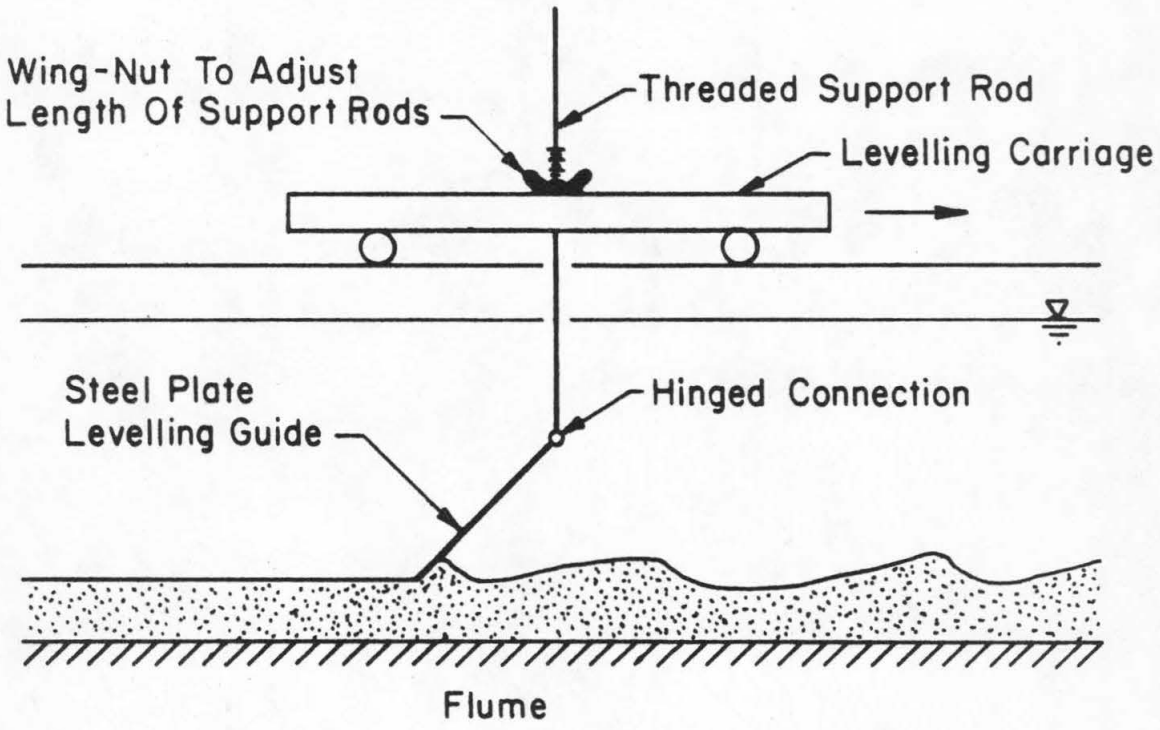

Fig. 3.7. Schematic diagram of modified bed leveling carriage used in 60-ft flume for rippled and dune bed experiments of Series F.

The plate was wired to the lower ends of the vertical support rods after the regular aluminum strip guides had been removed. The wire connectors acted as hinges, and by adjusting the length of the support rods the vertical angle the plate made with the loose bed could be set to any value between 0° and 90°. By traversing the bed with the vertical angle set at approximately 45° small wavelength bed features could be removed without altering mean bed elevations.

3.2.1 Sediment Discharge Sampling Apparatus

Sediment discharge in the low-transport experiments of Series E was measured using the same technique employed in the 40-ft flume, that is, all of the load was deposited in a slot at the lower end of the flume. The sampling slot is shown in Fig. 3.8. The cross members were made of wood strips attached to the flume bed and side walls with Dow-Corning silicon rubber. A fine-mesh screen 4 in. wide was nailed to the downstream cross member to prevent sediment particles that had been swept to the lower end of the slot from being washed over. A 0.625 in. I.D. aluminum tube with an 0.50 in. I.D. plastic hose connected to one end was used to siphon the sediment sample from the slot to a fine-mesh sieve placed on top of a plastic container. The sediment was caught in the sieve and the water drained into the plastic container below.

In the fine-sand experiments of Series F a sediment discharge sampling technique similar to that used in the 40-ft flume for experiments G-9 and G-10 was employed. The sediment discharge was

Fig. 3.8 Downstream End of 60-ft Flume Showing Slot Used To Catch Load in Series E. Siphoning tube to remove load samples is also shown. (Photo No. 11206)

sampled at the short vertical section of the return line just below the outlet basin. The sampling tube, originally used by Vanoni and Brooks (1957), consists of a 0.305 in. I.D. brass tube, 9 ft long with a 135° bend at the outlet end, and a manifold with four vertical sampling tips at the inlet. The manifold is shown schematically in Fig. 3.9. The four sampling tips are made from 0.136 in. I.D. brass tubing and are spaced 90° apart on the manifold. The diameters of two diametrically-opposed tips were reduced by soldering short 0.093 in. I.D. brass tubes in the ends. During an experiment only two of the tips were used for sampling. The inoperative tips were sealed off with masking tape.

The sampling tube was hung through a hole in a 4 in. aluminum channel mounted horizontally across the top of the outlet basin, by an adjustable metal collar. The tips were positioned 0.6 in. below the entrance to the 10 in. I.D. return pipe. A 0.375 in. I.D. plastic hose connected to the outlet of the sampling tube carried the water-sediment samples down over the side of the outlet basin to an elevation approximately 2 ft above the laboratory floor where it discharged the mixture into a conical filter paper. An adjustable metal clamp was attached to the plastic hose to control the flow rate in the siphon and thereby the sampling velocity. The sampling velocity was always made equal to the mean velocity in the pipe at the sampling level.

3.2.2 Bed Profile Measurement Apparatus

Longitudinal bed profiles were measured in Series F using a portable sonic sounder, a motorized instrument carriage, and an analog-to-digital tape recording system. A single-channel strip

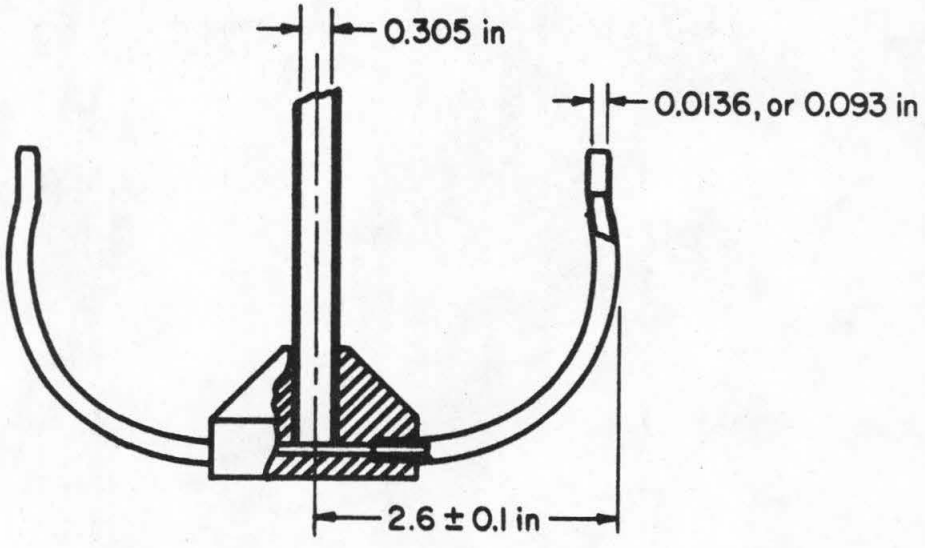

Fig. 3.9. Schematic diagram of sediment discharge sampling manifold used in 60-ft flume for Series F.

chart recorder was also used to provide a continuous check on the quality of the signal input to the digital recorder.

3.2.2.1 Motorized instrument carriage

The instrument carriage on the 60-ft flume has a steel plate which can be used for mounting a D-C electric motor. Vertical position of the motor can be adjusted so that a rubber-rimmed wheel mounted on the motor's shaft, makes contact with one of the carriage rails. In this position the variable-speed motor will drive the instrument carriage in either direction along the flume rails.

The electric motor was wired to a variable-resistance controller through a small box which enabled dead-man micro-switches at either end of the flume to open the circuit and prevent the motorized carriage from going much beyond the test reach. The micro-switches were activated by a small cam bolted to the side of the carriage.

An electric timer activated by two additional micro-switches located at the upstream and downstream ends of the 14-meter study reach was used to measure mean carriage speed over the reach.

Using a stop watch the variation in carriage speed along the study reach was measured by comparing the mean speed over short distances with the mean carriage speed over the 14-meter study reach. These checks indicated that the variation in speed was random and did not exceed 1% of the mean carriage speed.

3.2.2.2 Portable sonic sounder

The portable sonic sounder that was used is sold commercially as a Dual Channel Stream Monitor (DCSM), Model 1042 by Automation Industries, Inc. of Boulder, Colorado. A DCSM similar to the model used in this investigation has been described in detail by Karaki, et al (1961).

The DCSM was developed to monitor water surface and bed profiles in an alluvial channel. It operates on 115 volts AC or a small battery pack. The Model 1042 DCSM is shown in Fig. 3.10. The main unit is encased in a hard-plastic box. Two 40-ft coaxial cables connect this unit to the long end of a metal L-shaped probe. Acoustic transducers are attached to the other end of the probe. These transducers which are cylindrical in shape are made of ceramic barium titrate, rendered piezoelectric by permanent polarization. When an electric potential is placed across opposite sides of the piezoelectric material a deformation takes place along a specific axis. Conversely, when the material is subjected to stress along a certain axis an electric potential is produced. This property enables the transducers to transmit and receive acoustic signals in water.

The ceramic transducers are highly directional. By measuring the time it takes for an acoustic signal generated by the transducer and directed toward the stream bed to be reflected back the distance to the bed can be computed if the celerity of the acoustic signal is known.

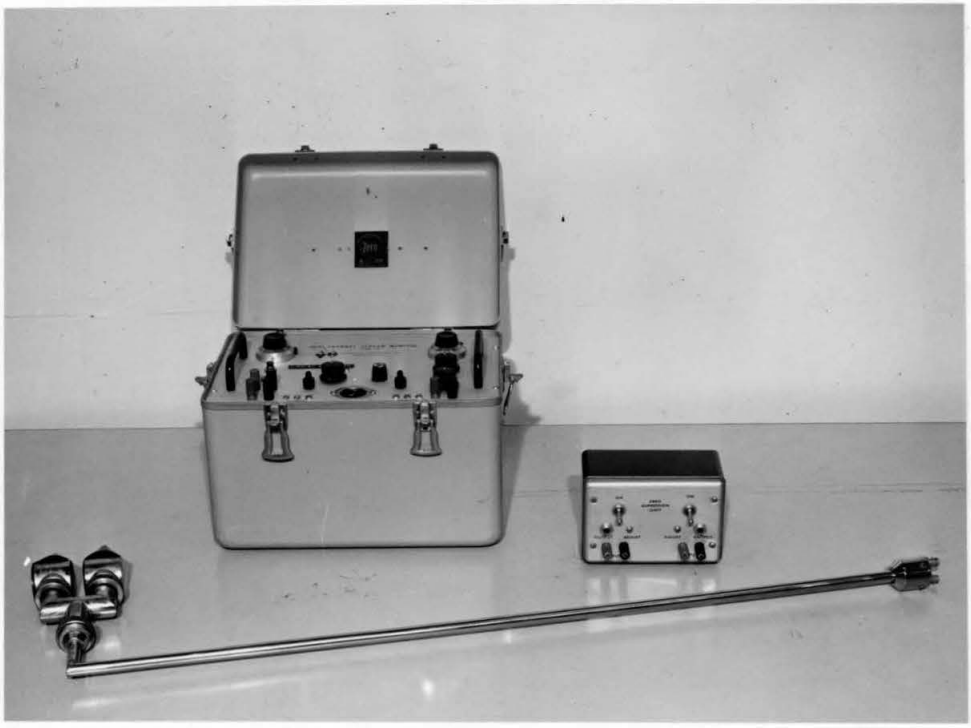

Fig. 3.10 Dual Channel Stream Monitor (left) With D-C Suppression Box (right) and L-Shaped Probe Used to Measure Bed Profiles. (Photo No. 11207)

There are five functional parts in the main unit of the DCSM: an electric clock, signal pulser, receiver, computer, and power supply. The electronic clock provides a time base. Signals from this clock are used to fire both pulsers and to set both computers. When a signal from the clock fires a pulser, a similar clock signal is fed to the appropriate computer. These signals start the timing cycle of the computer and activate the pulser such that an acoustic signal is generated at the transducer. When an echo is received it is fed into the appropriate computer as a reset signal which turns off the computer.

The output from the computer is a square-wave voltage. While the computer timer is operating the otherwise constant output voltage is reduced by 10 volts. A D-C Suppression Box integrates the square-wave signal from the computer and thereby provides a continuous D-C signal with a maximum variation of 10 volts. This box can also be used to reduce the base voltage of the output signal.

In order to eliminate the problem of multiple echoes a sensitivity control is provided on each channel. This control can be adjusted so that the computer will respond only to the primary echo.

The DCSM Model 1042 is built with an operating frequency of one megacycle and possible ranges of 1 ft, 5 ft, and 10 ft. Increasing the range reduces the electronic clock repetition rate, and thus reduces signal resolution. To increase signal resolution the unit used in this investigation had been modified during a prior study (Squarer (1970)) to operate on a frequency of 2.5 megacycles with ranges of 0.5 ft, 1 ft, and 10 ft.

The DCSM was calibrated in the 60-ft. flume with a flat bed and a water depth of approximately 19cm, for two different water temperatures 23°C, and 38°C. These were the water temperatures and depth which obtained during bed profile measurements in the experiments of Series F. At 23°C the calibration for the DCSM was 21.26 cm/v, and at 38°C 21.84 cm/v.

3.2.2.3 D-C Preamplifier and single-channel recorder

The preamplifier and recorder that were used to monitor the signal output from the DCSM are sold commercially as D-C Coupling Preamplifier, Model 151-1300; and Single-Channel Recorder, Model 151-100A by the Sanborn Company of Waltham, Mass. These units are shown in Fig. 3.11.

The input signal is fed to a preamplifier. This preamplifier amplifies the signal and supplies it to a driver amplifier which operates a galvanometer in the recorder. A heated stylus attached to the D'Arsonval movement galvanometer passes over a special plastic-coated paper with a rectilinear grid 5 cm wide manufactured by the Sanborn Company. The hot stylus melts the plastic coating to produce a thin permanent trace. Maximum deflection of this trace is ±2.5 cm. A second heated stylus triggered manually or by an automatic timer produces a marker trace along the lower margin of the strip chart. The recording paper can be driven at selected speeds ranging from 0.25 cm/sec to 10 cm/sec.

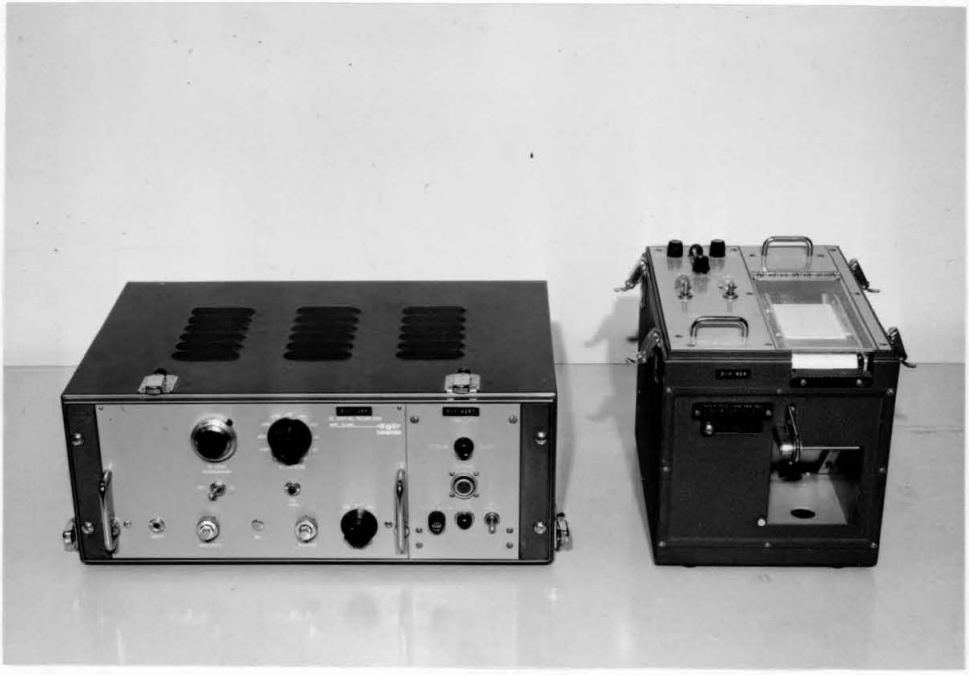

Fig. 3.11 D-C Coupling Preamplifier (left), and Single-Channel Recorder (right) Used to Monitor Input Signal to Digital Recorder. (Photo No. 11208)

The D-C Coupling Preamplifier has an attenuator control which introduces fixed attenuation factors between 1 and 1000, and a D-C suppression control which can be used to reduce the base voltage of the input signal.

3.2.2.4 Analog-to-digital recording unit

The analog-to- digital recorder used to store the bed profiles data on magnetic tape for computer processing is sold commercially as a Data Acquisition System (DAS), 1103 Series by Digital Data Systems of Northridge, Calif.

The DAS unit is shown in Fig. 3.12. It will accept up to eight channels of input voltages in the ranges ±1 v, ±5 v, ±10 v. Digitizing resolution is one part in 2047. Thus for the ±1 v range the digitized signal is given to ±0.001 v; whereas with the ±5 v and ±10 v ranges the digitized signal is given to ±0.01 v.

The input voltages are sampled by a high-speed switching circuit, ranging through eight channels in ten microseconds. This scanning rate is independent of actual signal sampling frequency. The sampling frequency can be set at selected values ranging from one sample per 100 seconds to 1600 samples per second (200 samples per second per channel if eight channels are used).

The sampled voltage from a particular channel goes to an analog-to-digital converter which converts the voltage to a binary signal which in turn is converted to a Binary Coded Decimal (Okoye and Raichlen (1969)). The digitized sample can then be displayed on the front face of the unit at the same time as its value is being stored

Fig. 3.12 Data Acquisition System Used to Digitize Analog Bed Profiles, and Store Digitized Output on Magnetic Tape. (After Okoye (1970))

in a memory unit. The DAS has two memory units. Each will hold 336 digitized samples. The digitized samples are fed into one of these memory units until its storage is exhausted. At this time the logic unit transfers the data flow into the other memory unit. Meanwhile the first memory unit has been emptied with its information stored on a 9-track magnetic tape.

Each 336-sample data set is placed on the magnetic tape as one record. In addition to the data set, at the beginning of the record header information is recorded on the tape. This information serves to identify each record individually. Seven items are included in the header information: day of year (as set on digital clock), hour of day, minute of hour, second of minute, number of channels being used, range, and a 4-digit head constant set arbitrarily by the experimenter. Between each record an inter-record gap (a blank section of tape) allows the tape recorder to accelerate to a constant speed which is used for recording.

At the end of a set of data which may include many records an End Of File button is depressed. This places a coded message on the tape which enables the computer to recognize the end of a data set.

Each magnetic tape is 600 ft long and will hold approximately 3600 records.

3.2.2.5 Bed profile measurement system

The four components used to measure bed profiles are shown in block diagram as they were assembled in Fig. 3.13.

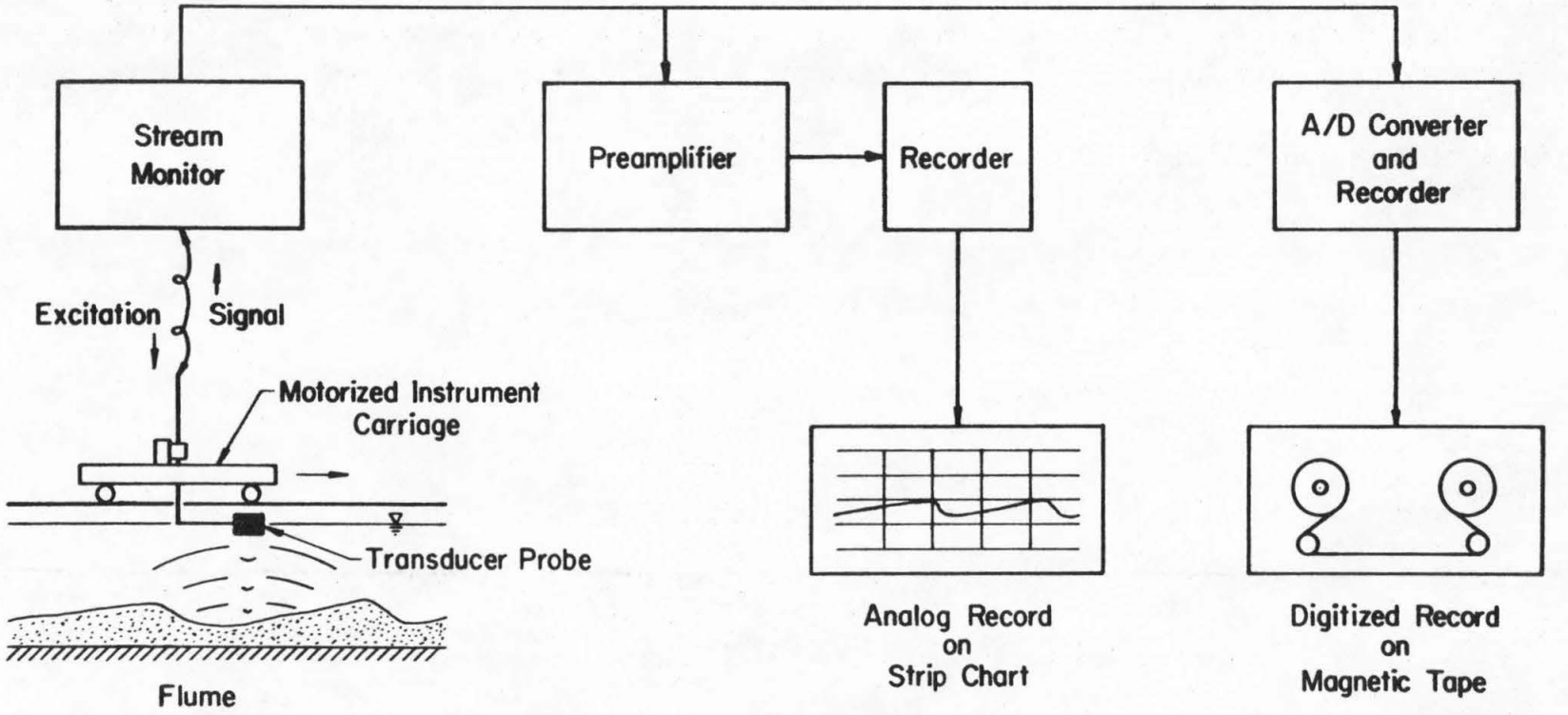

Fig. 3.13. Flow diagram of bed profile measurement system.

As the motorized instrument carriage traversed the flume a DCSM transducer monitored a profile of the bed configuration at one of seven lateral locations where profiles were measured. The output signal from the DCSM was fed simultaneously to the DAS unit and the Sanborn strip chart recording unit. The strip chart recording and the digitized signal display on the DAS console provided continual checks of the data being recorded on the magnetic tape.

The electric timer was used to determine the mean carriage speed, and thereby the distance between profile data points.

Bed profile data stored on the magnetic tapes were processed on an IBM 360/75 computer located in the Booth Computing Center at the California Institute of Technology.

The accuracy of the bed profile measurement system was checked by comparing point-gage measurements along a two-dimensional, artificially-created bed form, with measurements made with the DCSM system. The results are illustrated in Fig. 3.14. They show that the differences between the point-gage measurements and those obtained with the DCSM system are less than 2% of the bed form amplitude. Because the DCSM transducer heads are highly directional and focus on a relatively small area of the bed, it is felt that this relative error is approximately the same as obtained during three-dimensional bed form profile measurements.

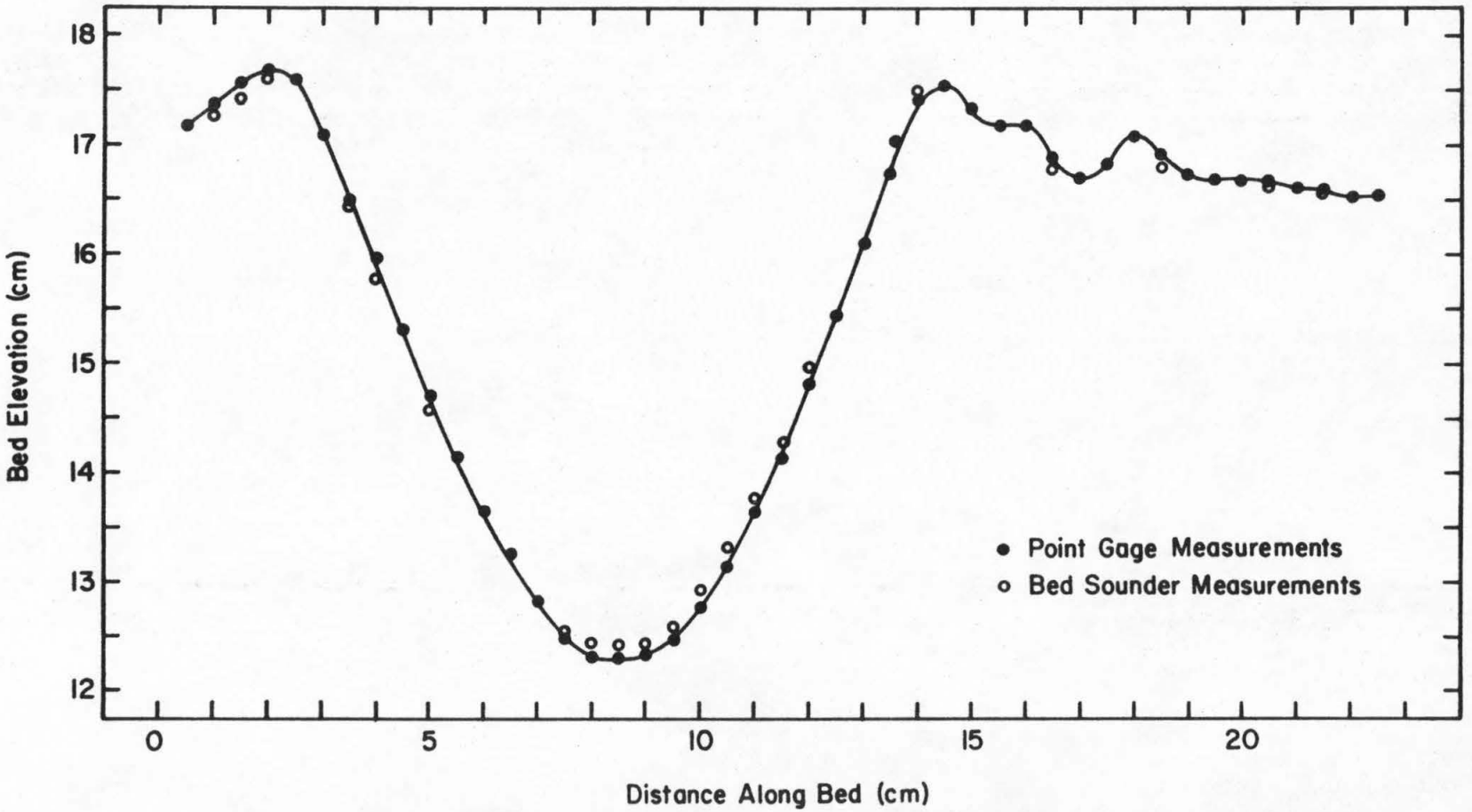

Fig. 3.14. Point-gage and DCSM-system measurements of artificially-formed, two-dimensional bed configuration.

3.3 SEDIMENT ANALYSIS APPARATUS

Sediment samples were oven-dried, and analyzed for particle size distribution and density. The oven has a temperature range of 38°C to 260°C, and a small blower to insure uniform heating.

Size distributions were obtained by separating sample material with a set of $\sqrt[4]{2}$ square-mesh seives manufactured by the W. S. Tyler Company of Cleveland, Ohio. A Ro-Tap mechanical shaker manufactured by the same company was used to shake the sediment through the seives. The Ro-Tap is controlled by a timer which can be set for vibration times of from 3 min. to 27 min.

An analytic balance was used to measure the dry weight of samples. This balance has an accuracy of ± 0.0005 gm. A triple-beam balance with an accuracy of ±0.005 gm, was used in determining specific gravities. The samples were placed in a small wire basket and weighed in air, and then basket and sample were submerged in a beaker of distilled water and weighed again under saturated conditions. Specific gravity of the coarse-particle samples (D_g = 18.5mm) from Series D was determined by measuring the change in water level in a graduated one-liter cylinder partially filled, when a sample of known weight was added.

3.4 SEDIMENTS USED AS BED MATERIAL

Nine different sediments were used as bed materials during the investigation. Size distributions of these sediments are shown in Fig. 3.15, and their physical properties are summarized in Table 3.1.

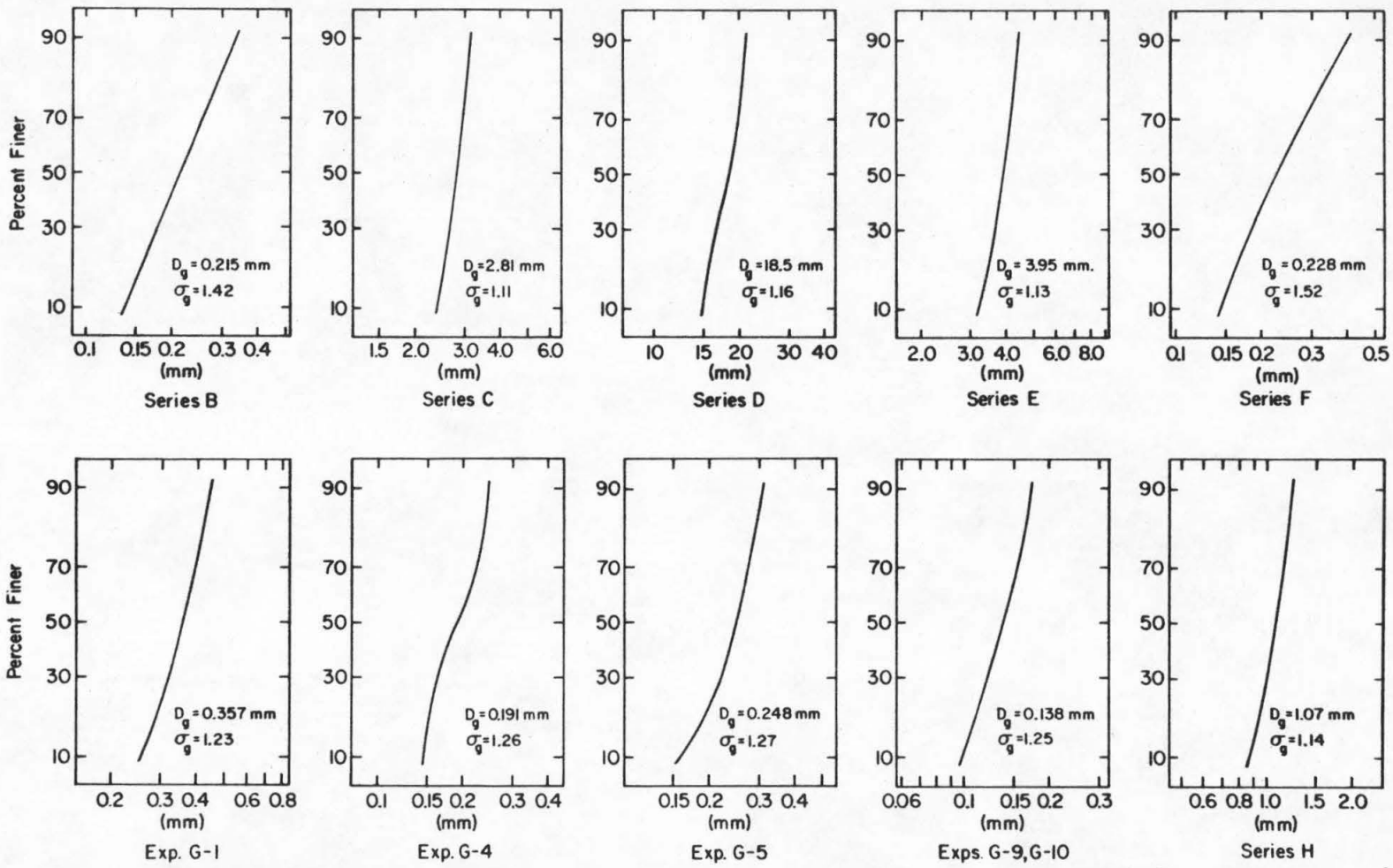

Fig. 3.15. Sieve size distributions of sediments used as bed material.

Table 3.1 Physical Characteristics of Sediments Used as Bed Materials

Run or Series	Description of Material	D_g Geom. Mean Size (mm)	σ_g Geom. Std. Deviation	ρ_s Mean Density (gm/cm^3)
B	Fine Silica Sand	0.215	1.42	2.65
C	Fine Gravel	2.81	1.11	2.61
D	Clay Aggregate	18.5	1.16	1.37
E	Fine Gravel	3.95	1.13	2.61
F	Fine Silica Sand	0.228	1.52	2.65
G-1	Fine Silica Sand	0.357	1.23	2.65
G-4	Fine Silica Sand	0.191	1.26	2.65
G-5	Fine Silica Sand	0.248	1.27	2.65
G-9, G-10	Fine Silica Sand	0.138	1.25	2.65
H	Coarse Sand	1.07	1.14	2.61

3.4.1 Fine Sands Used in Series B, F, and G

The fine sand from which the bed materials for Series B, F, and G were derived is sold commercially as Nevade #60 by Silica Products, Inc. of Overton, Nevada. The sand is pure silica except for slight mineral staining on the surfaces of approximately 5% of the grains. The sand has been naturally worn and the grains are fairly well rounded except for particle sizes finer than 0.088 mm wherein a large percentage of the grains are angular, sharp-edged fragments. A microphotograph of a small sample of the sand is shown in Fig. 3.16.

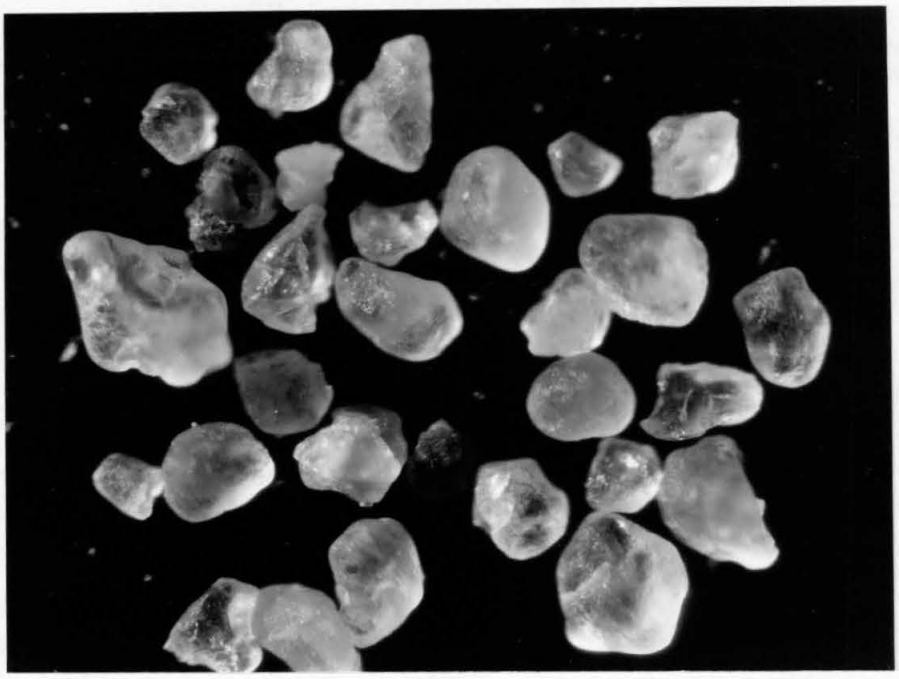

Fig. 3.16 Microphotograph of Silica Sand (Nevada #60) From Which Bed Materials Used in Series B, F, and G Were Derived. (Magnification: 75 times, Photo No. 11209)

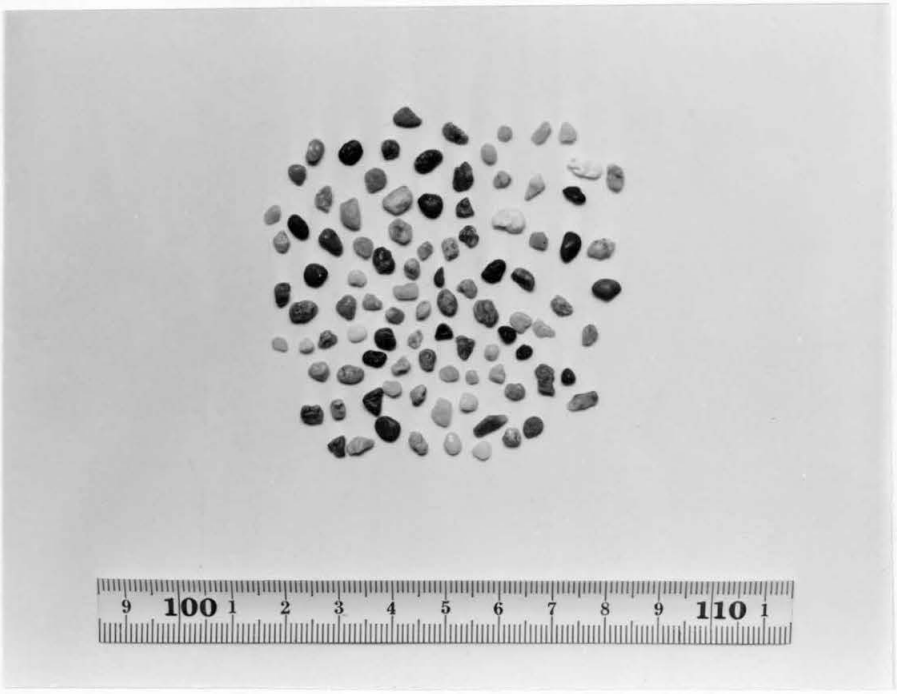

Fig. 3.17 Sample of Fine Gravel Used in Series C. (Scale is in cm, Photo No. 11210)

In Series B and F the sand was used as received from the supplier; but for the experiments of Series G, 7000 lbs of the sand was separated by fall velocity into eight well-sorted size fractions. A description of the apparatus and procedure used in this separation process is given in Appendix B. Sediments from four of these well-sorted size fractions were used as bed materials in Series G (see Table 3.1).

3.4.2 Fine Gravel Used in Series C

The fine gravel used in Series C is sold commercially as Aquarium No. 2 by the Monterey Sand Company of Monterey, California.

The Aquarium No. 2 was prepared for use by removing all of the material that would not pass a 3.327 mm square mesh sieve. Individual particles of the sorted material were of various colors indicating different mineral composition, but all of the particles were naturally worn and rounded. The variation in individual particle density was not measured.

A photograph of a small sample of the material is shown in Fig. 3.17.

3.4.3 Clay Aggregate Particles Used in Series D

Bed sediment for the experiments in Series D was derived from a synthetic, clay-aggregate material produced commercially by the Crestlite Company of San Clemente, California. The synthetic particles are formed by firing clay globules in a rotating cylindrical furnace.

The particles used in Series D were initially separated according to specific gravity. Material that floated in a saturated NaCl solution ($\rho \sim 1.2$ gm/cm^3) was discarded. The heavier particles were then sorted by hand for uniform size and shape (see Fig. 3.18). This material had a mean density of 1.37 gm/cm^3, but measured particle densities ranged from 1.2 gm/cm^3 to 2.0 gm/cm^3.

3.4.4 Fine Gravel Used in Series E

The fine gravel used in Series E was coarser than that of Series C (see Fig. 3.15). It was obtained from the Pioneer Pebble Company of Santa Monica, California. The individual particles were of various colors, and approximately 90% of them were naturally worn and somewhat round. In the experiments of Series E the densities of the load samples were significantly less than that of the bed material (see Table 5.1) indicating a variation in particle density; however, this variation was not measured directly. A photograph of a sample of the gravel is shown in Fig. 3.19.

3.4.5 Coarse Sand Used in Series H

The coarse sand used as bed material in Series H was obtained from the Monterey Sand Company. It is sold commercially as Crystal Amber No. 2.

This sand is 91% silica, and the particles are naturally worn and rounded. A photograph of a sample of the material that was used is shown in Fig. 3.20.

Fig. 3.18 Sample of Coarse, Synthetic Clay-Aggregate Particles Used in Series D. (Scale is in cm, Photo No. 11211)

Fig. 3.19 Sample of Fine Gravel Used in Series E. (Scale is in cm, Photo No. 11212)

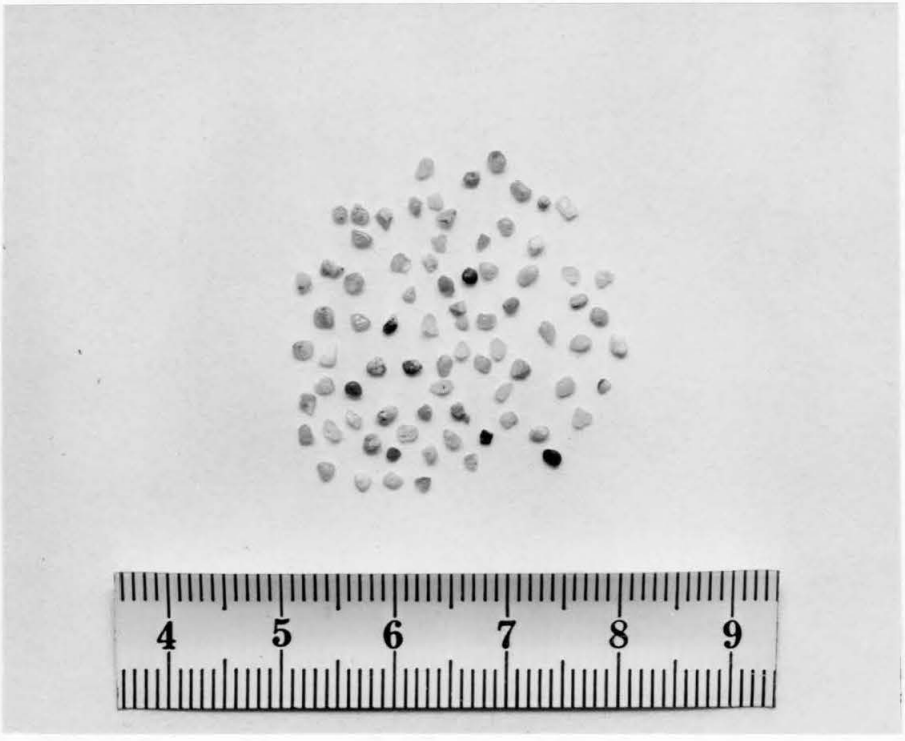

Fig. 3.20 Sample of Coarse Sand Used in Series H.
(Scale is in cm, Photo No. 11213)

CHAPTER 4

EXPERIMENTAL PROCEDURE

Three types of experiments in which there were important differences in procedure were made during the course of the investigation: 1) Low-transport flat-bed experiments, 2) High-transport flat-bed experiments, and 3) Ripple and dune bed experiments. 1) All experiments in Series B, C, D, E, and H, and experiments G-1, G-4, and G-5 were low-transport, flat-bed experiments. The bed materials ranged from fine sands to clay aggregate particles approximately 18.5 mm in diameter (see Table 3.1). In each experiment the loose bed was artificially leveled before the experiment was started; and all particle transport was by rolling and sliding along the bed. Sediment load was deposited in a slot near the lower end of the flume, and thus in these experiments there was no sediment recirculation. The experiments were made primarily to measure temperature effects on sediment discharge and friction slope. 2) Experiments F-23, F-24, F-27, F-28, G-9, and G-10 were high-transport, flat-bed experiments with fine sands. In each there was considerable suspended sediment discharge, and the natural bed form was flat. In these experiments centerline velocity and sediment concentration profiles were measured in addition to sediment discharge and friction slope. 3) The natural bed form in experiments F-3 through F-10 and F-31 through F-34 were

ripples and dunes. In each of these experiments sediment discharge and friction slope data were collected; and bed profiles were measured using a portable sonic sounder.

The experiments in Series B, C, D, G, and H were made in the 40-ft flume, and those of Series E and F were made in the 60-ft flume. Except in Series G, the bed material was the same for all of the experiments in a series.

With the exception of experiments G-1, G-4, and G-5 the experiments in each series were made in pairs. In each pair the mean velocity and depth were the same or nearly the same, but the water temperatures in the two experiments differed by at least $15^{\circ}C$. The velocity and depth were set by adjusting flume discharge and the amount of water in the flume; and sediment discharge and friction slope were measured as dependent variables.

During each experiment water was added to the flume to replace water lost through evaporation and leakage. In Series B, C, D, E, G, and H the water was replaced intermittently, whereas in the experiments of Series F water was constantly added at the inlet box through a small plastic hose with a needle valve to adjust the flow rate.

In experiment G-4 the maximum difference in water temperature from one end of the flume to the other was $0.5^{\circ}C$; in G-5 this difference was approximately $0.2^{\circ}C$. The maximum temperature difference along the flume in each of the other experiments was less than $0.1^{\circ}C$.

The variation in water temperature during an experiment was less than $\pm 1^{\circ}C$, except in E-1 and E-5 where the water temperature varied $\pm 3^{\circ}C$.

The procedures used in the low-transport, flat-bed experiments; the high-transport, flat-bed experiments; and the experiments wherein the bed was covered with ripples or dunes are outlined in Sections 4.1, 4.2, and 4.3, respectively.

4.1 PROCEDURE IN LOW-TRANSPORT, FLAT-BED EXPERIMENTS

In Series B prior to each experiment the fine sand bed was scarified, and then leveled using the carriage shown in Fig. 3.2. The leveled bed terminated with the upstream cross member of the slot forming the sediment trap near the lower end of the flume. At the upstream end of the flume the bed was contoured to provide a gradual change in flow depth from approximately 12 cm at the inlet to 6.10 cm at Station 1.0 (1.0 m below the upstream end of the flume) where the bed became flat.

After the bed preparation the water present in the flume during the leveling process was gradually replaced with water near the temperature desired in the experiment. This was accomplished by adding water in the outlet basin and simultaneously removing it through a drain pipe near the upstream end of the return line. When the correct water temperature and depth had been obtained the pump was started and discharge was slowly increased to the desired value. As the discharge was increased the flume slope was adjusted to give uniform flow over

the flat bed. The slope of the water surface relative to the flume was determined by fitting a straight line to the water surface profile obtained from point gage readings at different stations along the study reach. The criterion for uniform flow was that this relative slope be equal to zero. In each experiment the water surface was smooth and elevations could be measured ±0.05 mm.

The four 1000-watt electric heaters in the return pipe were used to maintain water temperature during the experiments.

After an initial run period of from 0.3 hours to 8 hours depending on sediment discharge (the initial run period was reduced for larger sediment discharges), the sampling slot was cleaned with a plastic siphoning tube and the first sediment discharge sampling period was begun. In each experiment two or more sediment discharge samples were collected. The sampling periods ranged from 1.2 hours in experiment B-2 to 60 hours. In experiments B-2 and B-4 the sampling periods were limited by the spontaneous formation of ripples on the bed (see Appendix F). After a sediment sample had been collected from the catch-slot the water taken from the flume in the siphoning process was returned to the outlet box. The amount of water removed was in each case less than two liters.

The sediment discharge samples were oven-dried at 118°C and then weighed and analyzed for size distribution.

The amount of water added to the flume during an experiment to replace the water lost through evaporation and leakage was determined by the change in mean flow depth over the study reach, as indicated by

surface elevation measurements. A loss of one liter corresponds to a 0.28 mm lowering of the mean water level in the 40-ft flume. With these additions the variation in flow depth during an experiment was less than 1%.

The procedure used in Series C was the same as that in Series B with the following exceptions. Whereas in the fine sand experiments of Series B bed elevations were obtained by direct measurements, in Series C they were computed using elevations measured near the tops of the bed particles. A 2 in. square brass plate 0.0625 in. thick was carefully placed on the fine gravel bed at the location where the bed elevation was desired and the elevation of the center of the plate was measured. The local bed elevation was computed by subtracting the plate thickness plus 0.2 D_g from the plate elevation. Einstein and El-Samni (1949) have presented data which indicate that by measuring the mean bed elevation in this way the velocity profile above the bed approximates a logarithmic distribution.

Water surface elevations in Series C were measured by taking spatial average readings along the flume centerline. This was necessary due to the small surface disturbances present in each experiment. The mean surface elevations were measured by moving the instrument carriage back and forth successively from 30 cm below to 30 cm above the station where the measurement was desired. The mean surface elevation was measured as the point gage elevation at which the surface was being intercepted over approximately half the traverse distance.

The sediment discharge samples were oven-dried and analyzed for weight, size distribution, and specific gravity. The specific gravity was determined by weighing the sample in air and then in a small wire basket submerged in a beaker of distilled water. The specific gravity, $S.G._w$, of the sample was computed using the following formula:

$$S.G._w = \frac{W_{sa}}{W_{sa} - W_{sw}} \qquad (4.1)$$

where W_{sa} = weight of the sample in air, in grams

and W_{sw} = weight of the sample submerged in distilled water, in grams.

The experiments in Series C were run for from 6 hours to 24 hours after an initial 1 hour to 3 hour adjustment period.

In Series D the experimental procedure was similar to that employed in Series C but due to the nature of the bed material the following modifications were necessary. The leveling carriage could not be used in these experiments. Instead a wooden board (0.875 in. x 15 in. x 10.25 in.) was used. The board had a leather strap connected to one side and could be worn on the hand like a paddle. Using this paddle as a guide the bed material was leveled such that the variations in bed elevation were less than ±0.5 mm along the study reach.

After the first experiment D-11 the bed particles that had been discharged during the previous experiment were returned to the flume before the bed was leveled for the next experiment. Thus in each experiment the bed material was virtually the same. The sediment

discharge samples were removed from the sampling slot one particle at a time with a pair of large metal tweezers. Because of the low transport rate it was possible to complete this removal in one or two minutes.

The clay aggregate used in Series D tended to absorb water. In a preliminary test it took approximately 30 hours for a small sample of the bed particles to become saturated. The specific gravity of the sample increased 4.5% during this saturation process. Because of the relatively long time required for the particles to become saturated and the significant change in specific gravity the sediment discharge samples were not oven-dried. The particles were individually surface dried, and then weighed and analyzed for size distribution and specific gravity. The sample material was sieved manually to prevent particle abrasion. Specific gravity was determined by weighing the particles in air and then measuring the change in water level in a graduated one-liter cylinder partially filled, when the sample particles were submerged therein. The specific gravity was computed using the following formula,

$$S.G._v = \frac{W_{sa}}{\Delta v \rho}$$

where Δv is the volumetric change in water level, in cm^3.

The experiments of Series E were conducted in the 60-ft flume but otherwise the experimental procedure was the same as that employed in Series C. The carriage described in Section 3.2 was used to level the bed material.

At the upstream end of the flume a fixed-bed section was used to create a boundary layer and prevent scour downstream from the inlet. The fixed-bed was made by covering one side of a 33.5 in. x 10 ft sheet of 24 ga. galvanized steel with glass resin and then sprinkling dry bed material on this surface. After the glass resin hardened the loose material that had not been bonded to the sheet was removed. The sheet was laid on the flume bed just below the inlet screens. The downstream one-third of the sheet overlaid loose bed material that increased in thickness to approximately 3 cm at the end of sheet where the depth of loose bed sediment became uniform.

Sediment discharge samples which were in fact the total sediment load during the sampling period, were removed from the catch-slot shown in Fig. 3.8 by siphoning.

In each experiment after E-1 prior to leveling the bed, sediment samples from the previous experiment were uniformly distributed over the bed, and then the loose bed was scarified.

Three 8460-watt electric heaters located in the return pipe of the 60-ft flume were used to maintain water temperature during the experiments of Series E.

The procedure used in experiments G-1, G-4, and G-5 was virtually the same as that for the experiments of Series B. In each of the three experiments a different size fraction of separated Nevada #60 sand was used as bed material (see Table 3.1).

Preliminary experiments were made prior to G-4 and G-5 to determine the water temperatures and mean velocity required to accomplish the experimental objectives. In experiment G-4 the objective was to match the boundary Reynolds number with that in G-1 by changing only the water temperature. In G-5 the water temperature and mean velocity were adjusted in order to match the boundary Reynolds number and the Shields stress with the values of these parameters in experiment G-1.

To maintain the water temperatures required in the experiments of Series G four 1000-watt heaters and two 8460-watt heaters located in the return line of the 40-ft flume were used.

In the experiments of Series H the procedure used was the same as that followed in Series C. However in Series H the water temperature differential was 20°C rather than approximately 15°C. Sediment discharge samples were collected for periods of from 3 hours to 6 hours after an initial 1 hour adjustment period.

4.2 PROCEDURE IN HIGH-TRANSPORT, FLAT-BED EXPERIMENTS

The experimental procedure was essentially the same for all of the high-transport, flat-bed experiments. After the water temperature, depth, and discharge were set, the flume was operated continuously, recirculating all sediment discharged through the flume, until equilibrium conditions obtained. This took from two hours to nine hours.

Experiments F-23, F-24, F-27, and F-28 were conducted in the 60-ft flume. In these experiments sediment discharge samples were collected at the beginning of the return pipe using the sampling tube described in Section 3.2.1. Three samples of 5 min. to 10 min. duration were collected in each experiment over a two hour period. The sampling velocity at the tips of the sampling tube was matched with the mean velocity in the 10-in. return pipe by measuring sample discharge with a graduated one-liter cylinder and a stop-watch. At the sampling section the velocity and sediment distribution were nearly uniform, but to help insure representative samples the tube was constantly moved about in the section during withdrawal.

Centerline velocity and sediment concentration profiles were measured in each experiment. The profiles were obtained at Station 10.0 (11.2 m below the upstream end of the flume) in F-23 and F-24, and at Station 12.0 (13.2 m below the upstream end of the flume) in F-27 and F-28.

The mean point velocities were measured using a Prandtl-type Pitot tube. A coefficient of 1.0 was assumed for the Pitot tube.

The point sampler illustrated in Fig. 3.3 was used to measure the sediment concentration profiles. Samples were collected after the sampling velocity had been matched with the mean velocity at the location as given by the measured velocity profile. Water removed from the flume during sampling was immediately replaced.

After the concentration profile measurements were completed water surface elevations were measured along the study reach. The pump was then shut off and when the water surface had become tranquil still water surface and bed elevations were measured. The dynamic water surface and bed elevations were measured by taking spacial average readings along the flume centerline using the same technique employed in the experiments of Series C. This was necessary due to small amplitude surface and bed disturbances present in each experiment.

The friction slope was determined graphically by measuring the slope of a straight line fitted to points computed along the energy grade line.

Experiments G-9 and G-10 were made in the 40-ft flume. In these experiments after equilibrium flow conditions obtained, four 4-min. sediment discharge samples were collected over a 1 hour period. The samples were removed at the vertical 9-in. I. D. section of the return pipe just below the outlet box as shown schematically in Fig. 3. 4.

The velocity and sediment concentration profile measurements were made at Station 9. 0 (9. 0 m below the upstream end of the flume).

All sediment samples collected in the high-transport, flat-bed experiments were oven-dried at 118^{o}C and then weighed and analyzed for size distribution.

4.3 PROCEDURE IN RIPPLE AND DUNE BED EXPERIMENTS

The ripple and dune bed experiments include F-3 through F-10 and F-31 through F-34. In these experiments the discharge was kept constant at 47.4 liters per sec.

At the beginning of each experiment the depth was set by adjusting the still water level at Station 3.0. The flume slope was set at 0.00088 in all of the experiments. Every twelve hours or so during an experiment the pump was shut off and after the water surface became tranquil the water level at Station 3.0 was checked and corrected if necessary. The pump was then started and the discharge slowly increased to the experimental value so that the bed disturbance was minimized. With these checks the variation in water level during an experiment did not exceed ±2 mm.

After from two days to nine days of continual flume operation equilibrium flow was obtained, and measurements were made over a period of three days. During the first day three 15-min. sediment discharge samples were collected using the same apparatus and procedure used in the high-transport, flat-bed experiments of Series F. When this sampling had been completed the flume discharge was reduced over a period of a few seconds to obtain a mean velocity in the flume of approximately 6 cm/sec. At this velocity there was no sediment transport. Water was then added at the inlet box to raise the mean depth to approximately 19 cm along the study reach in order to accomodate the optimum range of the DCSM transducer. The

purpose of slowly recirculating the water was to maintain uniform water temperature and thus uniform acoustic celerity in the flume. In the warm water experiments a water temperature of 38°C was maintained, and in the cold water experiments the temperature was 23°C.

When the correct water level and temperature had been established longitudinal bed profiles were measured along the flume centerline and at lateral positions 10 cm, 20 cm, and 30 cm on either side of the centerline. The profiles were measured using the component system described in Section 3.2.2. For the profile measurements the DCSM transducer was only partially submerged (see Fig. 3.13), and the motorized carriage was driven at a speed of approximately 6 cm/sec.

Following the bed profile measurements the still water level in the flume was reduced and the pump started. Eighteen to twenty hours later the sediment discharge and bed profile measurements were repeated.

On the third day after the three sediment discharge samples had been collected but before flume discharge was reduced for the bed profile measurements, water surface elevations were measured along the flume using the spatial averaging technique.

After the third set of bed profiles had been measured the bed was leveled with the hinged-plate carriage leveler described in Section 3.2 and shown schematically in Fig. 3.7. By traversing the study reach from six to ten times (three to five times each direction) with this leveler the bed was rendered smooth and laterally uniform; but not

longitudinally flat due to the long-wavelength, small-amplitude bed waves that were present in all of the ripple and dune bed experiments. Bed elevations were then measured along the flume centerline.

The friction slope was determined graphically by measuring the slope of the energy grade line along the central reach of the flume where uniform flow conditions prevailed.

CHAPTER 5

PRESENTATION OF EXPERIMENTAL RESULTS

To investigate the effect of a change in water temperature on sediment discharge near the bed, and on bed roughness three types of experiments were made: 1) Low-transport, flat-bed experiments with bed materials ranging from fine silica sand to coarse, synthetic clay-aggregate particles approximately 18.5 mm in diameter. In each of these experiments the mean bed shear stress was near the critical value for initiation of sediment movement; thus there was no suspended sediment discharge. 2) High-transport, flat-bed experiments with bed materials of fine sand in which there was considerable suspended sediment discharge. 3) A series of experiments wherein the discharge was held constant and the bed forms included ripples, dunes, and flat-bed, as defined by ASCE Task Committee on Preparation of Sedimentation Manual (1966).

In all of the experiments the mean bed shear stress was computed using the side-wall correction technique proposed by Johnson (1942), in conjunction with Eq. 5.1 for the friction factor of the channel walls.

$$f = \frac{0.324}{R^{\frac{1}{4}}} \tag{5.1}$$

where f is the Darcy-Weisbach friction factor, $R = 4Ur/\nu$, the flow Reynolds number, and r is the ratio of stream cross sectional area to

wetted perimeter, called the hydraulic radius. Eq. (5.1) was developed from clear-water experiments in the 40-ft flume.

The experiments are identified by series. In each series, with the exception of Series G, the bed material was the same for all experiments. The alphabetical order of the series refers to their chronology.

5.1 LOW-TRANSPORT, FLAT-BED EXPERIMENTS

The primary purpose of these experiments was to measure the temperature effect on sediment discharge in a flat bed regime wherein there is no suspended sediment discharge.

The experiments include those of Series B, C, D, E, and H; and experiments G-1, G-4, and G-5. Basic hydraulic data for these experiments are given in Table 5.1. With the exception of G-1, G-4, and G-5, the experiments were made in pairs. In each experiment-pair the mean velocity and depth were the same, but the two water temperatures differed by at least 15^{o}C. The warm water experiment in each pair is even numbered.

The low-transport, flat-bed experiments include flows where the condition at the bed was hydrodynamically smooth, in transition from smooth to rough, and fully rough. In this analysis the flow condition at the bed, smooth, transition, or rough is defined by the boundary Reynolds number of the bed $R_{*b} = U_{*b} D_g/\nu$, and the qualitative change in mean bed shear stress (τ_{ob}) when the water temperature is increased in a steady uniform flow of given velocity, depth, and bed material. When the boundary Reynolds number is small and τ_{ob} decreases with increase in water temperature the condition at

Table 5.1. Summary of Data, Low-Transport, Flat-Bed Experiments

Run No.	U Velocity (cm/sec)	H Depth (cm)	S_f Friction Slope	T [1] Water Temp. (°C)	g_s Sediment Discharge (gm/cm/sec x 10^8)	d_g Load Geom. Mean Size (mm)	s_g Load Geom. Std. Dev.	ρ_s Load Density (gm/cm^3)	F Froude No.	r_b Bed Hydr. Radius (cm)	f_b Bed Friction Factor	τ_{ob} Bed Shear Stress (newtons/cm^2 x 10^8)	U_{*b} Bed Shear Velocity (cm/sec)	q_{*b} Dimensionless Bed-Load Discharge (x 10^8)	τ_{*b} Shields Stress	R_{*b} Boundary Reynolds No.	$(\tau_{*b})_N$ Normalized Shields Stress	Run No.
Series B: D_g = 0.215 mm, σ_g = 1.42, ρ_s = 2.65 gm/cm^3; in 40-ft Flume																		
B-1	22.9	6.10	0.00035	21.0	2.57	0.301	1.31	2.65	0.30	4.11	0.0216	1.41	1.19	37.9	0.0405	2.61	1.08	B-1
B-2	22.9	6.10	0.00032	35.6	10.3	0.295	1.39	2.65	0.30	4.10	0.0197	1.27	1.13	159.	0.0366	3.43	1.17	B-2
B-3	21.3	6.10	0.00032	20.5	0.642	0.353	1.38	2.65	0.28	4.16	0.0230	1.30	1.14	9.86	0.0374	2.48	1.00	B-3
B-4	21.3	6.10	0.00029	36.4	1.86	0.330	1.36	2.65	0.28	4.14	0.0207	1.18	1.09	30.1	0.0335	3.34	1.07	B-4
B-5	19.8	6.10	0.00028	20.5	0.0330	- [2]	-	2.65	0.26	4.12	0.0227	1.12	1.06	0.549	0.0319	2.29	0.853	B-5
B-6	19.8	6.10	0.00025	35.6	0.124	0.365	1.31	2.65	0.26	4.10	0.0205	0.994	1.00	2.17	0.0286	3.04	0.911	B-6
Series C: D_g = 2.81 mm, σ_g = 1.11, ρ_s = 2.61 gm/cm^3; in 40-ft Flume																		
C-1	50.3	6.02	0.00326	20.6	6.50	2.98	1.09	2.60	0.65	5.03	0.0509	16.0	4.01	2.21	0.0361	114.	0.896	C-1
C-2	50.3	6.02	0.00330	35.5	1.54	2.94	1.09	2.62	0.65	5.10	0.0522	16.4	4.06	0.517	0.0368	160.	0.854	C-2
C-3	53.3	6.02	0.00365	20.5	33.9	2.98	1.08	2.60	0.69	5.03	0.0507	18.0	4.25	10.9	0.0405	121.	1.00	C-3
C-4	53.3	6.02	0.00372	34.6	17.6	2.98	1.08	2.60	0.69	5.11	0.0524	18.6	4.32	5.56	0.0416	167.	0.965	C-4
C-5	48.8	6.02	0.00308	20.5	1.46	2.97	1.08	2.63	0.63	5.02	0.0511	15.2	3.90	0.510	0.0341	111.	0.846	C-5
C-6	48.8	6.02	0.00309	35.4	0.672	2.99	1.09	2.66	0.63	5.09	0.0519	15.3	3.93	0.223	0.0344	155.	0.798	C-6
Series D: D_g = 18.5 mm, σ_g = 1.16, ρ_s = 1.37 gm/cm^3; in 40-ft Flume																		
D-11	50.3	6.10	0.00568	20.9	- [3]	19.3	1.06	1.28	0.65	5.46	0.0962	30.3	5.51	-	0.0449	1041.	-	D-11
D-12	50.3	6.10	0.00598	35.8	-	19.3	1.07	1.28	0.65	5.52	0.1025	32.2	5.69	-	0.0471	1487.	-	D-12
D-13	50.3	6.10	0.00567	20.9	-	19.8	1.06	1.27	0.65	5.45	0.0960	30.3	5.51	-	0.0448	1040.	-	D-13
D-14	50.3	6.10	0.00580	35.7	-	18.9	1.06	1.28	0.65	5.51	0.0991	31.2	5.60	-	0.0456	1460.	-	D-14
D-15	50.3	6.10	0.00559	20.7	-	18.8	1.07	1.26	0.65	5.45	0.0945	29.6	5.47	-	0.0442	1027.	-	D-15
D-16	50.3	6.10	0.00596	35.4	-	19.1	1.06	1.28	0.65	5.52	0.1021	32.2	5.68	-	0.0470	1473.	-	D-16
Series E: D_g = 3.95 mm, σ_g = 1.13, ρ_s = 2.61 gm/cm^3; in 60-ft Flume																		
E-1	68.6	18.3	0.00159	26.6	- [3]	4.15	1.13	2.50	0.51	15.8	0.0419	24.5	4.96	-	0.0393	228.	-	E-1
E-2	68.6	18.3	0.00157	41.0	-	4.13	1.12	2.46	0.51	15.9	0.0416	24.3	4.95	-	0.0387	305.	-	E-2
E-5	70.1	18.3	0.00163	26.1	-	4.11	1.11	2.47	0.52	15.7	0.0410	25.1	5.02	-	0.0401	228.	-	E-5
E-6	70.1	18.3	0.00161	41.1	-	4.10	1.12	2.42	0.52	15.9	0.0408	24.9	5.01	-	0.0396	309.	-	E-6
G-1: D_g = 0.357 mm, σ_g = 1.23, ρ_s = 2.65 gm/cm^3; in 40-ft Flume																		
G-1	22.9	6.06	0.00039	22.0	0.659	0.452	1.09	2.65	0.30	4.26	0.0250	1.63	1.28	5.46	0.0281	4.77	-	G-1
G-4: D_g = 0.191 mm, σ_g = 1.26, ρ_s = 2.65 gm/cm^3; in 40-ft Flume																		
G-4	22.9	6.06	0.00030	63.0	22.9	0.252	1.14	2.65	0.30	4.15	0.0187	1.21	1.11	409.	0.0384	4.73	-	G-4
G-5: D_g = 0.248 mm, σ_g = 1.27, ρ_s = 2.65 gm/cm^3; in 40-ft Flume																		
G-5	20.4	6.06	0.00027	49.0	0.308	0.329	1.16	2.65	0.26	4.21	0.0214	1.11	1.06	4.44	0.0273	4.71	-	G-5
Series H: D_g = 1.07 mm, σ_g = 1.14, ρ_s = 2.65 gm/cm^3; in 40-ft Flume																		
H-1	30.5	6.10	0.00081	22.0	0.991	1.16	1.10	- [2]	0.39	4.59	0.0314	3.64	1.91	1.86	0.0215	21.4	0.915	H-1
H-2	30.5	6.10	0.00084	42.0	0.675	1.17	1.09	-	0.39	4.75	0.0337	3.89	1.98	1.22	0.0228	33.6	0.891	H-2
H-3	33.5	6.10	0.00098	22.0	42.1	1.16	1.10	2.62	0.43	4.62	0.0316	4.44	2.11	71.5	0.0262	23.6	1.12	H-3
H-4	33.5	6.10	0.00102	42.0	23.0	1.15	1.10	2.62	0.43	4.78	0.0340	4.76	2.19	37.7	0.0279	37.2	1.09	H-4
H-5	32.0	6.10	0.00090	22.0	8.25	1.18	1.10	2.60	0.41	4.61	0.0318	4.07	2.02	14.6	0.0240	22.6	1.02	H-5
H-6	32.0	6.10	0.00093	42.0	4.98	1.16	1.09	2.61	0.41	4.77	0.0340	4.33	2.09	8.56	0.0254	35.5	0.992	H-6

[1] Temperature variations during each experiment was less than ±1°C, except in E-1 and E-5 where it was ±3°C.

[2] Sample too small for analysis.

[3] Equilibrium sediment discharge could not be measured.

the bed is described as hydrodynamically smooth. At intermediate values of R_{*b}, if τ_{ob} increases with increase in water temperature the bed flow is in transition from smooth to rough; and with large values of R_{*b} where τ_{ob} does not change with increase in temperature the flow condition at the bed is termed hydrodynamically rough.

In pipes artificially roughened with uniform sand grains it has been found (e. g. Rouse (1937)) that hydrodynamically smooth conditions obtain when the boundary Reynolds number ($R_* = U_* D_s/\nu$, where $U_* = \sqrt{\tau_o/\rho}$, τ_o is mean pipe shear stress, and D_s is mean sieve size of the sand grains) is less than a value near 10. For R_* larger than 10 but less than approximately 100 the flow is in transition according to the criteria previously outlined; and when R_* is larger than 100 flow is hydrodynamically rough.

Smooth bed conditions prevailed in the six fine sand experiments of Series B. The sediment discharge (g_s) and computed mean bed shear stress (τ_{ob}) for these experiments are plotted as functions of mean velocity and water temperature in Fig. 5. 1. In each experiment-pair the sediment discharge with warm water was from three to five times larger than that with cold water. However in each case the mean bed shear stress was smaller in the warm water flow.

In Series H and C the flows were in transition from smooth to rough. The bed materials were coarse sand and fine gravel respectively. Sediment discharge and mean bed shear stress

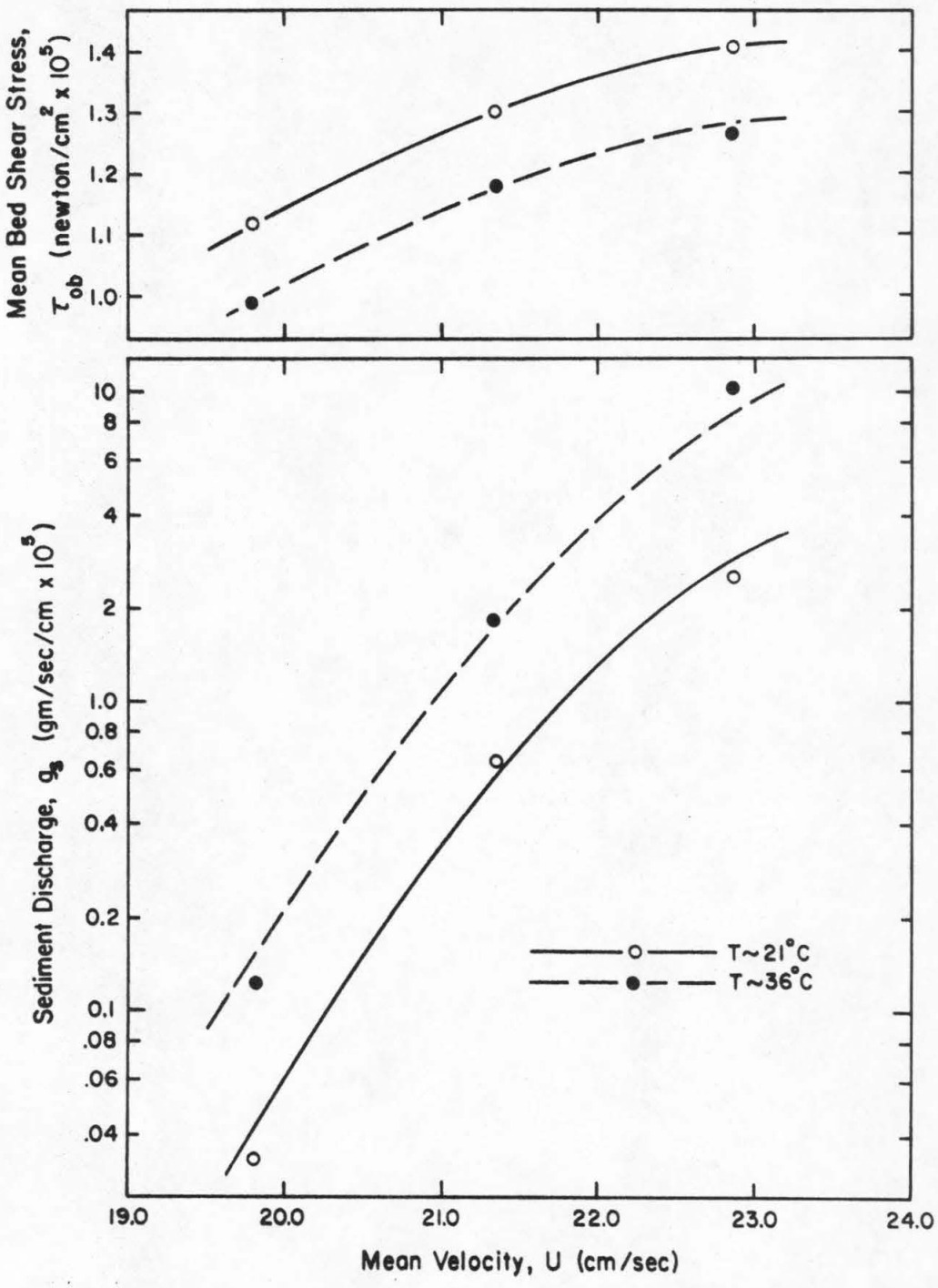

Fig. 5.1. Variation in τ_{ob} and g_s with velocity and water temperature for experiments of Series B. In each experiment H = 6.10 cm; and the bed material was fine, silica sand (D_g = 0.215 mm, σ_g = 1.42).

are plotted in Figs. 5.2 and 5.3 as functions of velocity and water temperature for the experiments of these two series. In each of the six experiment-pairs the sediment discharge was significantly smaller but the mean bed shear stress was larger in the warm water experiment.

These results indicate that the effect of an increase in water temperature on sediment discharge in a regime where the flow is in hydrodynamic transition is qualitatively opposite to the corresponding temperature effect in a smooth regime, under low-transport, flat-bed conditions.

In the experiments of Series C the boundary Reynolds numbers ($R_{*b} = U_{*b}D_g/\nu$) were larger than 100 but hydrodynamically rough flow was not obtained, as evidenced by the consistently larger mean bed shear stresses in the warm water experiments. These results suggest that in a flat bed regime fully-rough flow is first attained at a larger boundary Reynolds number than that required for fully-rough flow in pipes artificially roughened with uniform sand grains.

The small variation in mean bed shear stress with change in water temperature, and the relatively large boundary Reynolds numbers in the experiment-pairs of Series E and D (Table 5.1) indicate that in these experiments conditions at the bed closely approached those for fully-rough flow.

Sediment discharge is plotted as a function of experiment duration for the four experiments of Series E and the six experiments of Series D in Figs. 5.4 and 5.5, respectively. The five experiment-

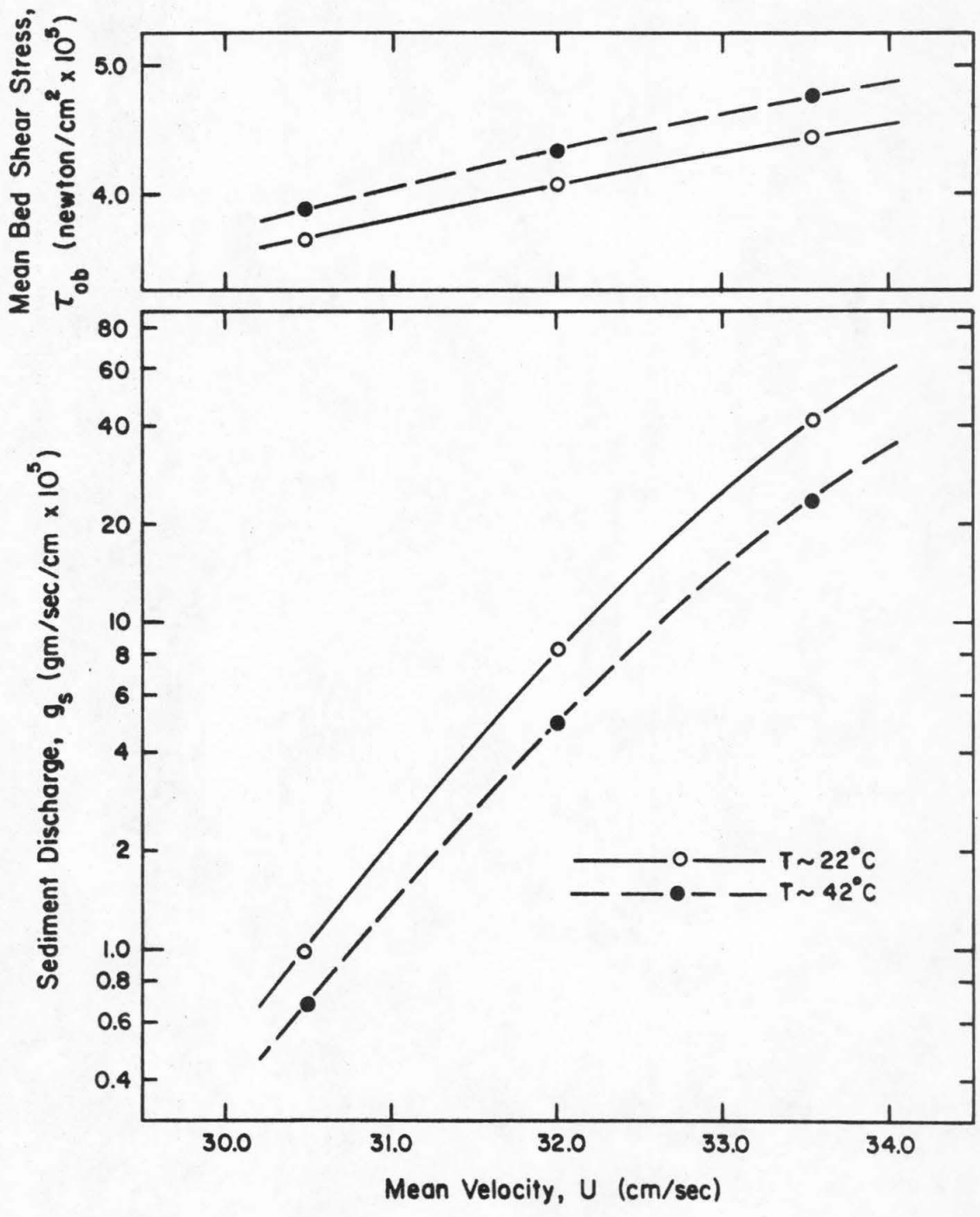

Fig. 5.2. Variation in τ_{ob} and g_s with velocity and water temperature for the experiments of Series H. In each experiment H = 6.10 cm; and the bed material was coarse sand (D_g = 1.07 mm, σ_g = 1.14, ρ_s = 2.61 gm/cm^3).

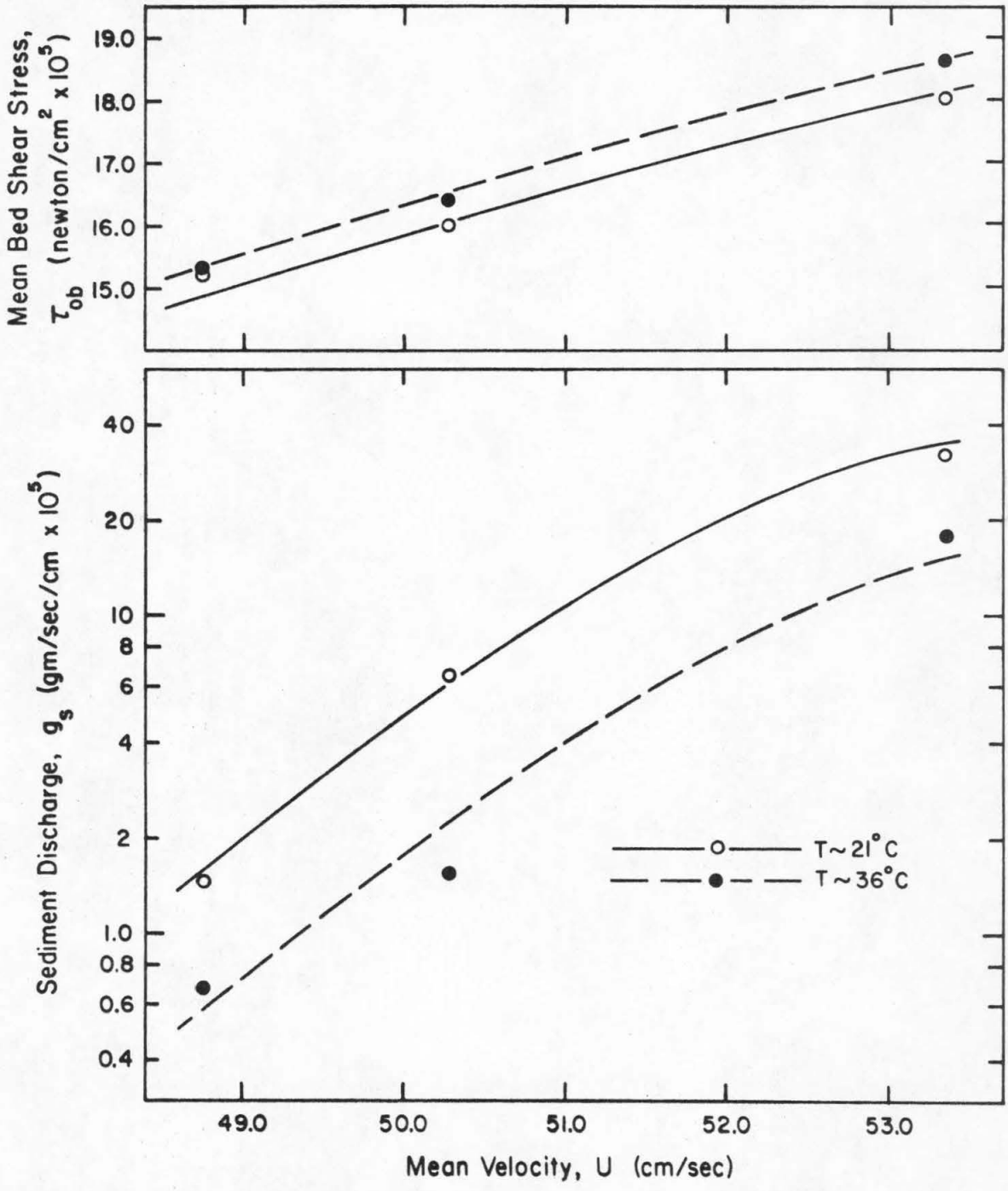

Fig. 5.3. Variation in τ_{ob} and g_s with velocity and water temperature for the experiments of Series C. In each experiment H = 6.02 cm; and the bed material was fine gravel (D_g = 2.81 mm, σ_g = 1.11, ρ_s = 2.61 gm/cm^3).

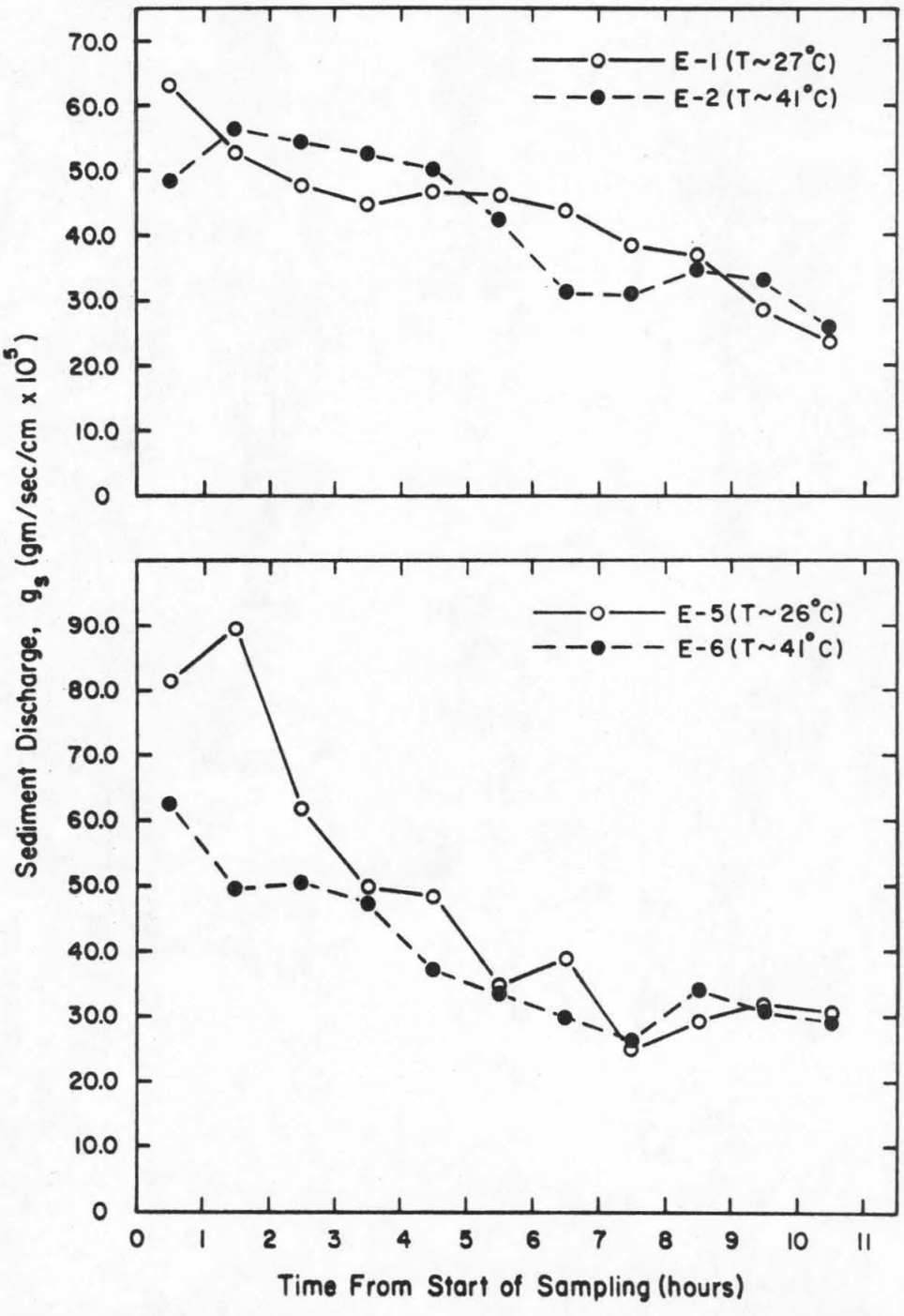

Fig. 5.4. Variation in g_s with run time and water temperature for experiments of Series E. In experiments E-1 and E-2 U = 68.6 cm/sec; and in E-5 and E-6 U = 70.1 cm/sec. In each experiment H = 18.3 cm; and the bed material was fine gravel (D_g = 3.95 mm, σ_g = 1.13, ρ_s = 2.61 gm/cm^3).

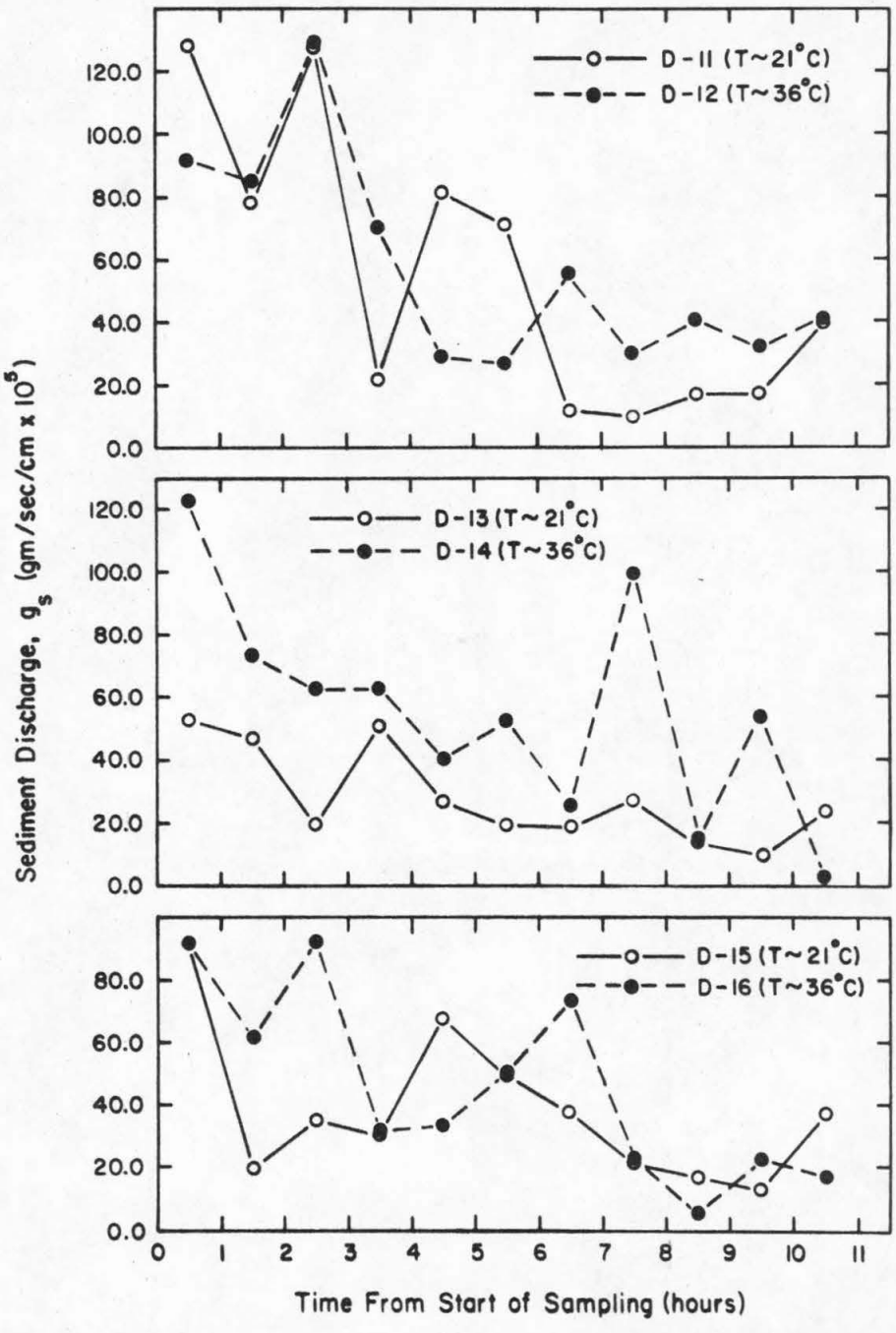

Fig. 5.5. Variation in g_s with run time and water temperature for the experiments of Series D. In each experiment U = 50.3 cm/sec and H = 6.10 cm; and the bed material was coarse clay-aggregate (D_g = 18.5 mm, σ_g = 1.16, ρ_s = 1.37 gm/cm^3).

pairs exhibit no characteristic difference in sediment discharge between the cold and warm water flows, thus indicating that in a low-transport, flat-bed regime with a hydrodynamically rough bed, sediment discharge does not depend on water temperature.

In each of the experiment-pairs of Series E and D the sediment discharge continually decreased during the period of measurement. It is felt that the variation in particle density in the bed materials of Series E and D as evidenced by the differences between load density and bed material density (see Table 5.1), produced bed armoring in these experiments; and that as this armoring progressed sediment discharge was reduced. Such armoring was not observed in any of the other low-transport, flat-bed experiments.

The data from Series B, C, D, E, and H indicate that in a low-transport, flat-bed flow where the velocity and depth are kept constant an increase in water temperature will produce a new equilibrium condition, i.e. sediment discharge, friction slope, and mean bed shear stress. The nature of the change in sediment discharge depends on the flow condition at the bed. Under hydrodynamically smooth conditions an increase in water temperature produced an increase in sediment discharge. In the transition from smooth to rough flow an increase in water temperature reduced sediment discharge; and when fully-rough flow obtained at the bed it was observed that an increase in water temperature had no effect on sediment discharge. These results are summarized in Fig. 5.6. The temperature effects on sediment

discharge predicted by the Einstein bed-load function (Section 2.3.2) for uniform bed material are qualitatively the same as those given in Fig. 5.6.

Temperature Effect On: / Flow Condition at Bed:	Sediment Discharge	Mean Bed Shear Stress
Hydrodynamically Smooth (Series B)	Increases as water temperature increases	Decreases as water temperature increases
Transition from Smooth to Rough (Series H and C)	Decreases as water temperature increases	Increases as water temperature increases
Hydrodynamically Rough (Series E and D)	No change with temperature increase	No change with temperature increase

Fig. 5.6 The Effect of Water Temperature on Sediment Discharge and Mean Shear Stress in a Flow of Low Sediment Transport Rate Over a Flat Bed.

5.1.1 Bed-Load Discharge Hypothesis

In a wide, flat bed alluvial channel wherein the flow is steady and uniform, neglecting the effects of surface tension the dynamic flow conditions are uniquely specified by the following parameters: mean bed shear stress, bed slope (S_b), dynamic viscosity

of the water (μ), fluid density, geometric mean size of the bed material, geometric standard deviation of bed material sizes; and particle shape factor (S. F.), density, and buoyant specific weight ($\gamma_s - \gamma$) where γ_s is the specific weight of the bed sediment, and γ is the specific weight of the water. Then volumetric sediment discharge per unit width on and near the bed, q_{sb} (bed-load discharge), must be a function of these variables and can be written,

$$q_{sb} = \varphi(\tau_{ob}, S_b, \mu, \rho, D_g, \sigma_g, \text{S. F.}, \rho_s, \gamma_s - \gamma) \qquad (5.2)$$

where $\varphi(\,)$ indicates a functional relation of the included variables. Bed slope affects particle transport by altering the gravitational forces which enhance and retard particle movement. In flat-bed regimes the bed slope is small and its influence on bed-load discharge may be neglected; and Eq. (5.2) is reduced to

$$q_{sb} = \varphi(\tau_{ob}, \mu, \rho, D_g, \sigma_g, \text{S. F.}, \rho_s, \gamma_s - \gamma) \qquad (5.3)$$

Using the Buckingham-Pi Theorem Eq. (5.3) can be non-dimensionalized as follows:

$$q_{*b} = \varphi(R_{*b}, \tau_{*b}, \frac{\rho_s}{\rho}, \sigma_g, \text{S. F.}) \qquad (5.4)$$

where

$$q_{*b} = \frac{q_{sb}}{U_{*b} D_g}$$

$$R_{*b} = \frac{U_{*b} D_g}{\nu}$$

the Shields stress $\tau_{*b} = \tau_{ob} / (\gamma_s - \gamma) D_g$, and the bed shear velocity is defined as $U_{*b} = \sqrt{\tau_{ob} / \rho}$.

Eq. (5.4) indicates that for given values of σ_g, ρ_s/ρ, and S. F., q_{*b} can be expressed as a function of R_{*b} and τ_{*b}. This transport function can be plotted by locating lines of constant q_{*b} on a two-dimensional graph with R_{*b} as the abscissa and τ_{*b} as the ordinate. In Fig. 5.7 the data from Series B, C, D, E, and H, and experiments G-1, G-4, and G-5 wherein the sediment discharge was all bed load, have been plotted on such a graph. The curve marked "Shields Curve" in Fig. 5.7 was fitted to Shields' (1936) data for incipient particle transport by Rouse (1939).

The experiment-pairs in each series are identified in Fig. 5.7 by the same data symbol. The q_{*b} contours of Series D and E are not quantitatively identified, because in these experiments an equilibrium sediment discharge could not be measured.

Fig. 5.7 is actually eight plots as defined above; for each of the eight bed materials used had a different σ_g. However in Series C and H, and experiments G-1, G-4, and G-5 the differences in σ_g, and particle density and shape are small and may be neglected. Thus Fig. 5.7 includes q_{*b} contours from four sets of ρ_s/ρ, σ_g, and S. F.

Fig. 5.7 affords a systematic presentation of the temperature effects described in Section 5.1. As shown in this plot in the experiment-pairs of Series B the boundary Reynolds numbers were small; and in each case an increase in water temperature effected a reduction in mean bed shear stress and τ_{*b}, but a large increase in absolute and dimensionless bed-load discharge. In Series H and C the values

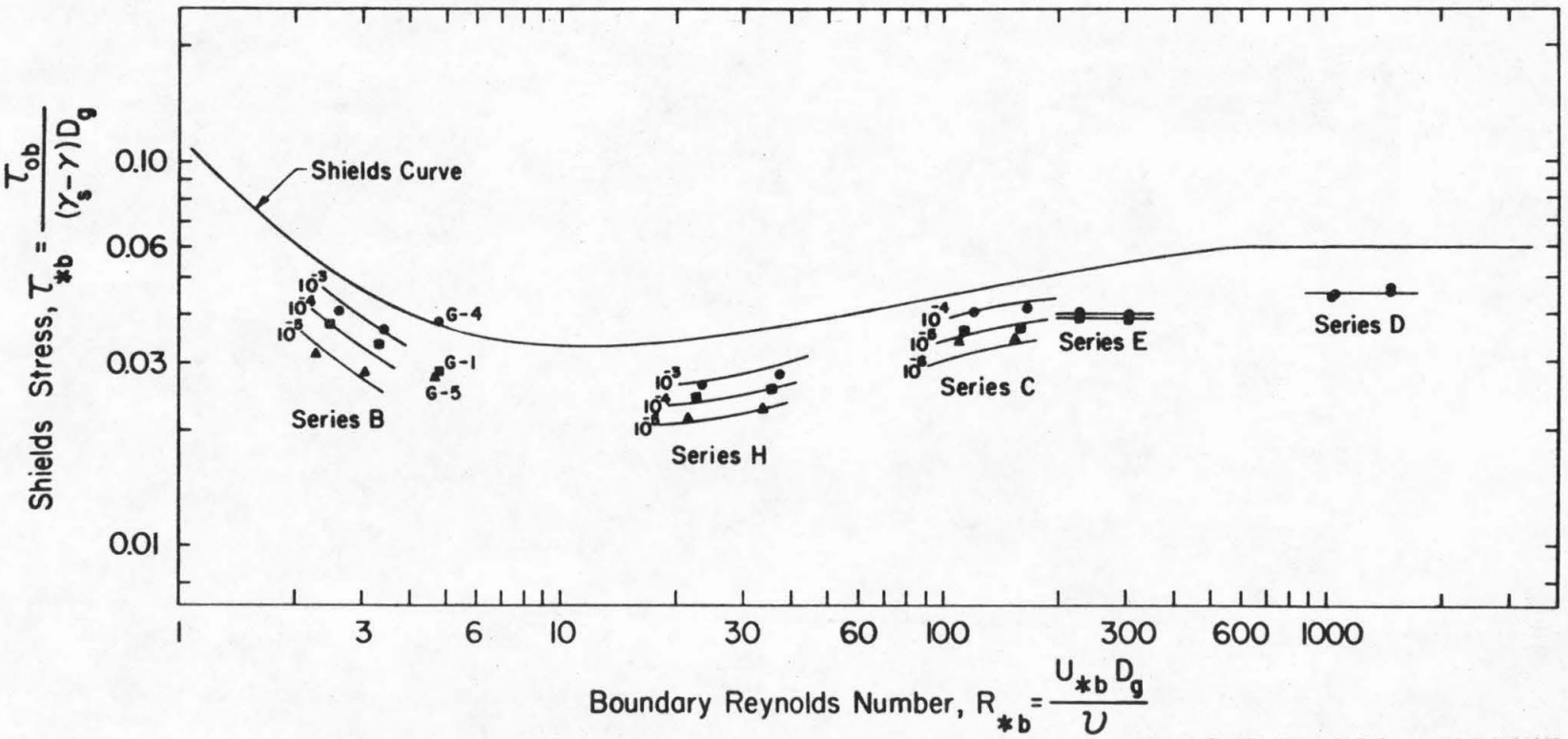

Fig. 5.7. Contours of dimensionless sediment discharge (q_{*b} = constant) versus τ_{*b} and R_{*b} for low-transport, flat-bed experiments. Numbers near the ends of the contours are values of q_{*b}. In each series the data points with the higher values of R_{*b} are for warm water; and constant velocity and depth experiment-pairs are indicated by the same data symbol.

of R_{*b} ranged from 21.4 to 167; and in the experiment-pairs of these series an increase in water temperature caused a small increase in the mean bed shear stress, but a significant decrease in sediment discharge and q_{*b}. Fig. 5.7 illustrates that with the large boundary Reynolds numbers of Series E and D hydrodynamically rough flow conditions were obtained, and there were no characteristic changes in mean bed shear stress or in sediment discharge with increase in water temperature.

The q_{*b} contours of Series B, C, and H in Fig. 5.7 illustrate the relatively large changes in sediment discharge that are produced by small changes in mean bed shear stress. With each bed material, at a given water temperature a 10% to 20% increase in τ_{ob} is accompanied by a 100% to 1000% increase in sediment discharge.

Eq. (5.4) indicates that a change in water temperature may alter bed-load discharge by effecting changes in the dynamic bed parameters R_{*b} and τ_{*b}; and that if the independent parameters in this equation are matched in flows satisfying the assumptions in its development, q_{*b} will have the same value in each case regardless of differences that may exist in water temperature.

Experiments G-1, G-4, and G-5 were made in an attempt to test the hypothesis expressed in Eq. (5.4). Hydraulic data for these experiments are summarized in Table 5.2. The bed materials used in the experiments came from a well-graded, naturally-worn silica sand that had been separated by fall velocity to produce several well-sorted size fractions. For a more complete description of the separation process see Appendix B.

Table 5.2 Data from Low-Transport, Flat-Bed Experiments With Well-Sorted, Naturally-Worn Silica Wherein Bed-Load Discharge Hypothesis was Tested.

Run No.	T Water Temperature (^{o}C)	τ_{*b} Shields Stress	R_{*b} Boundary Reynolds No.	q_{*b} Dimensionless Sed. Discharge ($\times 10^{5}$)
G-1	22.0	0.0281	4.77	5.46
G-4	63.0	0.0384	4.73	409.
G-5	49.0	0.0273	4.71	4.44

In experiments G-1 and G-4 the boundary Reynolds numbers were matched to within 1%. However in G-4 the Shields stress was 37% larger and q_{*b} was seventy-five times larger than in G-1.

By adjusting the velocity and water temperature in G-5 the values of R_{*b} and τ_{*b} in this experiment were matched to within 3% of the corresponding values in G-1, and q_{*b} was 0.81 times that measured in G-1. This difference in dimensionless bed-load discharge between experiments G-1 and G-5 can be explained by the respective differences in R_{*b} and τ_{*b}. Both parameters were slightly larger in experiment G-1, and in low-transport, hydrodynamically-smooth flows a small increase in these parameters will produce a relatively large increase in the dimensionless bed-load discharge.

Experiments G-1 and G-5 indicate that the hypothesis expressed in Eq. (5.3) is correct under the conditions assumed in its development.

Thus the effect of water temperature on bed-load discharge can be expressed in terms of R_{*b} and τ_{*b}, in a low-transport, flat-bed regime.

The results from experiments G-1 and G-4 illustrate the primary importance of τ_{*b} in Eq. (5.3), for low-transport flows. The experimental-pairs of Series B indicate that R_{*b} is also of importance in this equation. In Series B if τ_{*b} had been matched in each experimental-pair by increasing the mean velocity in the warm water flows the relative increase in sediment discharge with increase in water temperature in these experiments would have been even larger. Thus it was the 30% increase in R_{*b} that produced the several-fold increase in sediment discharge in the warm water flow of each experiment-pair in Series B.

5.1.2 Low-Transport, Flat-Bed Sediment Discharge Function

In Eq. (5.4) if R_{*b} is multiplied by R_{*b}/τ_{*b} and the product is raised to the 1/2 power, the dimensionless bed-load discharge function becomes

$$q_{*b} = \varphi(\tau_{*b},\ R_{\mu},\ \frac{\rho_s}{\rho},\ \sigma_g,\ \text{S. F.}) \qquad (5.5)$$

where

$$R_{\mu} = \frac{D_g^{3/2}}{\nu}\sqrt{g\left(\frac{\gamma_s-\gamma}{\gamma}\right)} \quad .$$

For a given bed material and water temperature Eq. (5.5) is reduced to

$$q_{*b} = \varphi(\tau_{*b}) \tag{5.6}$$

Eq. (5.6) may be normalized as follows,

$$\frac{q_{*b}}{q_{*b} = 10^{-4}} = \varphi\left[\frac{\tau_{*b}}{\tau_{*b}(q_{*b} = 10^{-4})}\right] \tag{5.7}$$

where $\tau_{*b}(q_{*b} = 10^{-4})$ is the value of τ_{*b} corresponding with $q_{*b} = 10^{-4}$ for a given bed material and water temperature.

In Fig. 5.8 Eq. (5.7) has been plotted for six values of R_μ using data from Series B, C, and H. The value of $\tau_{*b}(q_{*b} = 10^{-4})$ was determined in each case by a graphic interpolation of the dimensionless discharge function (Eq. 5.6) defined by the data.

The data plotted in Fig. 5.8 indicate that the normalized, dimensionless bed-load discharge function is approximately the same for all six values of R_μ. The small deviations from the straight line fitted to the data are not systematic, thus suggesting that these variations are the result of experimental error.

The straight-line fit of the data in Fig. 5.8 indicates that over the range of flow conditions of the experiments in Series B, C, and H the normalized bed-load discharge function can be closely approximated by the relation

$$(q_{*b})_N = (\tau_{*b})_N^{17.5} \tag{5.8}$$

where the subscript N denotes normalized parameters.

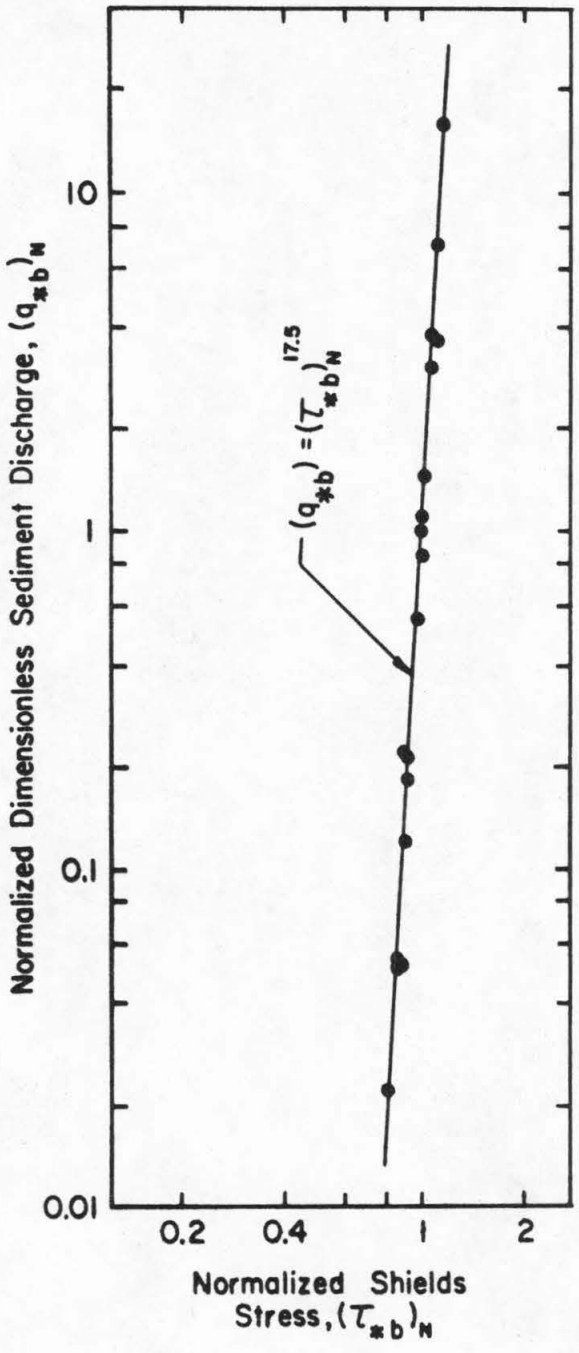

Fig. 5.8. Normalized dimensionless sediment discharge versus normalized Shields stress for the experiments of Series B, H, and C. In each experiment H ~ 6 cm; and the bed materials included fine sand (D_g = 0.215 mm, σ_g = 1.42), coarse sand (D_g = 1.07 mm, σ_g = 1.14), and fine gravel (D_g = 2.81 mm, σ_g = 1.11).

The experimental results presented in Fig. 5.8 suggest that for naturally-worn, silica particles the normalized, dimensionless bed-load discharge function is approximately the same for different values of D_g, σ_g, and different hydrodynamic flow conditions at the bed in low-transport, flat-bed flows.

5.1.3 Sediment Discharge Sorting in Low-Transport, Flat-Bed Experiments

The variations in particle size, shape, and density in the bed materials used in the low-transport, flat-bed experiments produced transport "sorting". In each experiment the physical characteristics of the load were different from those of the bed material. According to the development of Eq. (5.4) the load characteristics may also be expressed as a function of the independent parameters in this equation. Thus the geometric mean size of the load (d_g), and the geometric standard deviation of load sizes (s_g) can be written,

$$\frac{d_g}{D_g} = \varphi(R_{*b},\ \tau_{*b},\ \frac{\rho_s}{\rho},\ \sigma_g,\ \text{S. F.}) \tag{5.8}$$

and

$$s_g = \varphi(R_{*b},\ \tau_{*b},\ \frac{\rho_s}{\rho},\ \sigma_g,\ \text{S. F.}) \tag{5.9}$$

If it is assumed that for bed materials of given density and shape in a low-transport, flat-bed regime, the physical characteristics of the load are independent of flow conditions and depend only on the physical characteristics of the bed materials Eqs. (5.8) and (5.9) are reduced to

$$\frac{d_g}{D_g} = \varphi(\sigma_g) \tag{5.10}$$

$$s_g = \varphi(\sigma_g) \tag{5.11}$$

In Series B, C, and H and experiments G-1, G-4, and G-5 the bed materials were naturally-worn silica. Therefore in these experiments according to Eqs. (5.10) and (5.11) the differences in d_g/D_g and s_g must be the result of variations in σ_g. In the twenty experiments analyzed (see Table 5.3) it was found that d_g/D_g and s_g could be expressed as

$$\frac{d_g}{D_g} = C_1\sigma_g \tag{5.12}$$

and

$$s_g = C_2\sigma_g \tag{5.13}$$

where $C_1 = 1.00 \pm 5\%$ over 80% of the data, and $C_2 = 0.96 \pm 5\%$ for 90% of the data. The total sample mass collected in each experiment is also given in Table 5.3. These values indicate the relatively large variation in sample size among the different experiments; and show that C_1 and C_2 did not vary in a consistent way with sample size.

These results indicate that in a low-transport, flat-bed flow with a bed material of naturally-worn silica d_g and s_g are only very weakly dependent on flow conditions, i.e., on R_{*b}, and τ_{*b}; and their values can be predicted from D_g and σ_g.

Table 5.3 Sediment Discharge Sorting Constants for Low-Transport, Flat-Bed Experiments with Naturally-Worn Silica.

Run No.	Sample Mass (gm)	d_g Load Geom. Mean Dia. (mm)	s_g Load Geom. Std. Dev.	C_1 $\left(\frac{d_g}{D_g}\right)\frac{}{\sigma_g}$	C_2 $\frac{s_g}{\sigma_g}$
Bed Sediment: D_g = 0.215 mm, σ_g = 1.42					
B-1	154.	0.301	1.31	1.01	0.94
B-2	46.6	0.295	1.39	0.99	1.00
B-3	9.53	0.353	1.38	1.18	0.99
B-4	20.0	0.330	1.36	1.10	0.98
B-6	9.67	0.365	1.31	1.22	0.94
Bed Sediment: D_g = 2.81 mm, σ_g = 1.11					
C-1	112.	2.98	1.09	0.95	0.98
C-2	26.6	2.94	1.09	0.95	0.98
C-3	195.	2.98	1.08	0.95	0.97
C-4	101.	2.98	1.08	0.95	0.97
C-5	43.7	2.97	1.08	0.95	0.97
C-6	28.6	2.99	1.09	0.95	0.98
Bed Sediment: D_g = 0.357 mm, σ_g = 1.23					
G-1	5.06	0.452	1.09	1.03	0.89
Bed Sediment: D_g = 0.191 mm, σ_g = 1.26					
G-4	11.0	0.252	1.14	1.05	0.90
Bed Sediment: D_g = 0.248 mm, σ_g = 1.27					
G-5	2.38	0.329	1.16	1.05	0.91
Bed Sediment: D_g = 1.07 mm, σ_g = 1.14					
H-1	7.34	1.16	1.10	0.95	0.96
H-2	4.89	1.17	1.09	0.96	0.96
H-3	121.	1.16	1.10	0.95	0.96
H-4	63.3	1.15	1.10	0.94	0.96
H-5	31.6	1.18	1.10	0.96	0.96
H-6	19.1	1.16	1.09	0.95	0.96
			Mean Value:	1.00	0.96

For example, the data in Table 5.3 suggest that in hydrodynamically smooth flows (Series B, G-1, G-4, and G-5) C_1 is slightly larger than in the transition regimes (Series H and C).

5.2 HIGH-TRANSPORT, FLAT-BED EXPERIMENTS

The primary purpose of these experiments was to determine the effect of a change in water temperature on bed-load discharge in high-transport, flat-bed flows.

The high-transport experiments with flat beds include experiment-pairs F-23, F-24; F-27, F-28; and G-9, G-10. Basic hydraulic data for these experiments are given in Table 5.4. In each experiment-pair the mean velocity and depth were approximately the same, but the water temperature was 15°C higher in one experiment than in the other. The bed materials in these experiments were fine sands.

In each of the three experiment-pairs the warm water sediment discharge was slightly larger than the cold water sediment discharge.

The relatively broad spectrum of particle sizes in experiments F-23, F-24, F-27, and F-28 made it possible to separate the samples of sediment discharged through the flume into size fractions and thereby to determine the temperature effect on sediment discharge for several well-sorted size fractions. The sediment discharges for these size fractions are given in Table 5.5. In this tabulation each size fraction is identified by its geometric mean size. The geometric standard deviation of each size fraction is approximately 1.10.

Table 5.4. Summary of Data, High-Transport, Flat-Bed Experiments

Run No.	U Velocity (cm/sec)	H Depth (cm)	S_f Friction Slope	T [1] Water Temp. (^oC)	g_s Sediment Discharge (gm/cm/sec x 10^5)	d_g Load Geom. Mean Size (mm)	s_g Load Geom. Std. Dev.	p_s Load Density (gm/cm^3)	F Froude No.	r_b Bed Hydr. Radius (cm)	f_b Bed Friction Factor	U_{*b} Bed Shear Velocity (cm/sec)	τ_{*b} Shields Stress	R_{*b} Boundary Reynolds No.	U_{*cl} [2] Shear Vel. Along Centerline (cm/sec)	K Karman Constant
Series F: D_g = 0.228 mm, σ_g = 1.52, ρ_s = 2.65 gm/cm^3; in 60-ft Flume																
F-23	69.2	8.06	0.00205	23.0	89.9	0.181	1.44	2.65	0.78	7.12	0.0240	3.79	0.387	9.26	4.03	0.380
F-24	70.7	7.88	0.00208	38.0	92.7	0.162	1.50	2.65	0.80	7.01	0.0229	3.78	0.384	12.7	4.01	0.409
F-27	86.6	11.4	0.00198	24.5	263.	0.196	1.46	2.65	0.82	9.54	0.0198	4.30	0.500	10.9	4.70	0.348
F-28	87.8	11.2	0.00199	38.9	279.	0.185	1.43	2.65	0.84	9.48	0.0193	4.31	0.497	14.7	4.68	0.368
G-9, G-10: D_g = 0.138 mm, σ_g = 1.25, ρ_s = 2.65 gm/cm^3; in 40-Flume																
G-9	58.5	7.83	0.00187	48.0	55.3	0.142	1.20	2.65	0.67	5.60	0.0240	3.21	0.452	7.82	3.79	0.421
G-10	58.5	7.83	0.00191	33.0	53.0	0.141	1.21	2.65	0.67	5.51	0.0241	3.21	0.458	5.92	3.83	0.413

[1] Temperature variation during each experiment was less than $\pm 1^oC$.

[2] Computed as $\sqrt{gHS_f}$

Table 5.5. Summary of Concentration Profile Data For Different Size Fractions in Flat-Bed Experiment-Pairs F-23, F-24; F-27, F-28; and G-9, G-10

Run No.	d_s Geom. Mean Size of Fraction (mm)	g_s Sediment Discharge (gm/cm/sec x 10^6)	$\frac{g_s \text{ warm}}{g_s \text{ cold}}$ Sediment Discharge Ratio	R_{*b} Boundary Reynolds No.	Z Exponent Defined in Eq. (2.3)	w_s [1] Still-Water Particle Fall Velocity (cm/sec)
F-23	0.081	1.72	1.84	3.29	0.431	0.69
F-24	0.081	3.17		4.52	0.552	0.87
F-23	0.096	1.40	1.79	3.90	0.548	0.91
F-24	0.096	2.50		5.36	0.652	1.14
F-23	0.114	6.12	1.37	4.63	0.746	1.19
F-24	0.114	8.41		6.36	0.873	1.49
F-23	0.135	10.4	1.15	5.48	0.900	1.52
F-24	0.135	12.0		7.53	1.15	1.86
F-23	0.160	24.7	1.08	6.50	1.22	1.94
F-24	0.160	26.6		8.93	1.46	2.32
F-23	0.191	13.3	0.80	7.76	1.41	2.47
F-24	0.191	10.6		10.7	1.95	2.93
F-23	0.226	18.7	0.88	9.18	2.06	3.05
F-24	0.226	16.4		12.6	2.41	3.54
F-23	0.269	10.5	0.80	10.9	-	-
F-24	0.269	8.42		15.0	-	-
F-23	0.322	6.36	0.87	13.1	-	-
F-24	0.322	5.52		18.0	-	-
F-23	0.384	3.13	0.87	15.6	-	-
F-24	0.384	2.71		22.4	-	-
F-23	0.454	1.82	0.84	18.4	-	-
F-24	0.454	1.52		25.3	-	-
F-27	0.081	2.68	1.92	3.87	0.361	0.70
F-28	0.081	5.15		5.24	0.508	0.88
F-27	0.096	2.96	1.15	4.59	0.535	0.92
F-28	0.096	3.39		6.21	0.622	1.15
F-27	0.114	14.6	1.21	5.45	0.642	1.21
F-28	0.114	17.6		7.37	0.816	1.50
F-27	0.135	28.9	1.14	6.45	0.846	1.54
F-28	0.135	33.0		8.72	1.08	1.87
F-27	0.160	57.0	1.12	7.65	1.05	1.96
F-28	0.160	64.1		10.3	1.33	2.33
F-27	0.191	31.9	1.12	9.13	1.29	2.50
F-28	0.191	35.7		12.3	1.62	2.94
F-27	0.226	45.3	1.07	10.8	1.59	3.10
F-28	0.226	48.3		14.6	2.14	3.55
F-27	0.269	31.2	0.98	12.9	2.04	3.80
F-28	0.269	30.7		17.4	2.77	4.38
F-27	0.322	22.1	0.85	15.4	2.70	4.80
F-28	0.322	18.9		20.8	3.21	5.36
F-27	0.384	14.1	0.68	18.4	-	-
F-28	0.384	9.63		24.8	-	-
F-27	0.454	9.91	0.52	21.7	-	-
F-28	0.454	5.15		29.3	-	-
G-9	0.138	55.3	1.04	7.82	1.54	2.15
G-10	0.138	53.0		5.92	1.23	1.87

[1] From ASCE Task Committee on Preparation of Sedimentation Manual (1962).

In experiments F-23 and F-24 for size fractions finer than 0.191 mm the warm water sediment discharge was significantly larger than the cold water sediment discharge. Whereas for size fractions coarser than 0.160 mm the cold water sediment discharges were larger.

The sediment discharge data from experiments F-27 and F-28, also presented in Table 5.5, provide similar results. For each size fraction finer than 0.269 mm the sediment discharges in the warm water flow were larger; but with the four coarsest size fractions the cold water sediment discharges were larger.

Sediment concentration profile measurements were made along the flume centerline at station 10.0 (11.2 meters below the upstream end of the 60-ft flume) in experiments F-23 and F-24 and at flume station 12.0 (13.2 meters below the upstream end of the 60-ft flume) in experiments F-27 and F-28. These concentration profiles are helpful in interpreting the contrary temperature effects on sediment discharge that were observed among the different size fractions.

The cold and warm water concentration profiles measured in experiments F-23 and F-24 are plotted for seven size fractions in Figs. 5.9 to 5.12. The size-fraction samples finer than 0.081 mm and coarser than 0.226 mm were very small, and therefore the concentration profiles for these size fractions were not considered.

For size fractions 0.081 mm, 0.096 mm, and 0.114 mm (Figs. 5.9 and 5.10) the measured concentrations in the warm water flow are larger at each elevation than those in the cold water experiment.

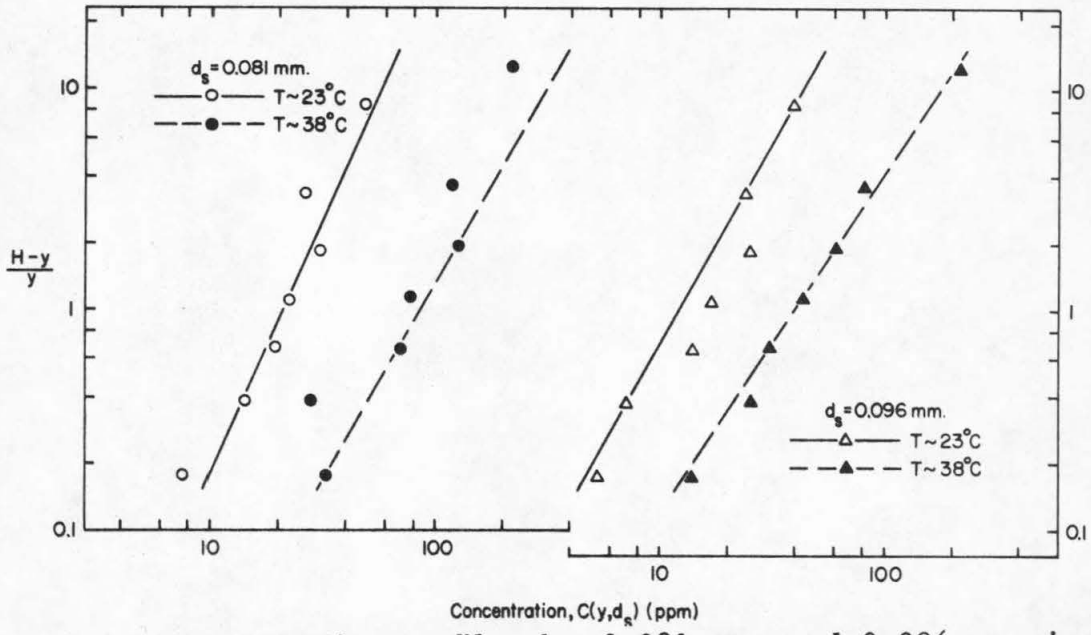

Fig. 5.9. Concentration profiles for 0.081 mm, and 0.096 mm size fractions measured along centerline of 60-ft flume in experiment-pair F-23, F-24. (U ~ 70 cm/sec, H ~ 8 cm; D_g = 0.228 mm, σ_g = 1.52.)

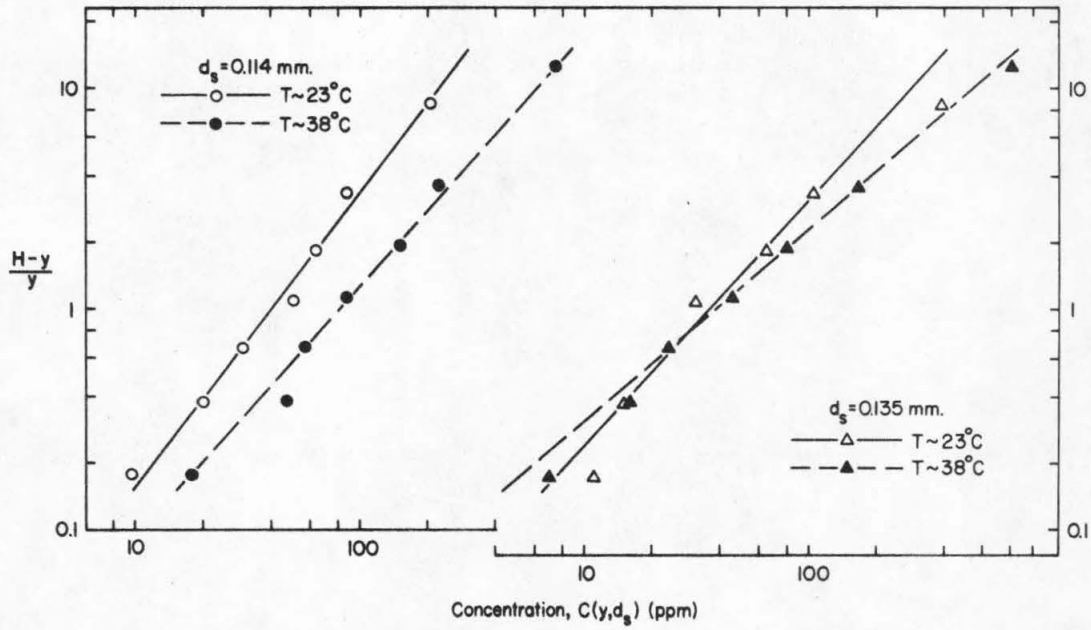

Fig. 5.10. Concentration profiles for 0.114 mm, and 0.135 mm size fractions measured along centerline of 60-ft flume in experiment-pair F-23, F-24. (U ~ 70 cm/sec, H ~ 8 cm; D_g = 0.228 mm, σ_g = 1.52.)

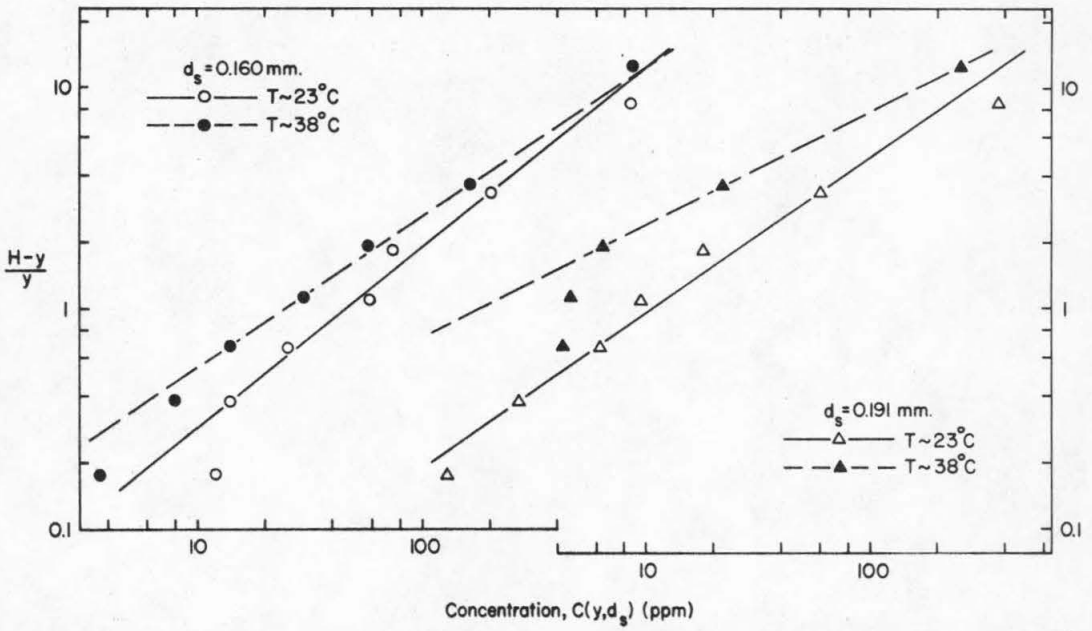

Fig. 5.11. Concentration profiles for 0.160 mm, and 0.191 mm size fractions measured along centerline of 60-ft flume in experiment-pair F-23, F-24. (U ~ 70 cm/sec, H ~ 8 cm; D_g = 0.228 mm, and σ_g = 1.52.)

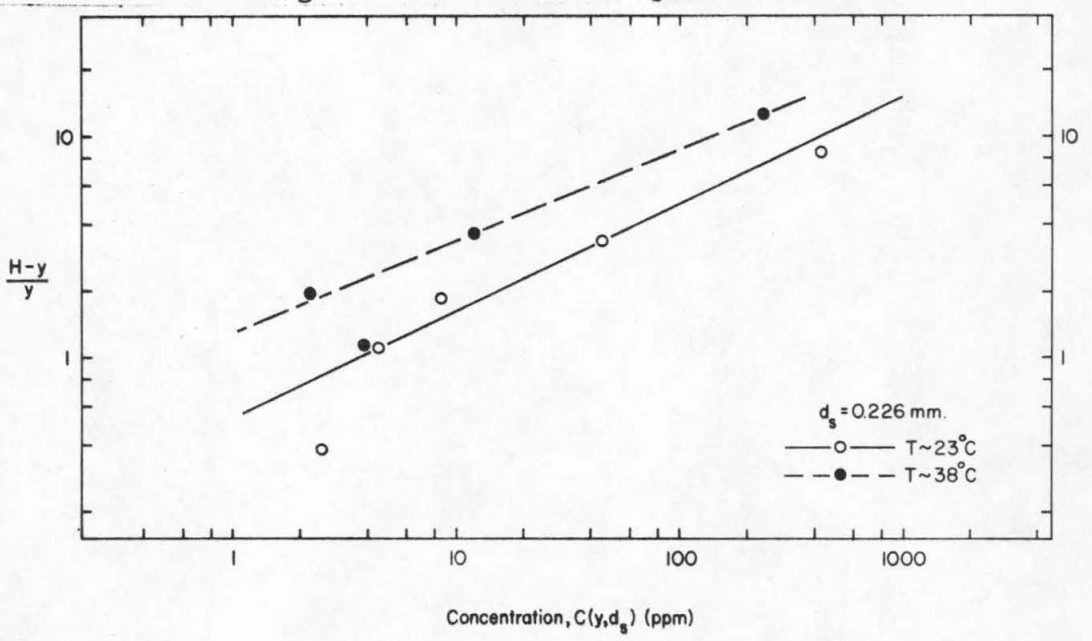

Fig. 5.12. Concentration profiles for 0.226 mm size fraction measured along centerline of 60-ft flume in experiment-pair F-23, F-24. (U ~ 70 cm/sec, H ~ 8 cm; D_g D_g = 0.228 mm, σ_g = 1.52.)

However for size fractions coarser than 0.135 mm (Figs. 5.11 and 5.12) the measured concentrations are uniformly larger in the cold water flow. In the concentration profiles for the 0.135 mm size fraction (Fig. 5.10) the cold and warm water curves intersect. This intersection suggests that in the lower half of the flows the warm water concentrations were larger, but that in the upper flow region the cold water concentrations exceeded those in the warm water flow.

The concentration profiles measured in experiments F-27 and F-28 are plotted for nine size fractions in Figs. 5.13 to 5.17. In experiments F-27 and F-28 larger sediment samples were collected thus allowing a wider resolution of size fractions than was possible in experiments F-23 and F-24. These concentration profiles exhibit the same qualitative temperature effects as observed in the concentration profiles of F-23 and F-24.

The concentration profiles in Figs. 5.13 and 5.14 show that for the three finest size fractions at each elevation where samples were collected the warm water concentrations were significantly larger than the respective cold water concentrations. Whereas in Figs. 5.15, 5.16 and 5.17 the data indicate that for size fractions coarser than 0.160 mm the cold water sediment concentrations were larger at each elevation. The cold and warm water concentration profiles for size fractions 0.135 mm and 0.160 mm intersect. With each size fraction the warm water sediment concentrations were larger near the bed, but in the upper flow region the cold water concentrations were larger.

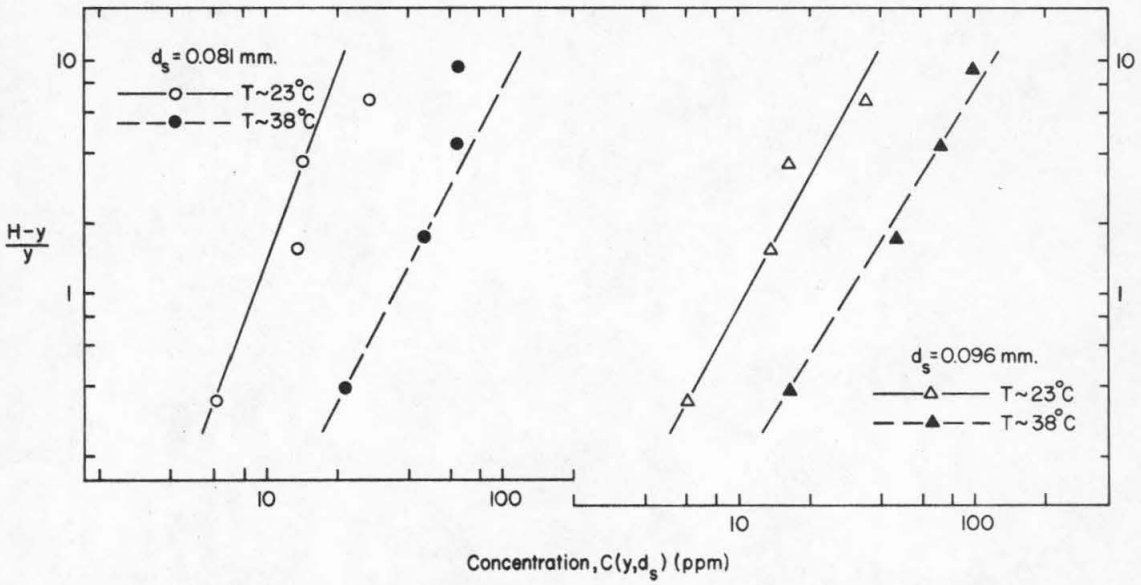

Fig. 5.13. Concentration profiles for 0.081 mm, and 0.096 mm size fractions measured along centerline of 60-ft flume in experiment-pair F-27, F-28. In these experiments U ~ 87 cm/sec, and H ~ 11.3 cm; and the bed material was well-graded silica sand (D_g = 0.228 mm, σ_g = 1.52).

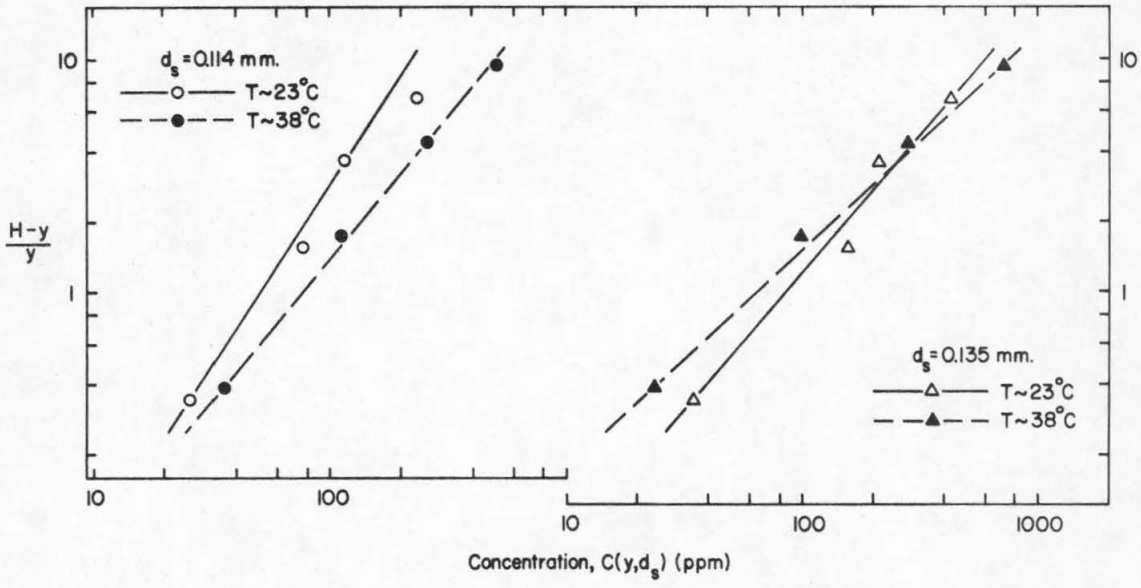

Fig. 5.14. Concentration profiles for 0.114 mm, and 0.135 mm size fractions measured along centerline of the 60-ft flume in experiment-pair F-27, F-28. In these experiments U ~ 87 cm/sec, and H ~ 11.3 cm; and the bed material was well-graded silica sand (D_g = 0.228 mm, σ_g = 1.52).

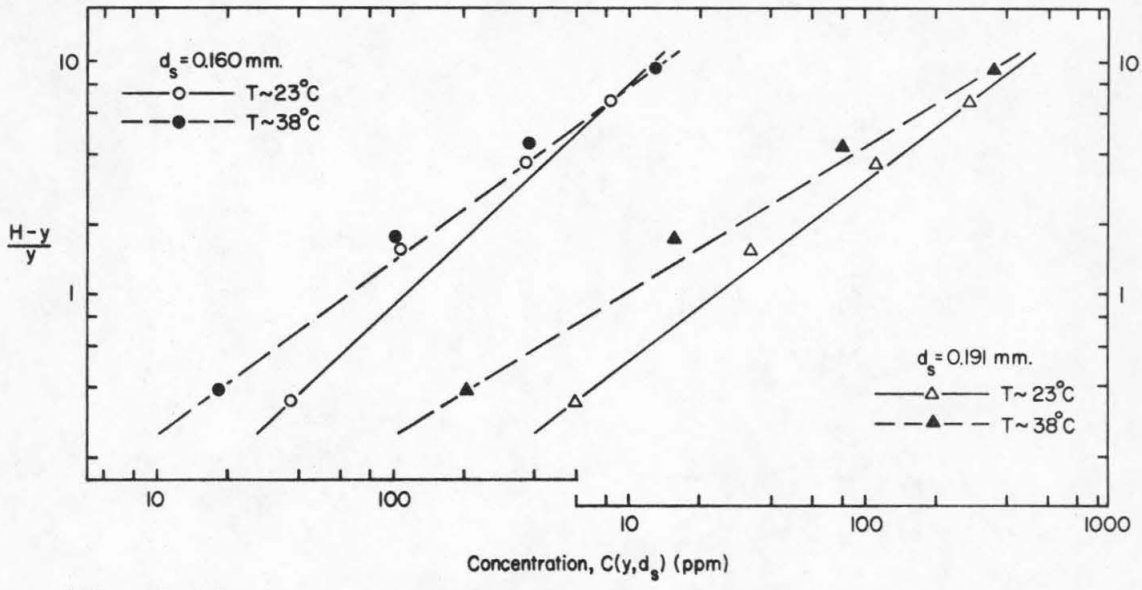

Fig. 5.15. Concentration profiles for 0.160 mm, and 0.191 mm size fractions measured along centerline of 60-ft flume in experiment-pair F-27, F-28. In these experiments U ~ 87 cm/sec, and H ~ 11.3 cm; and the bed material was well-graded silica sand (D_g = 0.228 mm, σ_g = 1.52).

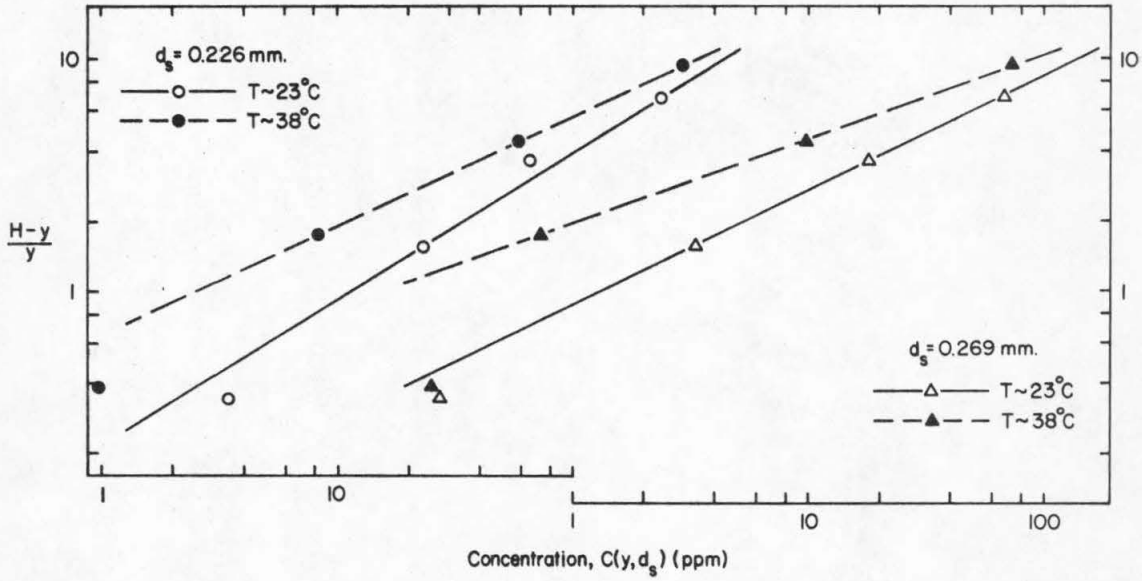

Fig. 5.16. Concentration profiles for 0.226 mm, and 0.269 mm size fractions measured along centerline of 60-ft flume in experiment-pair F-27, F-28. In these experiments U ~ 87 cm/sec, and H ~ 11.3 cm; and the bed material was well-graded silica sand (D_g = 0.228 mm, σ_g = 1.52).

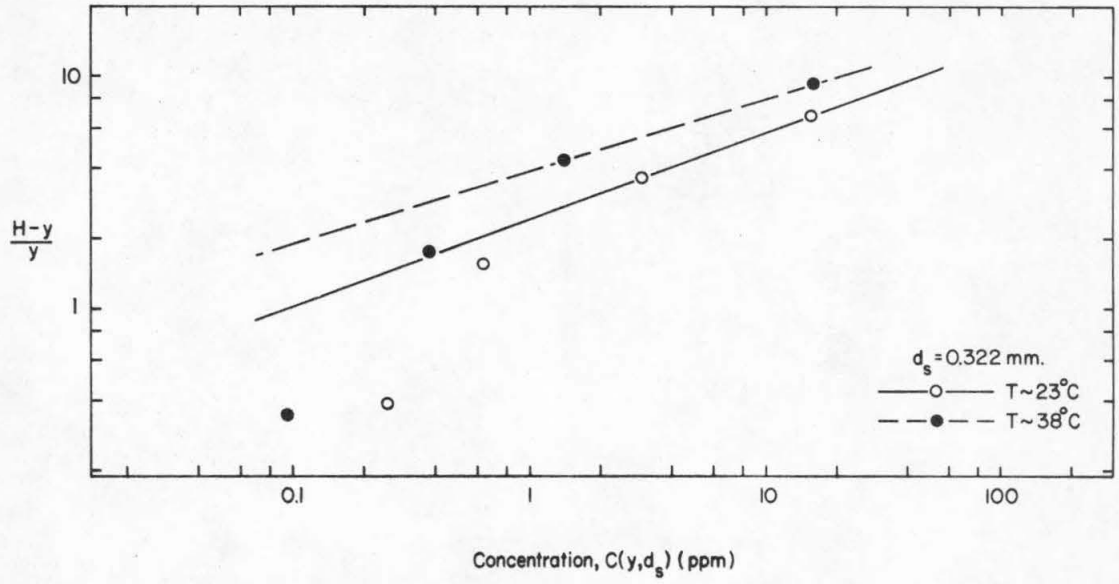

Fig. 5.17. Concentration profiles for 0.322 mm fraction measured along centerline of 60-ft flume in experiment-pair F-27, F-28. In these experiments U ~ 87 cm/sec, and H ~ 11.3 cm; and the bed material was well-graded silica sand (D_g = 0.228 mm, σ_g = 1.52).

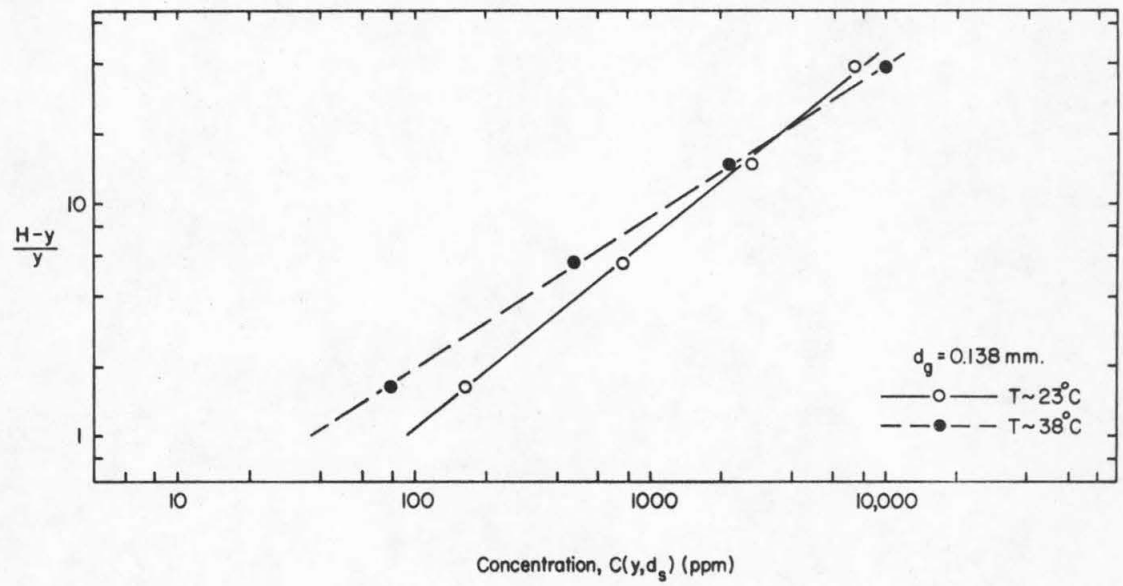

Fig. 5.18. Concentration profiles measured along centerline of 40-ft flume in experiment-pair G-9, G-10. In these experiments U = 52.8 cm/sec, and H = 7.83 cm; and the bed material was well-sorted silica sand (D_g = 0.138, σ_g = 1.25).

In Fig. 5.18 the concentration profiles from experiments G-9 and G-10 are plotted. These profiles were obtained along the flume centerline at station 9.0 (9.0 meters below the upstream end of the flume) in the 40-ft flume. Since the bed sediment and the load were well sorted the suspended load samples were not broken down into size fractions and only one profile was obtained in each experiment. The data plotted in Fig. 5.18 clearly illustrate the phenomenon suggested in Figs. 5.10 (d_s = 0.135 mm), 5.14 (d_s = 0.135 mm), and 5.15 (d_s = 0.160 mm) – cold and warm water profile intersection. The measured concentrations in the upper flow region were larger in the cold water experiment, but the warm water concentration nearest the bed was approximately 35% larger than the cold water concentration.

In Figs. 5.9 through 5.18 straight lines have been fitted to the data according to the relative suspended concentration theory expressed in Eq. (2.3). These straight-line profiles were fitted by the following procedure. Straight-line profiles were fitted to the data in plots where the location and slope of such a profile is unambiguous. Using values of Z from these straight-line profiles, and corresponding values of the bed shear velocity along the flume centerline ($U_{*cl} = \sqrt{gHS_f}$, where S_f is the friction slope) and von Karman constant, values of $ZU_{*cl}K$ were plotted against the still-water particle fall velocity as given by the ASCE Task Committee on Preparation of Sedimentation Manual (1962). A shape factor of 0.7 was assumed for all particle sizes. The von Karman

constant was determined graphically for each experiment from a velocity profile (see Fig. 5.19) measured along the flume centerline at the station where the sediment concentration profile was measured.

According to Eq. (2.3) a plot of $ZU_{*cl}K$ versus still-water particle fall velocity ω_s expresses the relation between ω/β and ω_s. The plotted data indicated that $ZU_{*cl}K$ varied linearly with ω_s in these six experiments. From a linear fit of these data probable values of Z were obtained for the remaining concentration profile data according to their respective still-water particle fall velocities. These probable Z values provided a guide for the final straight-line profiles; and in each case the profiles were fitted to the data which best accommodated a value of Z near the probable value.

The deviations of the data from a straight-line fit are in general larger in Figs. 5.9 through 5.17 than in Fig. 5.18. There are perhaps three factors which contributed to this difference. 1) In experiments G-9 and G-10 the sand bed was uniformly flat over the central flow region, whereas in experiments F-23, F-24, F-27, and F-28 long, small amplitude (approximately 0.2 cm) bed waves moving through the system effected continual changes in local bed elevation at the sampling station. These changes in local bed elevation produced differences between sampling velocity and local flow velocity during some of the profile measurements; and differences between the dimensionless coordinate during sampling and that computed from mean bed elevation measurements made after the concentration profile sampling had been

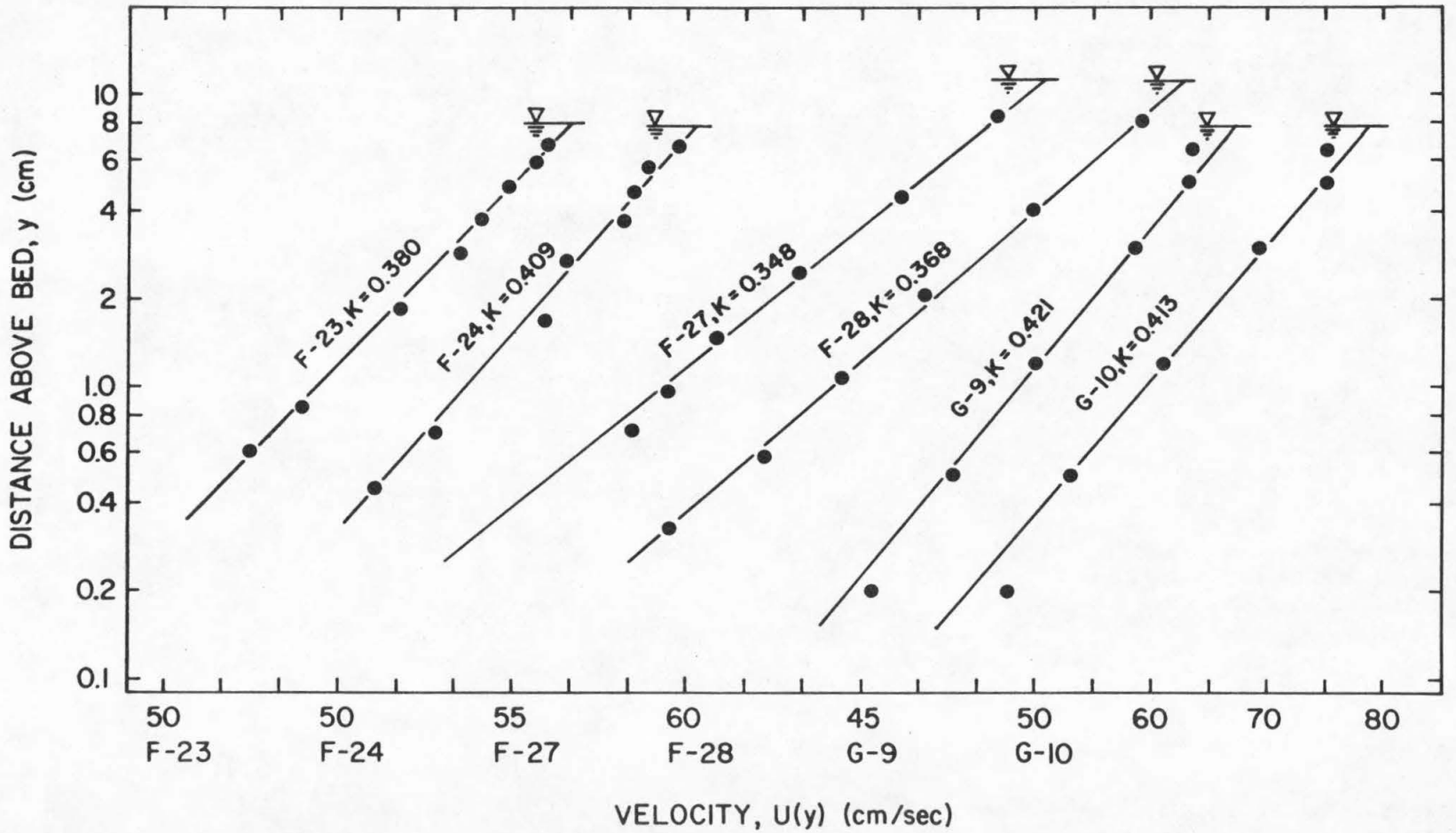

Fig. 5.19. Velocity profiles measured along flume centerline in experiments F-23, F-24, F-27, F-28, G-9, and G-10.

completed. Both types of error contributed to the data scattering in Figs. 5.9 through 5.17. 2) In experiments F-23, F-24, F-27, and F-28 the sample separation a) required that the samples be sieved, and b) reduced the size of the profile samples; both of which increased the relative errors introduced by sample analysis. Thus sample separation is partly responsible for the data scattering in the concentration profiles of F-23, F-24, F-27, and F-28, and the relative absence thereof in the profiles of experiments G-9 and G-10. 3) Experimental procedure was continually improved during the course of the experiments. It is therefore to be expected that the experimental results from G-9 and G-10 are somewhat more precise than those of F-23, F-24, F-27, and F-28.

The Z values for all of the concentration profiles are plotted in Fig. 5.20 as $\log_{10}(ZU_{*cl}K)$ versus $\log_{10}(\omega_s)$. A straight line representing the relation $ZU_{*cl}K = \omega_s$ has also been plotted. The data from experiments F-23, F-24, F-27, F-28, G-9 and G-10 suggest that this relation is fundamentally correct; and thus that if $\omega = \omega_s$ then β is constant and equal to unity for fine, naturally-worn silica sands.

5.2.1 Extension of Bed-Load Discharge Hypothesis

In Section 5.1.1 a hypothesis was presented for sediment discharge in a low-transport, flat-bed regime. This hypothesis can be extended to bed-load discharge in high-transport, flat-bed flows. Assuming these conditions obtained in experiments F-23, F-24, F-27

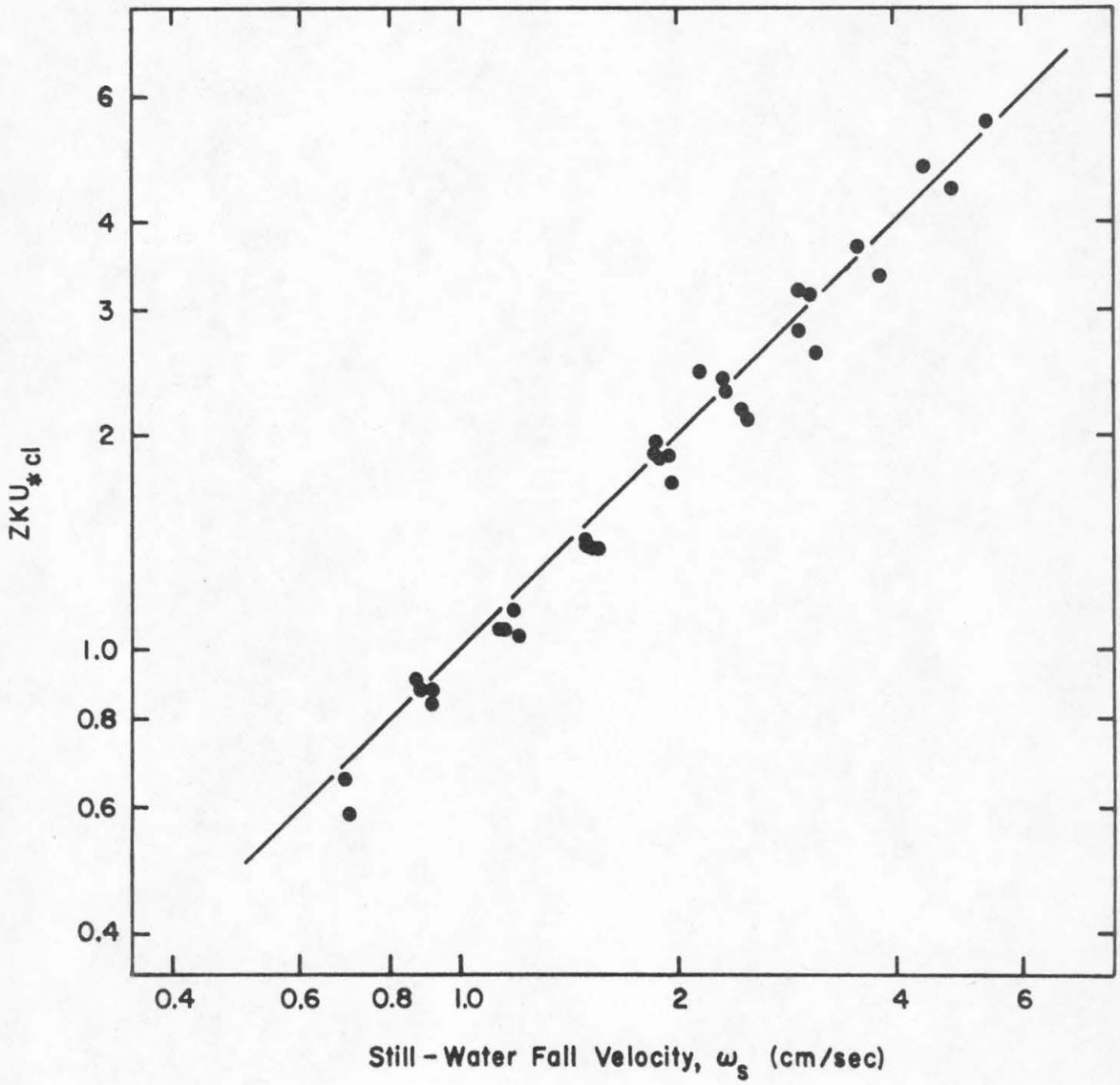

Fig. 5.20. Variation of $\log_{10} ZU_{*cl}K$ ($\log_{10} \omega/\beta$) with $\log_{10} \omega_s$ according to straight lines fitted to concentration profiles in Figs. 5.9 through 5.18.

F-28, G-9 and G-10 the inferred temperature effects on bed-load discharge in these experiments may be related to those observed in the low-transport, flat-bed experiments.

In Figs. 5.13 and 5.14 (d_s = 0.114 mm) the measured warm water concentrations are larger at each elevation, and the data indicate that the sediment concentration gradients are larger in the warm water flow. According to Eq. (2.3) these results indicate that the warm water sediment concentrations near the bed are also larger.

In a thin layer adjacent to the bed the relative sediment concentration distribution may be significantly different from that predicted by Eq. (2.3), as found by Einstein and Chien (1955). However the findings of Einstein and Chien indicate that if the sediment concentrations and concentration gradient are larger in the upper flow region where Eq. (2.3) closely approximates the relative concentration distribution, the concentrations are also larger in the bed layer.

Since the concentration of particles rolling and sliding along the bed must vary with the concentration just above the bed it is expected that sediment discharge on and near the bed (bed-load discharge) would also vary with this concentration. Therefore the larger concentrations and concentration gradients in Figs. 5.13 and 5.14 indicate that in experiment-pair F-27, F-28 the warm water bed-load discharges were larger for the three finest size fractions. These temperature effects on bed-load discharge are qualitatively the same as those observed in the experiments of Series B where the boundary Reynolds numbers were

approximately the same as the values of $R_{*b} = U_{*b}d_s/\nu$ for the three finest size fractions in experiments F-27 and F-28 (see Tables 5.1 and 5.5).

The concentration profiles given in Figs. 5.14 (d_s = 0.135 mm) and 5.15 (d_s = 0.160 mm) wherein the measured concentrations near the bed and the concentration gradients are larger in the warm water flow indicate that the bed-load discharge for 0.135 mm and 0.160 mm size fractions were also larger in the warm water flow. The sediment discharge ratios given in Table 5.5 for these two size fractions support this conclusion. In each case the warm water sediment discharge was larger, even though the warm water concentration gradient exceeded that in the cold water flow. This suggests that for each of these size fractions the bed-load discharge was larger in the warm water flow. The boundary Reynolds numbers for these size fractions are in each case less than 13 as given in Table 5.5. Thus these results also agree with the temperature effects on bed-load discharge suggested by the low-transport, flat-bed data presented in Fig. 5.7.

For the 0.191 mm, 0.226 mm, 0.269 mm, and 0.322 mm size fractions the concentration profiles (Figs. 5.15, 5.16 and 5.17), and the sediment discharge data are inconclusive. The low-transport flat-bed results suggest that over the range of boundary Reynolds numbers of these size fractions (approximately 10 to 20) the temperature effect on bed-load discharge may be small, for in this range the qualitative effect of an increase in water temperature on bed-load discharge changes.

The data from the experiments of Series H (Fig. 5.7) suggest that for boundary Reynolds numbers larger than 20 with an increase in water temperature there is a reduction in bed-load discharge. The boundary Reynolds numbers of the two coarsest size fractions in experiments F-27 and F-28 exceeded 18 (see Table 5.5), and the relatively small sediment discharge ratios 0.68 and 0.52, respectively, suggest that the bed-load discharge of these two size fractions was in fact larger in the cold water flow.

The concentration profile and sediment discharge data from experiments F-23 and F-24 suggest conclusions similar to those in experiments F-27 and F-28, and thus support these results. In experiments F-23 and F-24 the computed mean bed shear stresses were approximately 23% smaller than the values in F-27 and F-28, and therefore the boundary Reynolds numbers were also smaller. This difference in boundary Reynolds number explains why the increases in sediment discharge for the two coarsest size fractions in the cold water flow were larger in experiments F-27 and F-28 than in experiments F-23 and F-24.

In experiments G-9 and G-10 the boundary Reynolds numbers were less than 8. Thus the larger bed-load concentration and discharge in the warm water experiment of this pair also agrees with the low-transport, flat-bed results.

These results indicate that the temperature effects on bed-load discharge under high-transport, flat-bed conditions are qualitatively the same as those observed in the low-transport, flat-bed experiments presented in Fig. 5.7.

5.3 CONSTANT-DISCHARGE EXPERIMENTS

In experiments F-3 through F-10, F-23, F-24, and F-31 through F-34 the discharge was held constant. The purpose of these experiments was to measure changes in bed geometry and roughness, and sediment discharge with increase in water temperature over a range of bed forms common in natural, sand-bed streams. Bed forms present in the constant-discharge experiments included ripples, dunes, and flat-bed. Basic hydraulic data for these experiments are given in Table 5.6.

The experiments were made in pairs wherein the velocity and depth were nearly the same, but in one experiment the water temperature was approximately 23°C and in the other approximately 38°C. The warm water experiment in each pair is even numbered. In these experiments significant changes in bed roughness and sediment discharge were measured with increase in water temperature. These temperature effects are not consistent over the seven experiment-pairs.

The friction slope and computed bed friction factor ($f_b = 8\,U_{*b}^2/U^2$) for each of the experiments are plotted as functions of velocity and water temperature in Fig. 5.21. The sediment discharge is plotted as a function of mean velocity and water temperature in Fig. 5.22.

Table 5.6. Summary of Data, Constant-Discharge Experiments

D_g = 0.228 mm, σ_g = 1.52, ρ_s = 2.65 gm/cm³; in 60-ft Flume

Run No.	U Velocity (cm/sec)	H Depth (cm)	S_f Friction Slope	T[1] Water Temp. (°C)	g_s Sediment Discharge (gm/cm/sec x 10^6)	d_g Load Geom. Mean Size (mm)	s_g Load Geom. Std. Dev.	ρ_s Load Density (gm/cm³)	F Froude No.	r_b Bed Hydr. Radius (cm)	f_b Bed Friction Factor	U_{*b} Bed Shear Velocity (cm/sec)	τ_{*b} Shields Stress	R_{*b} Boundary Reynolds No.	$\overline{\sigma^2}$ Mean Variance of Bed Profiles (cm^2)	$\bar{\lambda}_o$ Mean Dist. Between Zero Crossings (cm)	Bed Form	Run No.
F-3	30.8	18.1	0.00056	22.4	0.196	0.154	1.54	2.65	0.23	16.2	0.0756	2.99	0.242	7.21	0.95	12.1	Ripples	F-3
F-4	30.8	18.1	0.00050	37.8	0.282	0.149	1.36	2.65	0.23	16.2	0.0669	2.82	0.212	9.43	0.70	11.0	Ripples	F-4
F-5	34.8	16.0	0.00089	22.9	0.973	0.124	1.56	2.65	0.28	14.7	0.0844	3.57	0.344	8.71	0.66	10.2	Ripples	F-5
F-6	34.4	16.2	0.00076	37.9	0.586	0.116	1.66	2.65	0.27	14.7	0.0745	3.32	0.296	11.2	0.67	11.6	Ripples	F-6
F-7	39.0	14.3	0.00128	23.0	9.66	0.154	1.66	2.65	0.33	13.2	0.0871	4.07	0.447	9.95	0.82	11.6	Ripples	F-7
F-8	39.0	14.3	0.00101	38.1	7.16	0.159	1.69	2.65	0.33	13.1	0.0678	3.59	0.346	12.1	0.89	14.4	Ripples	F-8
F-9	44.8	12.4	0.00160	23.2	30.0	0.149	1.78	2.65	0.41	11.5	0.0719	4.25	0.487	10.4	1.13	15.4	Ripples	F-9
F-10	45.1	12.3	0.00141	37.8	23.7	0.150	1.85	2.65	0.41	11.4	0.0617	3.96	0.420	13.3	1.34	21.8	Ripples	F-10
F-33	48.2	11.6	0.00177	22.9	39.6	0.139	1.85	2.65	0.45	10.7	0.0640	4.31	0.500	10.5	1.14	18.7	Ripples	F-33
F-34	46.9	11.9	0.00187	38.3	47.0	0.149	1.84	2.65	0.43	11.1	0.0738	4.51	0.544	15.2	3.47	38.6	Dunes	F-34
F-31	53.3	10.4	0.00209	23.2	59.7	0.138	1.82	2.65	0.53	9.6	0.0554	4.44	0.531	10.9	2.35	33.6	Dunes	F-31
F-32	52.4	10.6	0.00208	38.4	58.2	0.148	1.78	2.65	0.51	9.9	0.0586	4.49	0.539	15.2	3.38	51.1	Dunes	F-32
F-23	69.2	8.06	0.00205	23.0	89.9	0.181	1.44	2.65	0.78	7.1	0.0240	3.79	0.387	9.26	-	-	Flat	F-23
F-24	70.7	7.88	0.00208	38.0	92.7	0.162	1.50	2.65	0.80	7.0	0.0229	3.78	0.384	12.7	-	-	Flat	F-24

[1] Temperature variation during each experiment was less than ±1°C.

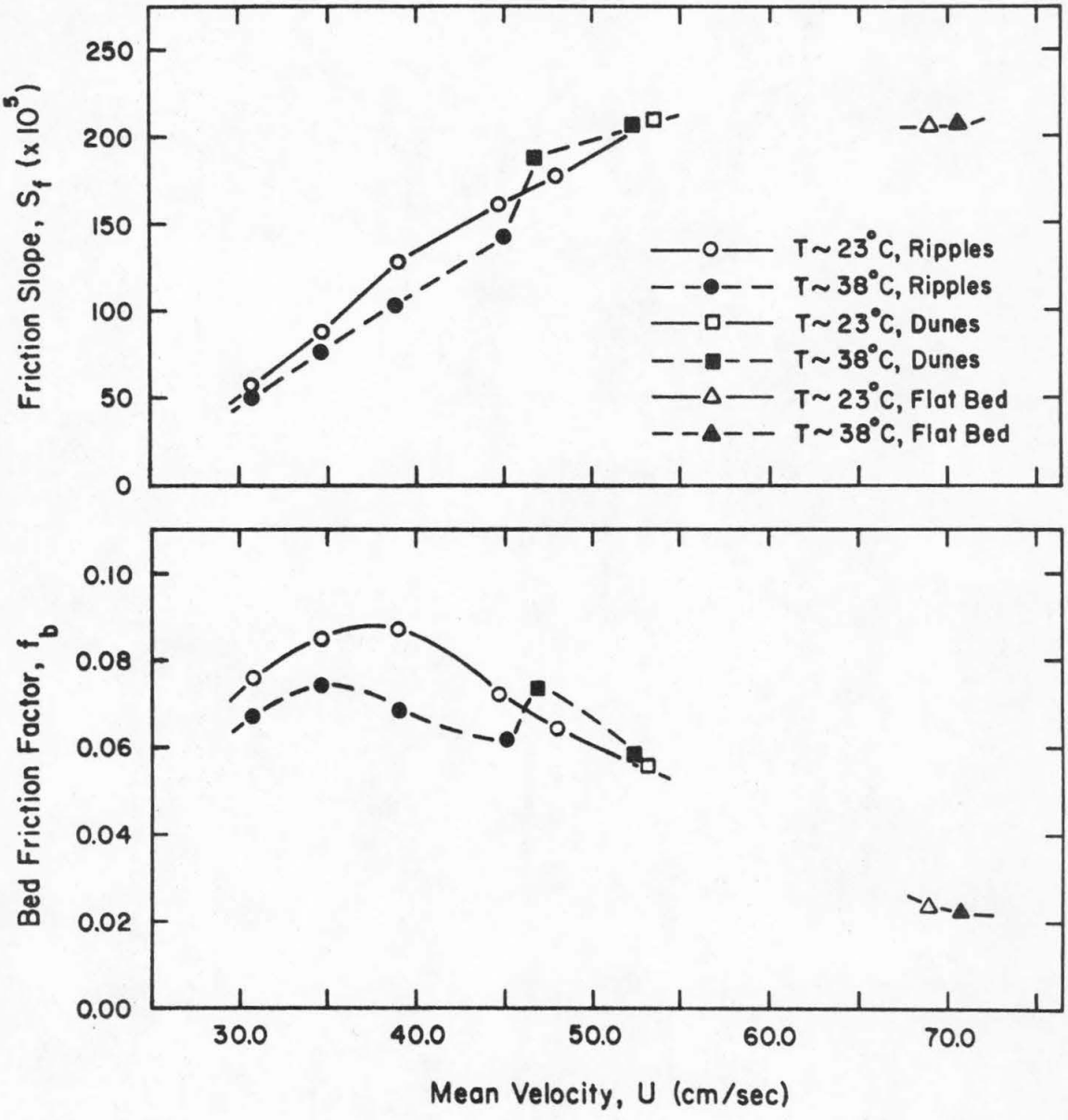

Fig. 5.21. Variation in S_f and f_b with velocity and water temperature for the constant-discharge (Q = 47.4 l/sec) experiments of Series F. These experiments were made in the 60-ft flume with a bed material of fine silica sand (D_g = 0.228 mm, σ_g = 1.52).

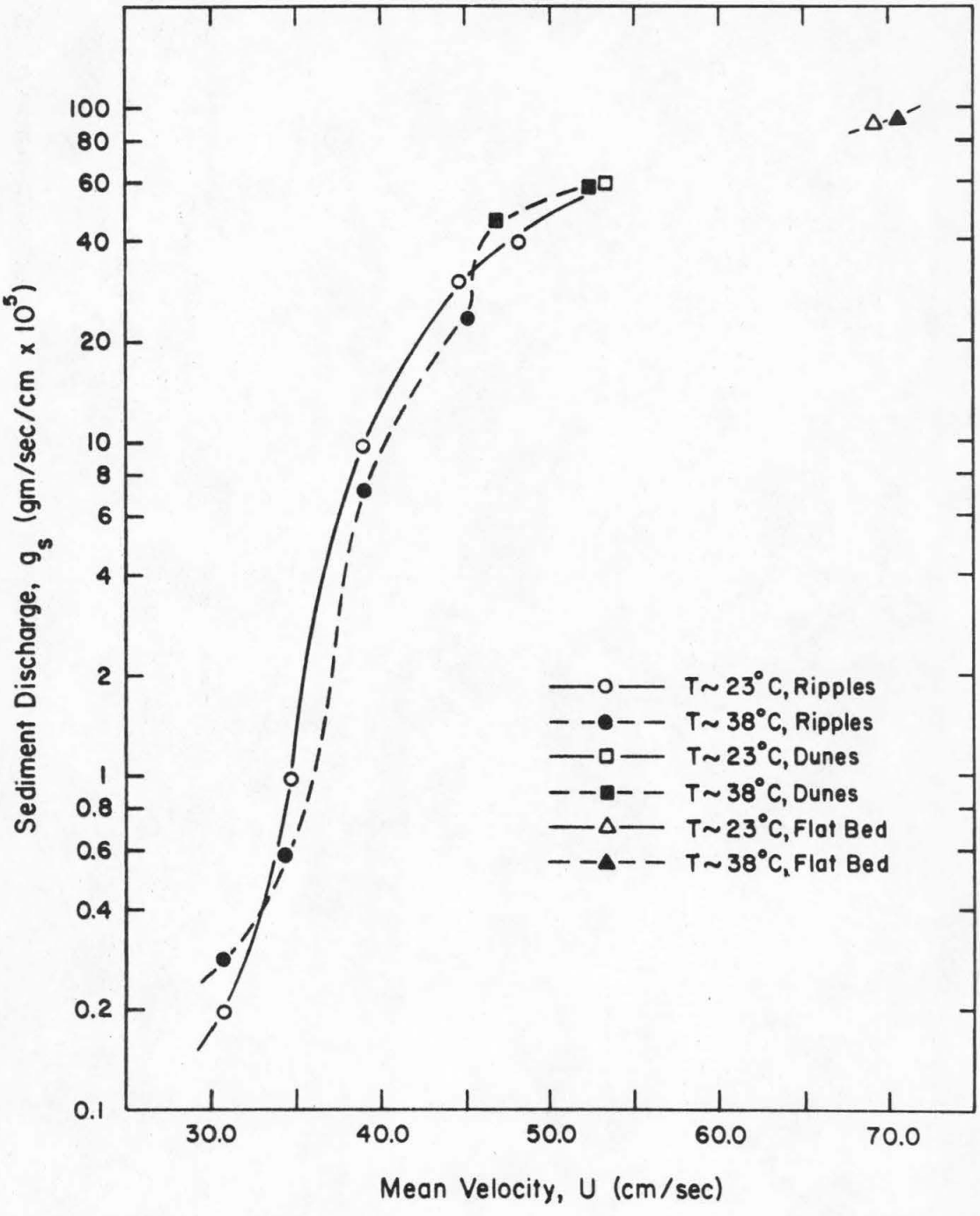

Fig. 5.22. Variation in g_s with velocity and water temperature for the constant discharge (Q = 47.4 l/sec) experiments of Series F. These experiments were made in the 60-ft flume with a bed material of fine silica sand (D_g = 0.228 mm, σ_g = 1.52).

As shown in Fig. 5.21 in the four lowest-velocity experiment-pairs, F-3 through F-10, the bed form was ripples; and in each pair S_f and f_b were significantly larger in the cold water flow. These data suggest that a rippled bed formed by a cold water flow is characteristically rougher than one formed by a warm water flow at the same velocity and depth. Franco (1968) has presented data from constant-discharge experiments in a feed-type flume with fine sand that also suggest this characteristic difference in cold water and warm water ripple roughness.

Vanoni and Hwang (1967) have shown that a naturally-formed ripple bed is hydrodynamically rough. Thus the differences in bed roughness measured in experiments F-3 through F-10 indicate that with each experiment-pair there were geometric differences between the rippled beds formed by the cold and warm water flows.

In experiment F-10 (U = 45.1 cm/sec) it was observed that the ripples were noticeably longer and more nearly two-dimensional than in the experiments with smaller velocities, indicating that the warm water bed was in transition to a dune configuration. In F-34 (U = 46.9 cm/sec), the transition had been accomplished and the bed was covered with dunes; but the cold water experiment of the pair, F-33 (U =48.2 cm/sec) still had a rippled bed (see Fig. 5.23). As shown in Fig. 5.21 the warm water friction slope and bed friction factor in this experiment-pair were larger than the respective values for the cold water flow, indicating that with the change in bed form to dunes in the warm water experiment there was also a relatively large increase in channel roughness.

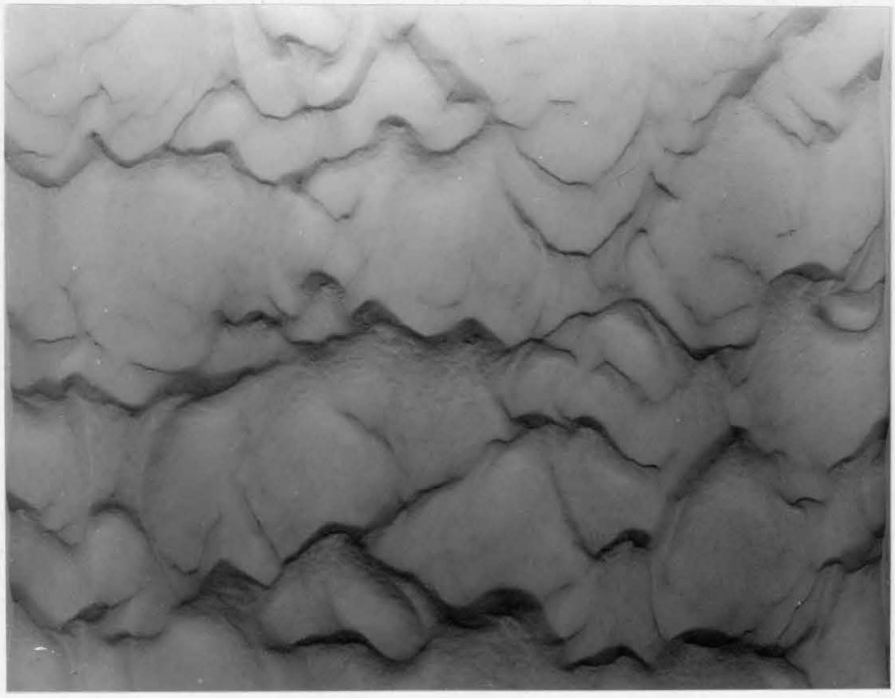

(a) Ripple Bed Configuration in F-33 ($T \sim 23^{\circ}C$). (Photo No. 11214)

(b) Typical Dune Front in F-34 ($T \sim 38^{\circ}C$). (Smaller ripples on bed were formed during flume shutdown, Photo No. 11215.)

Fig. 5.23 Ripple and Dune Bed Configurations in Experiments F-33 ($T \sim 23^{\circ}C$) and F-34 ($T \sim 38^{\circ}C$). In these experiments $U \sim 47.5$ cm/sec, and $H \sim 11.7$ cm. (Flow is from top to bottom, and scale is given by width of photographs which corresponds to 85 cm width of flume.)

In experiment F-31 (U = 53.3 cm/sec) the cold water transition to dunes had been accomplished and thus in this experiment-pair (F-31 and F-32) the bed forms were again the same.

The data presented in Fig. 5.21 indicate that under certain conditions the transition to a dune configuration occurs at a lower velocity in a warm water flow than in a cold water flow; and that this characteristic difference can produce a flow regime where the warm water bed roughness is greater than that in a cold water flow of the same discharge and depth.

Not enough data are available from this series of experiments to determine whether there is a characteristic difference in bed roughness when there are dunes on the bed in both cold and warm water flows. The data from experiments F-31 and F-32 (U $\sim$ 53.0 cm/sec) suggest however, that if such a difference does exist it is small.

In experiment-pair F-23 and F-24 (U $\sim$ 70.0 cm/sec) flat-bed conditions obtained, and the differences in S_f and f_b between the cold and warm water flows were small.

The data plotted in Fig. 5.22 show that with the exception of the lowest-velocity experiment-pair F-3 and F-4 (U = 30.8 cm/sec), the temperature effect on sediment discharge was qualitatively the same as that on channel roughness. The anomaly in experiments F-3 and F-4 may be explained by a characteristic difference between this experiment-pair and the higher-velocity experiments. In each of the higher-

velocity experiments there was a significant amount of suspended sediment discharge; whereas in the lowest-velocity experiment-pair virtually all of the sediment discharge moved close to the bed. Visual observations during the two experiments indicated that a few particles were suspended briefly as they were transported from ripple crest to trough, but otherwise particle movement was by rolling and sliding along the bed.

The temperature effect on sediment discharge in experiments F-3 and F-4 agree qualitatively with those observed in the low-transport, flat-bed experiments of Series B wherein the depth was kept constant. The boundary Reynolds numbers were in each case less than 10, as shown in Table 5.7. These results indicate that the qualitative temperature effects on bed-load discharge observed in the flat-bed experiments of Series B may also obtain in flows where the bed configuration is non-planar.

5.3.1 Spectral Analysis of Ripple and Dune Bed Profiles

The irregular geometry of a ripple or dune covered bed is not amenable to clear and concise mathematical description. These bed waves are generally three-dimensional, and rather than having a simple periodicity there usually is a broad range of wave lengths superimposed in a somewhat random manner.

In 1966 Nordin and Algert (1966) proposed the use of spectral analysis in characterizing the complex geometry of ripple, and dune covered beds. This technique has since been employed by others

(Ashida and Tanaka (1967), Hino (1968), and Squarer (1970)). As a mode of bed wave description, spectral analysis has considerable advantage; it is objective, concise, and may be readily applied to both laboratory and field data. The primary disadvantage of spectral analysis of bed waves is that as yet the results obtained have not been clearly related to bed geometry, or roughness.

Table 5.7 Data From Fine-Sand Experiments in Series B and Experiments F-3 and F-4.

Run No.	T Water Temperature (^{o}C)	τ_{*b} Shields Stress	R_{*b} Boundary Reynolds No.	$g_s \times 10^5$ Sediment Discharge (gm/sec/cm x 10^5)	Bed Form
B-1	21.0	0.0405	2.61	2.57	Flat
B-2	35.6	0.0366	3.43	10.3	Flat
B-3	20.5	0.0374	2.48	0.642	Flat
B-4	36.4	0.0335	3.34	1.86	Flat
B-5	20.4	0.0319	2.29	0.033	Flat
B-6	35.6	0.0286	3.04	0.124	Flat
F-3	22.4	0.242	7.29	0.196	Ripples
F-4	37.8	0.212	9.43	0.282	Ripples

5.3.1.1 Spectral distribution function

The spectral distribution function S(k) (also called the power spectrum (Blackman and Tukey (1958)) approximates the distribution of the variance of a function f(x) among its mean periodic

components. The variance of f(x) is defined as

$$\sigma^2 = \lim_{L \to \infty} \frac{1}{L} \int_{-L/2}^{L/2} f(x)^2 dx \qquad (5.14)$$

where f(x) is the bed profile function adjusted to zero mean, x is the longitudinal coordinate, and L is the bed profile length.

This spectral distribution function is defined by the cosine transform of the autocovariance function $R(\tau)$, of f(x)

$$S(k) = 4 \int_0^{\infty} R(\tau) \cos (k\tau) d\tau \qquad (5.15)$$

where k is the wave number, $2\pi/\lambda$; λ is the bed wave length,

$$R(\tau) = \lim_{L \to \infty} \frac{1}{L-\tau} \int_{-L/2}^{L/2-\tau} f(x) f(x+\tau) dx ,$$

is the autocovariance function, and τ is the lag interval. The integral of S(k) is equal to the variance of the bed function f(x),

$$\sigma^2 = \int_0^{\infty} S(k) dk \qquad (5.16)$$

The autocovariance function may be approximated from a discrete evaluation of f(x) over the domain (x_1, x_N), by

$$R(m\Delta x) = \frac{1}{N-m} \sum_{i=1}^{N-m} f(x_i) f(x_{i+m}) \qquad (5.17)$$

$$m = 0, 1, 2 \ldots M$$

where $m = \tau/\Delta x$,

and $\Delta x = x_{i+1} - x_i$; the interval between values of f(x).

The spectral distribution function may then be estimated from this discrete autocovariance function by employing the trapezoidal rule for integration,

$$S(k_m) \sim 2\Delta x\left(R(0) + R(M\Delta x)\cos(Mk_m\Delta x) + 2\sum_{i=1}^{M-1} R(i\Delta x)\cos(ik_m\Delta x)\right)$$

$$m = 0, 1, 2 \ldots M \qquad (5.18)$$

where $k_m = \frac{m\pi}{M\Delta x}$

The accuracy and resolution of Eqs. (5.17) and (5.18) depend upon the length of the sample record (N), the interval between data points (Δx), and the maximum autocovariance lag (M) (Fleck (1957)).

The high wave number resolution of the spectral distribution function is effectively limited by the size of the sampling interval Δx, according to the relation

$$k_{max} = \frac{\pi}{\Delta x} \qquad (5.19)$$

Over the interval ($k = 0, k_{max}$) the computational procedure outlined in Eqs. (5.18) and (5.19) yields M + 1 points in the spectrum S(k). These spectral estimates are spaced at equal intervals of

$$\Delta k = \frac{k_{max}}{M} \qquad (5.20)$$

Whereas the parameters Δx and M determine the characteristic resolution of the computed spectral distribution function (Eq. (5.18)), the accuracy of the spectral estimates depends primarily on N, the length of the sample record. The spectral estimates are computed using the autocovariance function defined by Eq. (5.17). This autocovariance function is a statistical estimate of the expected or mean values of $(f(x) \cdot f(x + m\Delta x))$ over the infinite domain $(-\infty < x < \infty)$. The accuracy of these estimates depends on the number of samples (N-m) used in the computation. A precise relation for the accuracy of these estimates as a function of sample number (N-m) is not available. However a practical estimate of the probable error in $R(m\Delta x)$ may be obtained by comparing autocovariance functions computed over different sample intervals or lengths.

Fleck (1957) has presented data which indicate that the spectral estimates given by Eq. (5.18) may be improved by the simple smoothing operation,

$$S(0) = \frac{1}{2} S(0) + \frac{1}{2} S(k_1) \tag{5.21a}$$

$$S(k_m) = \frac{1}{4} S(_{m-1}) + \frac{1}{2} S(k_m) + \frac{1}{4} S(k_{m+1}) \tag{5.21b}$$

$$m = 1, 2 \ldots M-1$$

$$S(k_M) = \frac{1}{2} S(k_{M-1}) + \frac{1}{2} S(k_M) \tag{5.21c}$$

performed on the computed values of the spectral distribution function.

This smoothing operation tends to reduce the width of the computed spectral response (Eq. 5.18) to a particular wavelength present in the bed function. Thus, by this smoothing a better spectral filter is achieved.

5.3.1.2 Measurement and analysis of bed profiles

In experiments F-3 through F-10; and F-31 through F-34 where there were ripples or dunes on the bed, longitudinal bed profiles were measured in each experiment with a portable sonic sounder. A description of the apparatus and procedure used in the measurement of these profiles is given in Sections 3.2.2 and 4.3, respectively. In each experiment bed profiles were measured on three consecutive days after equilibrium flow conditions had been approached. Bed profiles were measured along the flume centerline and at lateral positions 10 cm, 20 cm, and 30 cm on either side of the flume centerline. Thus three sets of seven bed profiles were obtained in each experiment.

A visual analysis of all bed profiles from the constant discharge experiments indicated that there were no bed waves present of wave length less than 2 cm; thus $\Delta x = 1$ cm was chosen as the sampling interval for the numerical computation of $R(\tau)$ and $S(k)$. The maximum lag interval decided upon for these computations was $M = 150$. This value of M with $\Delta x = 1$ cm provides a wave number resolution in the computed spectral density function of $\Delta k = \pi/150$ rad/cm. Greater resolution could not be justified in view of the probable errors in the spectral estimates that were suggested by the variations among the spectral distribution functions computed over different sample intervals (lateral position and time) in each experiment.

The sample length of the bed profiles was limited by the physical length of the flume. The bed profiles were measured over a 14.0 meter reach, from station 2.0 (3.2 meters below the upstream end of the flume) to station 16.0. This 14.0 meter sample length was reduced to approximately 12 meters for analysis in order to remove the effect of flume inlet and outlet disturbances. Therefore the sample size N for each bed profile was approximately 1200.

In each experiment the bed profiles were measured after the flume discharge had been reduced such that there was no longer sediment transport. If the reduction was accomplished instantaneously an abrupt wave was created. This wave traveled upstream through the flume producing a slight backwash on the bed wave crests. Whereas if the reduction in discharge was effected over a period of several seconds to avoid an abrupt surface wave, small ripples formed on the bed waves during the shutdown operation (see Fig. 5.29(b)). In experiments F-33 and F-34 ($U \sim 47.5$ cm/sec) bed profiles were measured after both types of flume shutdown; and the computed spectral distributions were compared. The results indicated that the bed wave distortions produced during shutdown had little effect on the shape of S(k).

In most cases the flume shutdown procedure used was a compromise, producing some wave backwash and the growth of small ripples near the crests of the larger bed waves.

Examples of the bed profiles measured in experiments F-3 through F-10, and F-31 through F-34 are given in Figs. 5.24 and 5.25. In each case a least-squares fit of the data has been used to remove the non-zero linear trend in the bed profiles.

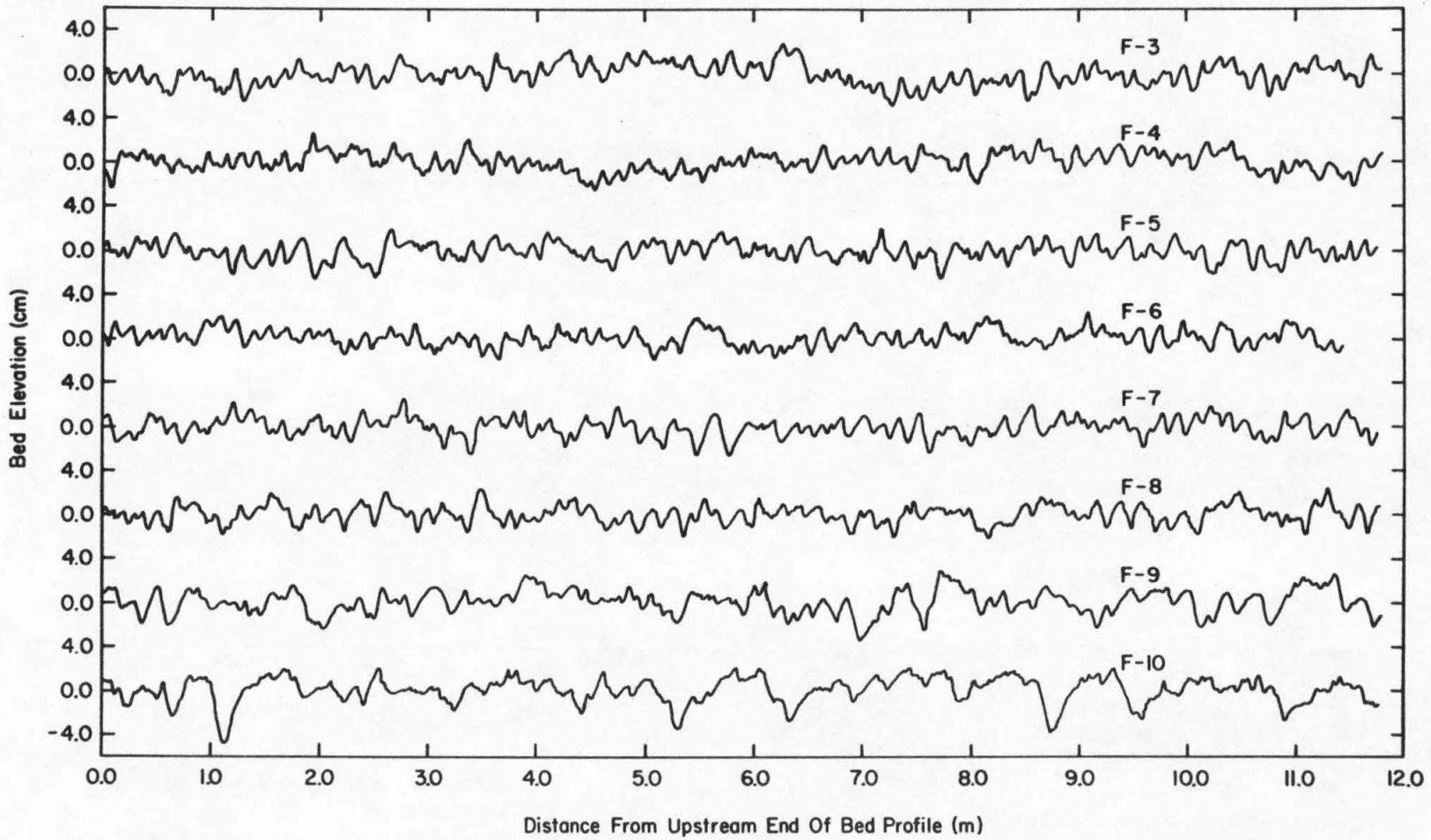

Fig. 5.24. Longitudinal bed profiles measured along centerline of 60-ft flume in experiments F-3 through F-10. In these experiments Q = 47.4 lit/sec and the bed material was fine silica sand (D_g = 0.228 mm, σ_g = 1.52).

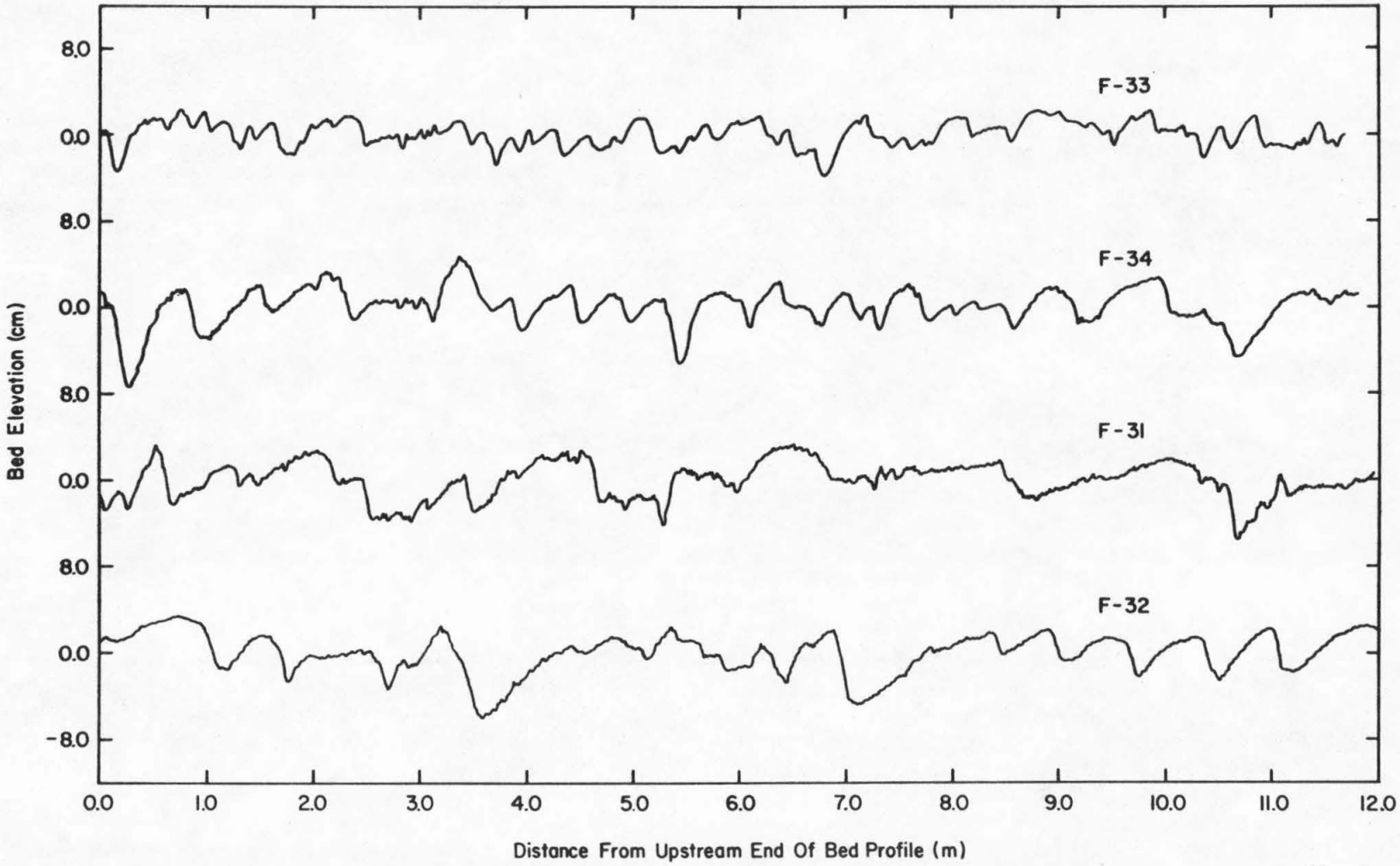

Fig. 5.25. Longitudinal bed profiles measured along centerline of 60-ft flume in experiments F-31 through F-34. In these experiments Q = 47.4 lit/sec and the bed material was fine silica sand (D_g = 0.228 mm, σ_g = 1.52).

5.3.1.3 Spectral distributions of ripple and dune beds

Spectral distribution functions were computed using Eqs. (5.17), (5.18), and (5.21a, b, and c) for each of the bed profiles measured in experiments F-3 through F-10, and F-31 through F-34.

The computed spectral distribution functions from each experiment were plotted as $\log_{10} S(k)$ versus $\log_{10} k$ and visually compared. In each case there appeared to be no systematic variation in S(k) with lateral position or time after the first day of bed profile measurement. These results suggest that the last fourteen bed profiles measured in each experiment approximate samples from the same bed function f(x). Thus by using two or more of these bed profiles jointly a better estimate may be obtained for the spectral distribution of the bed function.

This technique was applied to each set of bed profiles measured, and improved spectral estimates were obtained by averaging the spectral estimates from the seven individual bed profiles. In these experiments the crest lengths of the dominant ripple and dune bed waves exceeded 10 cm. This indicates that some bed waves were multiply recorded in each bed profile set, and thus the profile sets do not contain seven statistically independent samples. Because of this lack of profile independence, in each set the spectral averaging did not increase the effective sample length seven-fold as would have been the case if the bed profiles were statistically independent, but by some lesser amount.

In Fig. 5.26 examples are given of the spectral variations present in the ripple and dune profile sets; and in Figs. 5.27 and 5.28 averaged (mean) spectral estimates are given for experiments F-3 through F-10 and F-31 through F-34. In each case the smoothed spectral estimates have been normalized ($S(k)_N$) with respect to the computed variance of the sample:

$$\sigma^2 = \frac{1}{N-1} \sum_{i=1}^{N} f(x_i)^2 \qquad (5.21)$$

In the experiment-pairs where the bed form consisted of ripples in both the cold and warm water flows the variations among the spectral estimates from the bed profiles of each set (Fig. 5.26) were considerably larger than the differences between the cold and warm water mean spectral estimates (Fig. 5.27). Therefore the relatively small differences between the cold and warm water mean spectral estimates in the rippled-bed experiment-pairs are not statistically significant, and do not admit of clear interpretation. In the higher-velocity experiment-pairs the differences between the cold and warm water mean spectral estimates (Fig. 5.28) are larger, and thus suggest true inequality.

In experiment-pair F-9 and F-10, as explained in Section 5.3, the bed ripples formed by the warm water flow (F-10) were noticably longer than those in the cold water flow. This difference in bed wave length is also suggested in the mean spectral distribution functions shown in Fig. 5.28. In the warm water experiment F-10, the mean

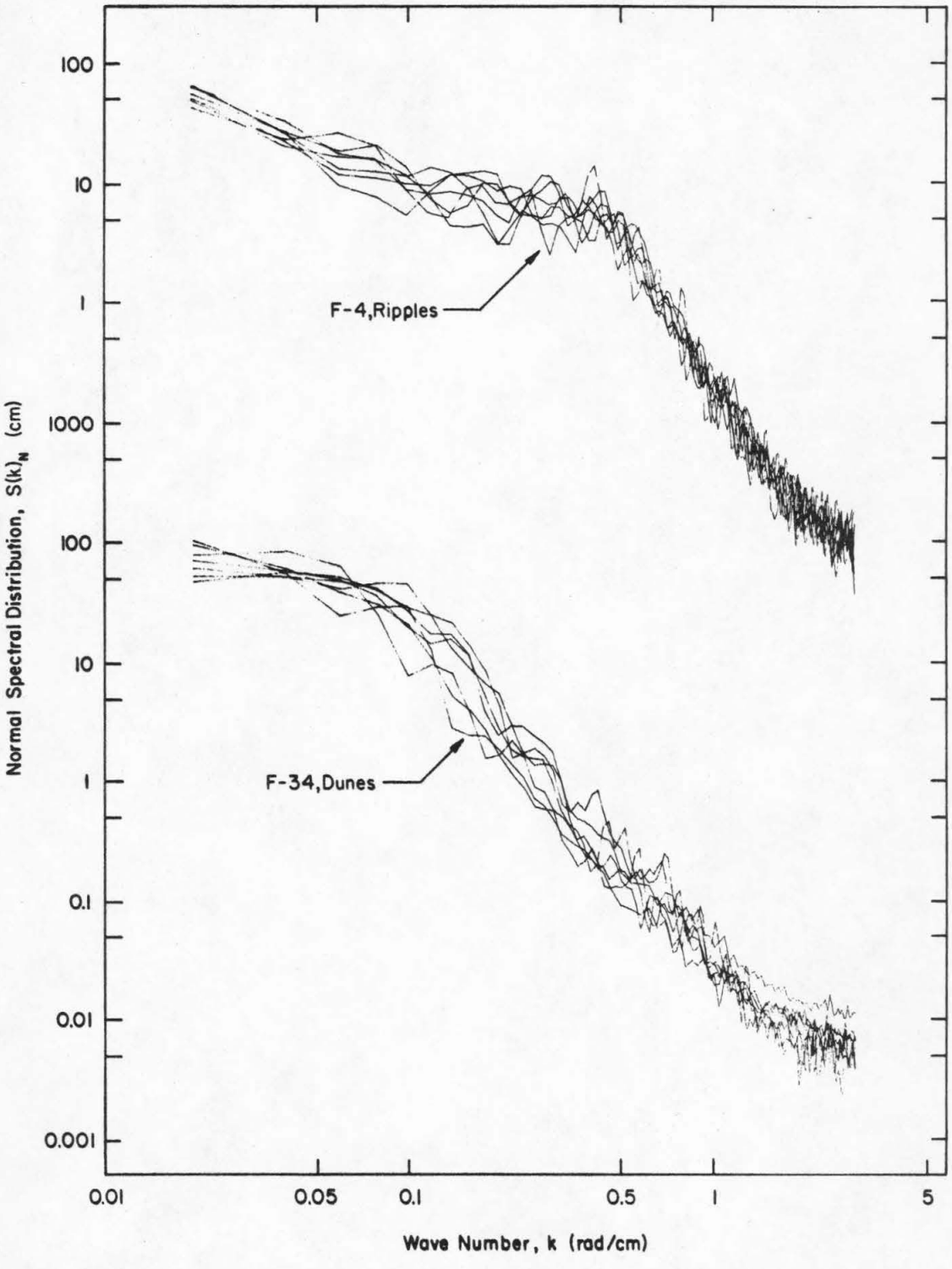

Fig. 5.26. Examples of variation in spectral distributions computed for ripple (F-4) and dune (F-34) bed profile sets.

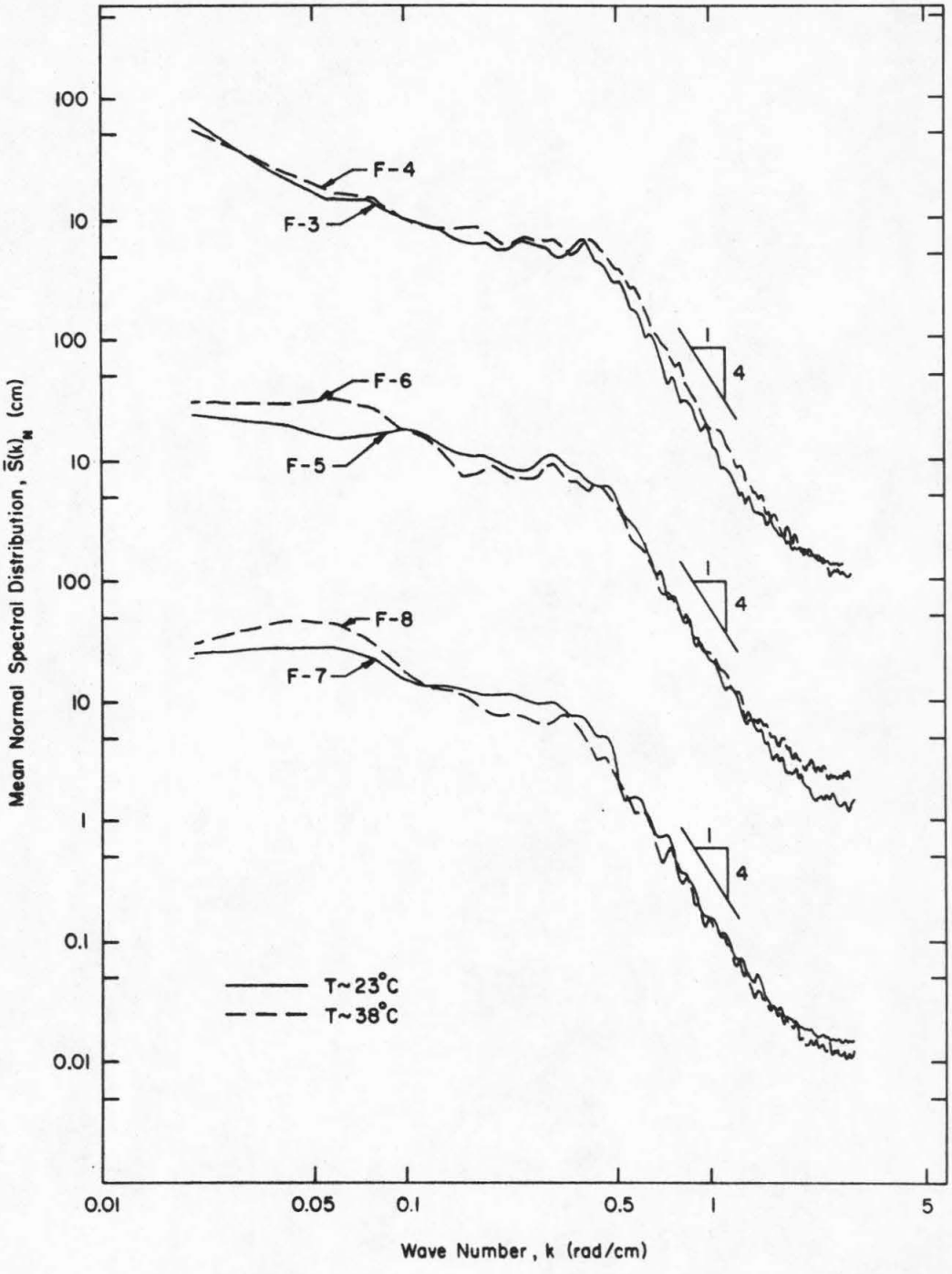

Fig. 5.27. Mean spectral distributions computed for ripple bed profile sets measured in experiment-pairs F-3, F-4; F-5, F-6; and F-7, F-8. In these experiments Q = 47.4 lit /sec; and the bed material was fine silica sand (D_g = 0.228 mm, σ_g = 1.52).

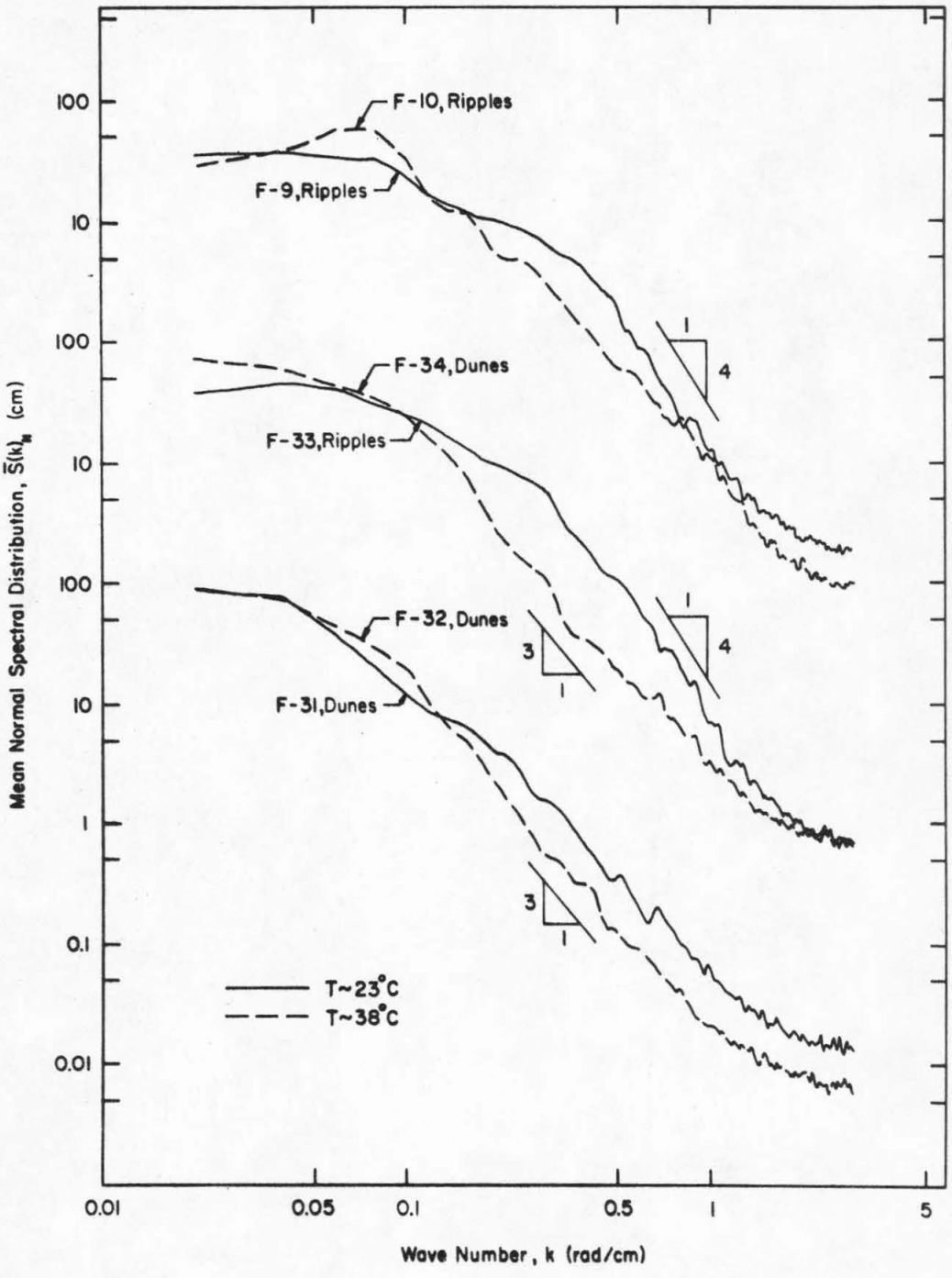

Fig. 5.28. Mean spectral distributions computed for bed profile sets measured in experiment-pairs F-9, F-10; F-33, F-34; and F-31, F-32. In these experiments Q = 47.4 lit /sec; and the bed material was fine silica sand (D_g = 0.228 mm, σ_g = 1.52).

spectral estimates for $k > 0.16$ rad/cm are less than in the cold water experiment F-9, but over the range $k = 0.04$ to 0.12 rad/cm the warm water spectral estimates are considerably larger than those for the cold water flow. These differences suggest that the relative contribution to the bed variance of the longer bed wave lengths was greater in experiment F-10 than in F-9, and thus are similar to those that might be expected if the dominant bed wave lengths in F-10 were larger than those in F-9.

The differences in experiment-pair F-33 and F-34 between the cold and warm water spectral distributions resemble those in F-9 and F-10, but are more pronounced. In experiment F-34 (Fig. 5.28) the mean spectral estimates are significantly less than those of F-33 for $k > 0.1$ rad/cm; but for wave numbers smaller than 0.1 rad/cm the warm water mean spectral estimates are larger. These differences again are suggestive of the actual observed differences between the two bed configurations. In F-34 the dune bed waves were significantly longer than the bed ripples present in experiment F-33; and thus it might be expected that the relative spectral contributions of the smaller wave numbers (larger bed wave lengths) in F-34 would be larger than those in F-33.

In experiments F-31 and F-32 the bed form was dunes in both the cold and warm water flows. The spectral distributions for these experiments given in Fig. 5.28 are similar in shape. However, the differences between the cold and warm water spectral distributions

over the intermediate wave numbers (near k = 0.09 rad/cm) and the higher wave numbers (k > 0.13 rad/cm) allude to larger bed wave lengths in the warm water flow, F-32.

In Table 5.6 the mean distance between alternate zero crossings ($\overline{\lambda}_o$) and mean variance ($\overline{\sigma}^2$) are given for the bed profiles used in the computation of the mean spectral distributions in Figs. 5.27 and 5.28. These data also reflect the changes in bed form observed in the constant-discharge experiments. In the experiments where there were dunes on the bed the measured values of $\overline{\sigma}^2$ and $\overline{\lambda}_o$ are more than twice as large as the corresponding values in the rippled-bed experiments. Crickmore (1970) has presented data which indicate that the average of the highest one-third differences between bed wave crest elevation and the next downstream trough, also called the significant wave height, is directly proportional to $\overline{\sigma}$, the standard deviation of the bed function. His data also indicate that the average wave length based on alternate changes in slope varies directly with $\overline{\lambda}_o$. Therefore the differences in $\overline{\sigma}^2$ and $\overline{\lambda}_o$ measured in the constant-discharge experiments suggest that in the dune bed experiments the bed waves were significantly longer and of greater amplitude than those in the ripple-bed flows. Visual observations and the bed profiles measured during these experiments confirm these results.

The bed friction factor is plotted as a function of $\overline{\sigma}^2/\overline{\lambda}_o r_b$ in Fig. 5.29. $\overline{\sigma}^2/\overline{\lambda}_o r_b$ is similar to the bed roughness parameter $\overline{h}^2/\overline{\lambda} r_b$ where $\overline{h}$ is the mean height of bed waves, and $\overline{\lambda}$ is the mean bed length, proposed by Vanoni and Hwang (1967). In Fig. 5.29 the

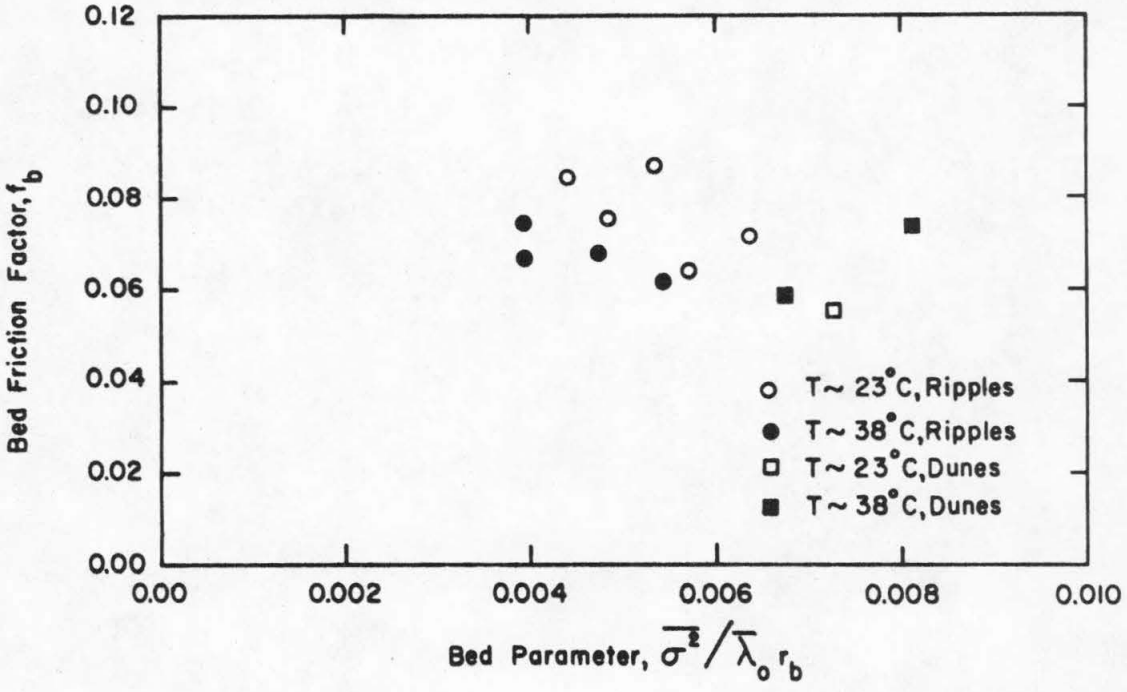

Fig. 5.29. Variation in $\overline{\sigma^2}/\overline{\lambda}_o r_b$ with bed friction factor for ripple and dune bed experiments of Series F. In these experiments Q = 47.4 l/sec; and the bed material was fine silica sand (D_g = 0.228 mm, σ_g = 1.52).

correlation between f_b and $\overline{\sigma}^2/\overline{\lambda}_o r_b$ is small; and the data indicate that this statistical parameter alone cannot be used to describe the hydraulic roughness of the bed.

The spectral distribution functions of Figs. 5.27 and 5.28 illustrate characteristically different shapes for the ripple and dune beds. With the ripple bed experiments (F-3 through F-9) the computed spectral distributions are relatively flat for wave numbers smaller than approximately 0.4 rad/cm; and for higher wave numbers the mean spectral estimates decrease at a rate proportional to k^{-4}. Whereas in the dune bed experiments (F-31, F-32, and F-34) the computed spectral distributions are relatively flat for k smaller than approximately 0.07 rad/cm, but the high wave number decay rate of the spectral distributions is reduced to k^{-3}.

These differences in shape suggest that in the rippled beds there was a broader range of wavelengths which contributed significantly to the bed variance than in the dune beds; but that the range of bed wavelengths present in the bed function was as large with dunes as with ripples. The ripple and dune bed profiles in Figs. 5.24 and 5.25 also indicate these bed form characteristics.

CHAPTER 6

DISCUSSION OF RESULTS

In this chapter consideration is given to experimental results presented in Chapter 5. The observed temperature effects on sediment discharge in low-transport, flat-bed flows are interpreted phenomenologically; and in the last section temperature effects on sediment discharge and bed configuration in natural streams are discussed, in view of results obtained in this study, and field observations.

6.1 LOW-TRANSPORT, FLAT-BED FLOWS

The different temperature effects on mean bed shear stress and sediment discharge observed in the low-transport, flat-bed experiments (Fig. 5.6) are suggestive of the complexity of the resistance and particle transport phenomena at the bed. These phenomena are not yet well understood, and thus the experimental results obtained in this study cannot be clearly interpreted phenomenologically. However in view of some recent turbulence measurements near the bed by Blinco and Partheniades (1971) it is possible to advance a plausible explanation for the observed temperature effects on sediment discharge.

Under low-transport, flat-bed conditions it is primarily the infrequent high-intensity turbulence bursts at the bed which accomplish the dislodgment and transport of bed particles. An increase in the

frequency of high-intensity bursts per unit area of the bed produces an increase in sediment discharge; and with a reduction in the frequency of bursts there is a reduction in sediment discharge.

Blinco and Partheniades measured turbulence intensities near the bed in clear-water flows with a smooth, flat bed; a bed covered with fixed sand particles (0.345 mm); and a bed of fixed silicon-carbide particles (2.45 mm). Their results given in Fig. 6.1, suggest that the dimensionless turbulence intensity $\sqrt{\overline{u'^2}}/U_{*b}$ (where $\sqrt{\overline{u'^2}}$ is the root-mean-square value of the longitudinal turbulence), near the bed is only weakly dependent on the size of the roughness elements and is primarily a function of the dimensionless elevation $y_* = U_{*b}y/\nu$. In these experiments y was measured from an elevation $0.27\ D_s$ below the tops of the particles, where D_s is the mean diameter of the uniform bed particles. Thus $y_* = 0.27\ R_{*b}$ at the top edge of the bed particles.

The results given in Fig. 6.1 indicate that for boundary Reynolds numbers less than a value near 36 ($y_* < 10$) with an increase in water temperature there is an increase in turbulence intensity near the tops of the bed particles. But for values of R_{*b} larger than 36 with an increase in temperature there is a reduction in $\sqrt{\overline{u'^2}}$ near the tops of the particles. These changes in $\sqrt{\overline{u'^2}}$ with temperature are similar to those observed on sediment discharge in Series B, H, and C. The increase in sediment discharge with increase in water temperature in the experiment-pairs of Series B ($R_{*b} < 13$) corresponds with an increase in $\sqrt{\overline{u'^2}}$ according to the results given in

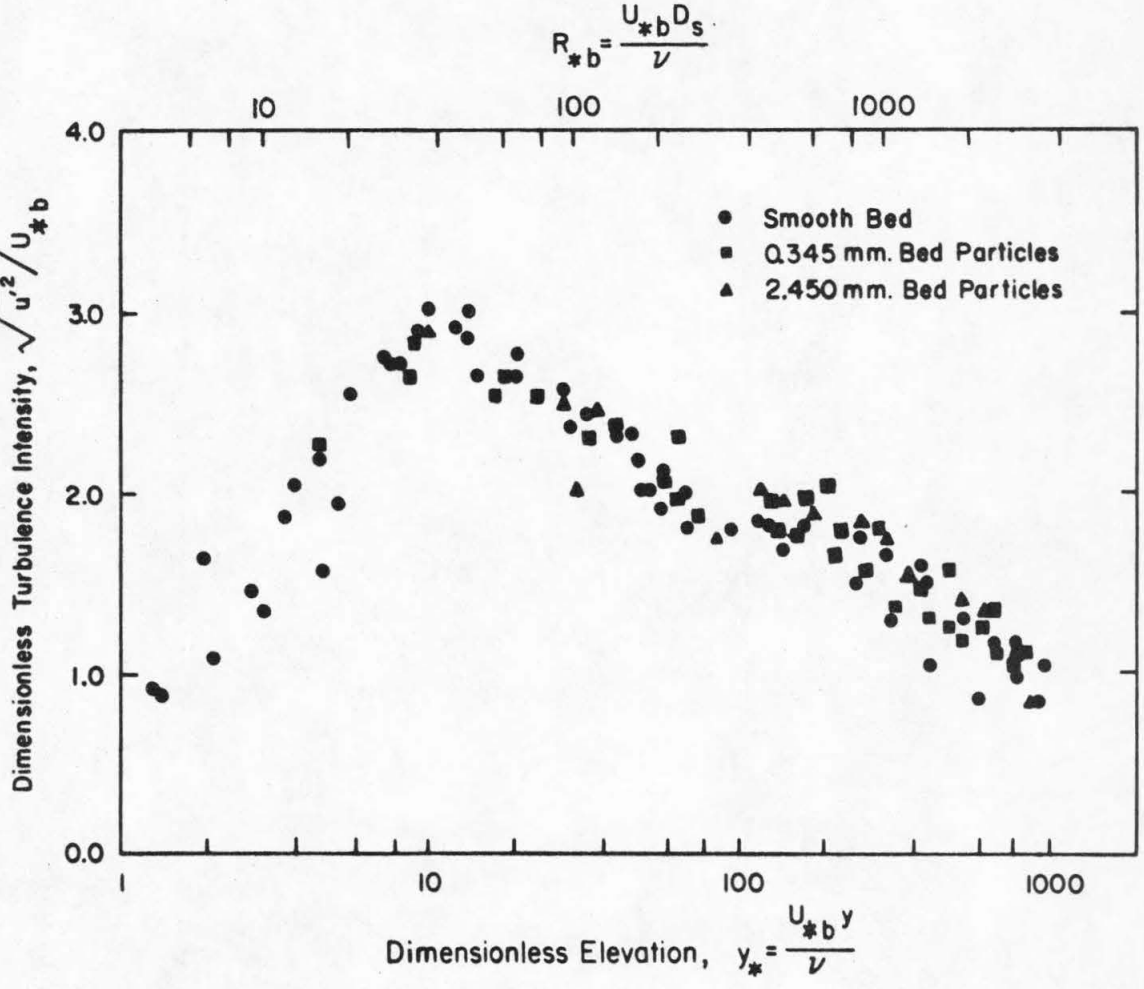

Fig. 6.1. Dimensionless turbulence intensity versus dimensionless distance above bed for clear-water experiments with a smooth, flat bed; a bed covered with 0.345 mm sand particles; and a bed covered with 2.45 mm silicon-carbide particles. (After Blinco and Partheniades (1971)).

Fig. 6.1. In Series H and C where the values of R_{*b} were larger the decreases in sediment discharge with increase in water temperature may correspond to reductions in $\sqrt{\overline{u'^2}}$ according to Fig. 6.1.

The data presented in Fig. 6.1 also indicate that the relative change in $\sqrt{\overline{u'^2}}$ with increase in water temperature is larger for values of $U_{*b}y/\nu$ less than 36 than for higher values. If the prior hypothesis relating changes in $\sqrt{\overline{u'^2}}$ with changes in sediment discharge is correct, these results suggest that the relative change in sediment discharge with increase in water temperature would be larger in flows wherein the boundary Reynolds numbers are small than in those having values of R_{*b} larger than approximately 36. The data from Series B, H and C reflect this difference. In Series B where the boundary Reynolds numbers were small three to five-fold changes in sediment discharge were observed with an increase in water temperature of approximately $15^{\circ}C$; whereas in Series H and C ($R_{*b} > 21$) with temperature increases of $15^{\circ}C$ to $20^{\circ}C$ the relative changes in sediment discharge were perhaps half as large as those in Series B.

The observed temperature effects on τ_{ob} in the low-transport, flat-bed experiments are similar to those observed in pipe flows. However, whereas in pipes it has been observed that fully-rough flow obtains at boundary Reynolds numbers larger than 100, the data from Series C and E indicate that fully-rough flow is first achieved at a value of R_{*b} near 200 with a flat bed.

Data from Series B, C and H suggest that the normalized function

$$(q_{*b})_N = (\tau_{ob})_N^{17.5} \tag{6.1}$$

closely approximates the normalized sediment discharge functions defined by the experiments in these series (see Fig. 5.8). By extrapolating Eq. (6.1) six points on the dimensionless transport contour $q_{*b} = 10^{-2}$ have been solved for using data from Series B, C, and H. The six points are plotted in Fig. 6.2. A smooth transport contour fitted to these points lies near the Shields Curve. This contour indicates that the incipient transport data compiled by Shields and others corresponds with a dimensionless sediment discharge on the order of 10^{-2}. It also suggests that the dimensionless sediment discharge contours in this region have a somewhat narrower and deeper trough than the curve constructed by Rouse. These differences in shape are qualitatively the same as those between the Shields Curve and the theoretical curve for incipient particle transport presented by Egiazaroff (1967).

Data from Series B, C, G, and H show that in low-transport, flat-bed flows the load characteristics of a silica bed material depend primarily on D_g and σ_g. It was found that the geometric mean size of the load could be closely approximated by the relation

$$d_g = D_g \sigma_g \tag{6.2}$$

and the geometric standard deviation of the load by

$$s_g = 0.96 \sigma_g \tag{6.3}$$

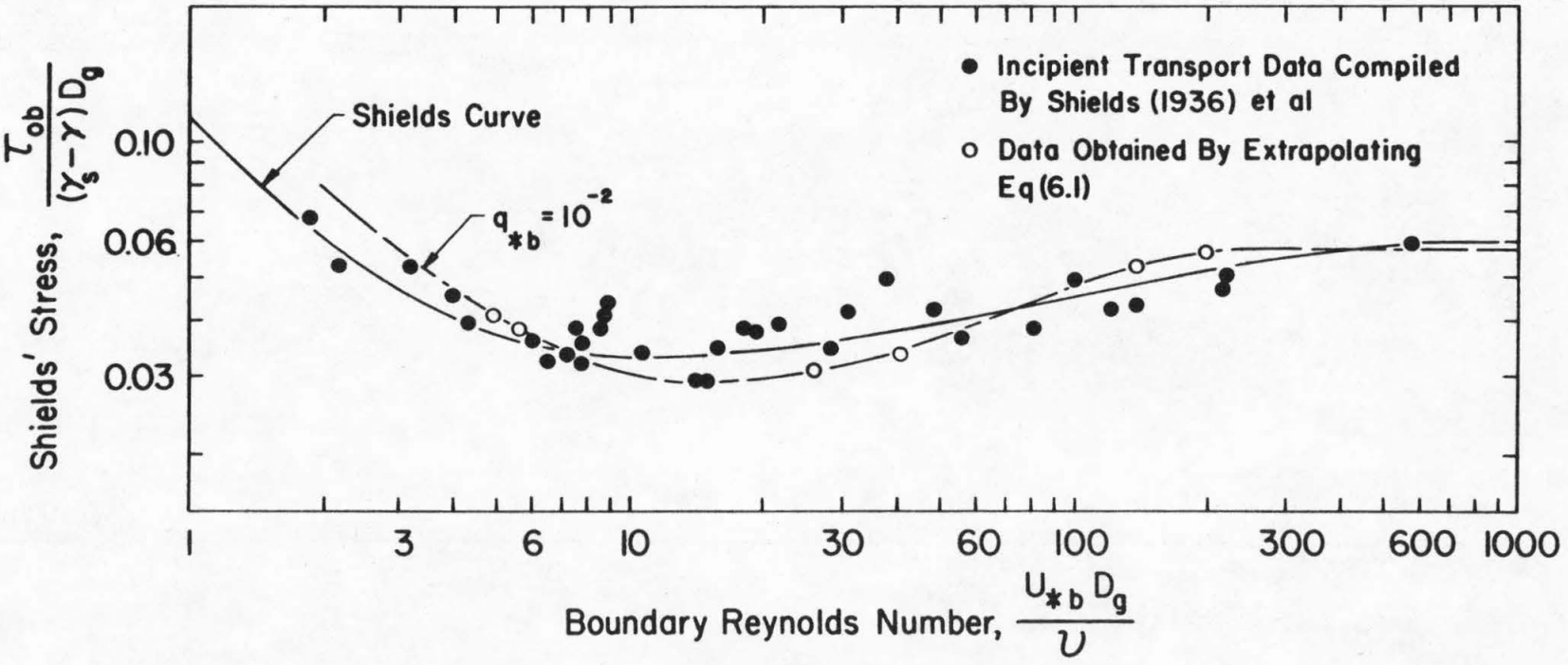

Fig. 6.2. Plot of dimensionless transport contour $q_{*b} = 10^{-2}$, and incipient transport curve fitted to Shields (1936) data by Rouse (1939).

These results however, were obtained with bed materials of $\sigma_g < 1.5$, and may not be correct in flows where there are larger size differences in the bed material.

6.2 HIGH-TRANSPORT, FLAT-BED FLOWS

In the high-transport, flat-bed experiments (F-23, F-24, F-27, F-28, G-9, and G-10) where there was suspended sediment transport, the temperature effects on bed-load discharge based on particle boundary Reynolds numbers were qualitatively the same as those which obtain in low-transport, flat-bed flows. These results indicate that under high-transport, flat-bed conditions the boundary Reynolds numbers of individual bed material sizes based on mean bed shear stress may be used to characterize the different flow conditions experienced by the bed particles. The data from experiment-pair F-27, F-28 also indicate that there can be contrary temperature effects on bed-load discharge among different size fractions of the bed material, i.e. an increase in the discharge of particles in some size fractions and a decrease in others.

6.3 CONSTANT-DISCHARGE FLOWS

The results obtained in the constant-discharge experiments illustrate the complex effects that water temperature can have on sediment discharge and bed geometry in a stream with a fine sand bed.

It is not possible to give a clear interpretation of these results. However, with the data presented in Section 5.3 and data from other experiments made during this investigation it is possible to identify pertinent variables and how they affect sediment discharge and bed configuration.

Data from experiment-pair F-23 and F-24 wherein the bed was flat, indicate that the bed-load discharge was larger in the warm water flow. In these experiments the boundary Reynolds numbers were less than 13. According to the bed-load discharge hypothesis presented in Section 5.2.1 for this range of boundary Reynolds numbers with an increase in water temperature there will be an increase in bed-load discharge. Also it may be argued that in flows over ripple and dune beds wherein the boundary Reynolds numbers, ($R'_{*b} = U'_{*b}D_g/\nu$) based on grain roughness bed shear stress are less than 13 the bed-load discharge in a warm water flow would be larger than in a cold water flow at the same velocity and depth. In all of the constant-discharge experiments wherein there were ripples and dunes on the bed the values of R'_{*b} were less than 13 because of the lower velocities in these experiments. Thus it might be expected that in each of these experiment-pairs, F-3, F-4; F-5, F-6; F-7, F-8; F-9, F-10; F-33, F-34; and F-31, F-32, the bed load discharge was larger in the warm water flow. In experiment-pair F-3 and F-4 wherein the bed was rippled and all of the sediment discharge moved as bed load, a larger bed-load discharge was in fact measured in the warm water flow.

In the ripple and dune experiment-pairs it was observed that the transition to dunes, a bed wave phenomenon generally associated with higher velocities than ripples, was accomplished at a lower velocity in the warm water flow. Thus the warm water development of the bed "led" that in the cold water flow. In experiments F-33 and F-34 wherein the change in bed form with increase in water temperature was observed, $R'_{*b} \sim 4$, and 6, respectively.

Similar temperature effects on bed form were observed in high-transport experiments G-8 and G-9 made in the 40-ft flume. The basic hydraulic data for these experiments are given in Table 6.1.

Table 6.1 Data From High-Transport, Flat-Bed Experiments G-8 and G-9 wherein H = 7.83 cm, and the Bed Material was Well-Sorted ($\sigma_g \sim 1.25$), Naturally-Worn Silica.

Run	U Mean Velocity (cm/sec)	T Water Temperature (^{o}C)	D_g Geom. Mean Diameter (mm)	R_{*b} Boundary Reynolds No.	Bed Form
G-8	65.2	23.0	0.191	7.70	Flat
G-9	58.5	48.0	0.138	7.82	Flat

In experiments G-8 and G-9 the beds were uniformly flat. After these experiments had been completed the water temperature was changed to study its effect on the flows. When the water temperature was increased approximately 25^{o}C in G-8 the bed form changed to mild antidunes with in-phase surface waves; and in G-9 when the

temperature was reduced 25°C relatively long, small amplitude, dune-like waves appeared on the bed. Since the R_{*b} values in these experiments were between 7 and 8, it is to be expected that an increase in temperature of 25°C will cause a significant increase in bed-load discharge, and conversely with a temperature reduction of 25°C the bed-load discharge will be reduced.

These experimental results (F-33, F-34, G-8, and G-9) indicate that in flows where the values of R'_{*b} are small, with an increase in water temperature and thereby a probable increase in bed-load discharge, warm water bed development leads that in a cold water flow at the same discharge and depth.

6.4 TEMPERATURE EFFECTS IN NATURAL STREAMS

Flow conditions in a natural stream may be considerably different from those which obtain in a laboratory flume. Natural streams are usually much larger than laboratory flows, and as explained by Kennedy and Brooks (1963) the constraints-slope, depth, and velocity, are somewhat different. In addition natural streams are generally unsteady and non-uniform. These differences sometimes make it difficult to extend laboratory results to the case of a natural stream. However, the basic mechanisms involved in sediment transport and bed deformation must be similar, and in this regard a natural stream is closely related to laboratory flows.

In natural streams including the Missouri River at Omaha, Nebraska it has been observed that at a given discharge as water temperature is reduced large bed waves present in the warm water flow are washed out and the cold water bed configuration approaches a flat bed. With this reduction in temperature and change in bed form large increases in suspended load discharge have also been measured. Observations of the Missouri River indicate that the water temperature varies from 80°F in August to 45°F in November, and that in the central section of the channel H ~ 16 ft, and S_f ~ 0.8 ft/mile. Thus boundary Reynolds numbers for the cold and warm water flows are approximately 13 and 21, respectively (D_g ~ 0.22 mm).

In Table 6.2 R_{*b} values are given for the Middle Loup River in Nebraska, the Lower Colorado, and the Lower Mississippi wherein observed temperature effects on suspended sediment discharge, and bed roughness are similar to those on the Missouri River. In each case the cold and warm water values of R_{*b} are approximately the same as those in the Missouri River. In these rivers R'_{*b} is perhaps 30% to 60% less than the values of R_{*b} given in Table 6.2. (At 45°F the bed is more nearly flat and thus the values of $R_{*b}(45^\circ F)$ are reduced less than those at 80°F.) This reduction in R_{*b} places the R'_{*b} values for the rivers in the range ~10 to 20. In this range, the temperature effect on bed-load discharge probably changes sign. A transition of this kind is suggested in the low-transport, flat-bed experiments (Fig. 5.7), and the concentration profiles of high-transport, flat-bed experiments F-23, F-24, F-27, and F-28. With boundary Reynolds

Table 6.2 Data From Natural Streams

	D_g Geom. Mean Size of Bed Sediment (mm)	H Depth (ft)	S_f Friction Slope	$R_{*b}(45^oF)$ Boundary Reynolds No. at 45^oF	$R_{*b}(80^oF)$ Boundary Reynolds No. at 80^oF
Missouri River	0.22	16	0.000151	13	21
Middle Loup River	0.32	1	0.00133	14	23
Lower Colorado	0.32	10	0.000217	18	30
Lower Mississippi	0.30	30	0.000085	18	29

numbers (R'_{*b}) below this range an increase in bed-load discharge with increase in water temperature is expected; and above this range a reduction in bed-load discharge with increase in water temperature is expected. Thus between 10 and 20 the net temperature effect on bed-load discharge will depend on the distribution of bed material sizes, and the corresponding particle boundary Reynolds numbers.

The temperature effect on bed configuration over the range ~10 to 20 may be different from those which obtain at lower values of R'_{*b}. In a pair of experiments (F-25e, F-26e; in which U ~ 67 cm/sec, H ~ 8.3 cm) made in conjunction with the constant-discharge experiments, it was observed that the bed was uniformly flat with a water temperature of 23°C but at 38°C small intermittent dune-like wave fronts passed through the flume. In F-25e and F-26e the values of R'_{*b} were near the lower end of the 10 to 20 range. These observations indicate that in F-25e and F-26e the cold water bed development led that in the warm water flow; and a flat bed obtained at a lower velocity with the cold water. However in these experiments the velocity and thus the values of R'_{*b} were less than those in experiments F-23 and F-24 where there was a larger bed-load discharge in the warm water flow. Thus in F-25e and F-26e the bed-load discharge was probably larger in the warm water experiment. These data suggest that at a given velocity and depth an increase in bed-load discharge with increase in water temperature does not necessarily indicate that warm water bed development will lead that in the cold water flow. Or stated another way, bed development is not uniquely determined by bed-load discharge. This conclusion is also suggested by results obtained in the low-transport, flat-bed, instability experiments presented in Appendix F.

The temperature effect on bed form observed in experiment-pair F-25e and F-26e is similar to those observed in natural streams, where the values of R'_{*b} are also in the ~10 to 20

range. In each case dune-like bed waves were observed in the warm water flow but at a lower water temperature the bed form became flat.

These results may explain the contrary temperature effects on bed roughness observed in laboratory flows and natural streams. In laboratory flows the bed form is usually ripples, and R'_{*b} is small. Under these conditions the warm water bed development leads the cold water development; with the result that at a given velocity (discharge constant) cold water ripples are characteristically rougher, whereas in natural streams the bed form is dunes and the values of R'_{*b} are somewhat larger. In this case the cold water bed development leads and a flat bed, with a corresponding reduction in bed roughness, may obtain at a lower velocity than in a warm water flow at the same discharge.

CHAPTER 7

SUMMARY OF CONCLUSIONS

The conclusions listed below are based on data from 1) the low-transport, flat-bed experiments wherein the bed materials ranged from fine sand to coarse, clay-aggregate particles approximately 18.5 mm in diameter. In these experiments the bed shear stresses were near the critical values for incipient particle transport and all sediment discharge was by rolling and sliding along the bed; 2) the high-transport experiments with fine sands where the bed was flat, and there was considerable suspended load discharge; and 3) the experiments with fine sand wherein the discharge was held constant and the velocity was varied to produce ripple, dune, and flat bed forms.

In each case experiments were made in pairs wherein the mean velocity and depth were the same or nearly the same, but in one experiment of the pair the water temperature was from 15°C to 25°C higher than in the other.

7.1 CONCLUSIONS BASED ON DATA FROM LOW-TRANSPORT, FLAT-BED EXPERIMENTS

1. In flat-bed flows where all of the sediment discharged moves by rolling and sliding along the bed the effect of a change in water temperature on sediment discharge depends on the flow condition

at the bed. Under hydrodynamically smooth conditions with an increase in water temperature there is an increase in sediment discharge; whereas in the transition between smooth and rough with an increase in temperature sediment discharge is reduced. With fully-rough flow at the bed sediment discharge does not change with change in water temperature.

2. In low-transport, flat-bed flows the dimensionless sediment discharge function may be expressed as

$$q_{*b} = \varphi\left(\tau_{*b},\ R_{*b},\ \frac{\rho_s}{\rho},\ \sigma_g,\ \text{S. F.}\right) \qquad (7.1)$$

and thus the temperature effect on sediment discharge can be given in terms of τ_{*b} and R_{*b}.

3. In low-transport, flat-bed flows hydrodynamically smooth conditions obtain for R_{*b} less than a value near 13, and fully-rough flow is achieved at R_{*b} larger than approximately 200. Between these values of R_{*b} the flow is in transition.

4. The transport contour $q_{*b} = 10^{-2}$ follows closely the incipient transport data compiled by Shields (1936). This contour has the same characteristic shape as the incipient transport curve constructed by Rouse (1939), but has a deeper and narrower trough than Rouse's curve. Also the minimum value of τ_{*b} on the transport contour is achieved near $R_{*b} = 13$ whereas Rouse's minimum is reached at $R_{*b} \sim 10$.

5. In low-transport, flat-bed flows with a naturally-worn, silica bed material the load characteristics depend only weakly on sediment discharge and the flow condition at the bed; and may be predicted from the bed material characteristics according to the following relations,

$$d_g = \sigma_g D_g \tag{7.3}$$

$$s_g = 0.96 \sigma_g \tag{7.4}$$

7.2 CONCLUSIONS BASED ON DATA FROM HIGH-TRANSPORT, FLAT-BED EXPERIMENTS

1. In flat bed flows wherein there is suspended sediment discharge, the effects of temperature on bed-load discharge are similar to those in low-transport, flat-bed flows. For boundary Reynolds numbers less than a value near 13 with an increase in water temperature there is an increase in bed-load discharge, whereas for boundary Reynolds numbers larger than approximately 20 with a temperature increase there is a reduction in bed-load discharge.

2. The qualitative temperature effects on bed-load discharge of different size particles in a graded bed sediment can be characterized by the boundary Reynolds numbers of the particles based on mean bed shear stress. Thus in flows where the particle boundary Reynolds numbers range from values less than approximately 13 to values larger than 20, an increase in temperature may produce an increase in bed-load discharge for the finer particles and a decrease for the coarser ones.

3. For fine sands a plot of ω/β versus ω_s approximates a linear relation. This linear relation indicates that for $\omega = \omega_s$, $\beta = 1.0$.

7.3 CONCLUSIONS BASED ON DATA FROM CONSTANT-DISCHARGE EXPERIMENTS

1. In a stream with a rippled bed of fine sand an increase in water temperature (discharge and depth held constant) may effect either an increase or a reduction in sediment discharge and bed roughness.
2. In rippled-bed flows over fine sand the hydraulic roughness of the bed with warm water is less than that which obtains in a cold water flow at the same discharge and depth.
3. Under certain conditions an increase in water temperature alone can accomplish a change in bed form.
4. The observed changes in bed form with change in water temperature indicate that in flows where R'_{*b} is less than a value near 8 warm water bed development leads that which obtains in a cold water flow at the same discharge; and thus the transition from ripples to dunes is accomplished at a lower velocity in the warm water flow.
5. The normalized spectral distributions for ripples are characteristically different from those for dunes. These characteristic differences correspond with observable geometric differences in the bed forms.
6. The statistical bed parameter $\overline{\sigma^2}/\overline{\lambda}_o r_b$ alone cannot be used to describe the hydraulic roughness of an alluvial bed.

7. Field data from the Missouri, Middle Loup, Lower Colorado, and Lower Mississippi Rivers indicate that in these natural streams the boundary Reynolds numbers based on grain roughness shear stress are between ~10 and 20. For these values of R'_{*b} laboratory and field data indicate that: a) the net temperature effect on bed-load discharge depends on the distribution of bed material sizes, and the corresponding particle boundary Reynolds numbers; and b) bed development in a cold water flow leads that which obtains in a warm water flow at the same discharge; and thus the transition from dunes to a flat bed is accomplished at a lower velocity in the cold water flow.

LIST OF REFERENCES

Ashida, K., and Tanaka, Y., "A Statistical Study of Sand Waves", Proc. 12th Congress, IAHR, Vol. 2, 1967, pp. 103-110.

Blackman, R. B., and Tukey, J. W., The Measurement of Power Spectra, from the Point of View of Communications Engineering, Dover Publications, New York, 1958.

Blinco, P. H., and Partheniades, E., "Turbulence Characteristics in Free Surface Flows over Smooth and Rough Boundaries", Jour. of Hydr. Res., Vol. 9, No. 8, 1971, pp. 43-69.

Burke, P. P., "Effect of Water Temperature on Discharge and Bed Configuration, Mississippi River at Red River Landing, Louisiana", U. S. Army Engineering District, New Orleans, 1965.

Carey, W. C., "Effect of Temperature on Riverbed Configuration: Its Possible Stage-Discharge Implications", Proc. of Fed. Inter-Agency Sed. Conf. Misc. Publ. No. 970, Agricultural Research Service, USDA, 1963, pp. 237-272.

Colby, B. R., "Discharge of Sands and Mean-Velocity Relationships in Sand-Bed Streams", U. S. Geol. Survey Professional Paper 462-A, 1964.

Colby, B. R., and Scott, C. H., "Effects of Water Temperature on the Discharge of Bed Material", U. S. Geol. Survey Water-Supply Paper 462-G, 1965.

LIST OF REFERENCES (continued)

Crickmore, M. J., "Effect of Flume Width on Bed-Form Characteristics", Jour. of Hyd. Div., ASCE, Vol. 92, No. HY2, 1970, pp. 473-496.

Einstein, H. A., "The Bed-Load Function for Sediment Transportation in Open Channel Flows", U. S. Dept. Agriculture Tech. Bull. 1026, 1950.

Einstein, H. A., and Chien, N., "Effects of Heavy Sediment Concentration Near the Bed on Velocity and Sediment Distribution", Univ. of Calif., Inst. of Eng. Research, U. S. Army Corps of Engineers, Missouri River Div. Sediment Ser. No. 3, 1955.

Einstein, H. A., and El-Samni, E. A., "Hydrodynamic Forces on a Rough Wall", Reviews of Modern Physics, Vol. 21, No. 3, 1949, pp. 520-524.

Fleck, J. T., "Power Spectrum Measurements by Numerical Methods", Cornell Aero. Lab., Report No. 85-440-1, 1957.

Franco, J. J., "Effects of Water Temperature on Bed-Load Movement", Jour. of Waterways and Harbours Div., ASCE, Vol. 94, WW3, 1968, pp. 343-352.

Hino, M., "Equilibrium - Range Spectra of Sand Waves Formed by Flowing Water", Jour. of Fluid Mech., Vol. 34, Part 3, 1968, pp. 565-573.

LIST OF REFERENCES (continued)

Ho, P., "Abhangigkeit der Geschiebebewegung von der Kornform und der Temperature", Mitteilungen der Preubischen Versuchsanstalt fur Wasser-, Erd- und Schiffbau, Berlin, Germany; translated to English by Q. M. Saleh, Nat. Bur. of Stds., Washington, D. C., 1939.

Hubbel, D. W., and Ali, K. A., "Qualitative Effects of Temperature on Flow Phenomena in Alluvial Channels", U. S. Geol. Survey Short Papers in Geologic and Hydraulic Sciences, Art. No. 301, 1961, pp. D21-D23.

Igiazaroff, I. V., Discussion of "Sediment Transportation Mechanics: Initiation of Motion" by Task Committee on Preparation of Sedimentation Manual, ASCE, Jour. of Hyd. Div., ASCE, Vol. 93, No. HY4, 1967, pp. 281-287.

Johnson, J. W., "The Importance of Side-Wall Friction on Bed-Load Investigations", Civil Engineering, Vol. 12, No. 6, 1942, pp. 329-331.

Karaki, S. S., Gray, E. E., and Collins, J., "Dual Channel Stream Monitor", Jour. of Hyd. Div., ASCE, Vol. 87, No. HY6, 1961, pp. 1-16.

Kennedy, J. F., and Brooks, N. H., "Laboratory Study of an Alluvial Stream at Constant Discharge", Proc. of Fed. Inter-Agency Sed. Conf., Misc. Publ. No. 970, Agricultural Research Agency, USDA, 1963, pp. 320-330.

LIST OF REFERENCES (continued)

Keulegan, G. H., "Laws of Turbulent Flow in Open Channels", Nat. Bur. of Stds., Jour. of Res., Vol. 21, 1938, pp. 707-741.

Lane, E. W., Carlson, E. J., and Hanson, C. S., "Low Temperature Increases Sediment Transportation in Colorado River", Civil Engineering, Vol. 19, No. 9, 1949, pp. 45-46.

Mostafa, M. G., "Analytical and Experimental Study of the Effects of Flow Characteristics and Fluid Viscosity Upon the Movement of Bed-Load in an Open Channel", Ph. D. Thesis in Civil Engineering, Univ. of Minnesota, 1949.

Nordin, C. F., and Algert, J. H., "Spectral Analysis of Sand Waves", Jour. of Hyd. Div., ASCE, Vol. 92, No. HY5, 1966, pp. 95-114.

Okoye, J. K., "Characteristics of Transverse Mixing in Open-Channel Flows", W. M. Keck Lab. of Hydraulics and Water Resources, Report No. KH-R-23, California Institute of Technology, 1970.

Okoye, J. K., and Raichlen, F., "Description and Operation of Analog-To-Digital Data Acquisition System," W. M. Keck Lab. of Hydraulics and Water Resources, Tech. Memo 69-9, California Institute of Technology, 1969.

Rouse, H., "Modern Conceptions of the Mechanics of Fluid Turbulence", Transactions, ASCE, Vol. 102, 1937, pp. 463-505.

Rouse, H., "An Analysis of Sediment Transportation in the Light of Fluid Turbulence", Soil Conservation Service Report No. SCS-TP-25, USDA, 1939.

LIST OF REFERENCES (continued)

Shields, A., "Anwendung der Aenlichkeitsmechanik und der Turbulentzforschung auf die Geschiebebewegung", Mitteilungen der Preussischen Versuchsanstalt fur Wasserbau und Schieffbau, Berlin, Germany; translated to English by W. P. Ott and J. C. van Uchelen, California Institute of Technology, 1936.

Squarer, D., "Friction Factors and Bed Forms In Fluvial Channels", Jour. of Hyd. Div., ASCE, Vol. 96, No. HY4, 1970, pp. 995-1017.

Straub, L. G., Anderson, A. G., and Flammer, G. H., "Experiments on the Influence of Temperature on the Sediment Load", Univ. of Minn., St. Anthony Falls Hydraulic Lab., U. S. Army Corps of Engineers, Missouri River Div. Sediment Ser. No. 10, 1958.

Task Committee on Preparation of Sedimentation Manual, ASCE, "Sediment Transportation Mechanics: Introduction and Properties of Sediment", Jour. of Hyd. Div., ASCE, Vol. 88, No. HY4, 1962, pp. 77-107.

Task Committee on Preparation of Sedimentation Manual, ASCE, "Nomenclature for Bed Forms In Alluvial Streams", Jour. of Hyd. Div., ASCE, Vol. 92, No. HY3, 1966, pp. 51-64.

U. S. Army Corps of Engineers, "Missouri River Channel Regime Studies", U. S. Army Corps of Engineers, Missouri River Div. Sediment Ser. No. 13B, 1969.

LIST OF REFERENCES (continued)

Vanoni, V. A., "Transportation of Suspended Sediment in Water", Transactions, ASCE, Vol. 111, 1946, pp. 67-133.

Vanoni, V. A., and Brooks, N. H., "Laboratory Studies of the Roughness and Suspended Load of Alluvial Streams", California Institute of Technology, Sedimentation Lab., U. S. Army Corps of Engineers, Missouri River Div. Sediment Ser. No. 11, 1957.

Vanoni, V. A., and Hwang, L., "Relation Between Bed Forms and Friction in Streams", Jour. of Hyd. Div., ASCE, Vol. 93, No. HY3, 1967.

APPENDIX A

SUMMARY OF NOTATION

a	distance from stream bed to some arbitrary reference level
A	empirical coefficient in sediment discharge equation $Q_{ss} = AU^b$
A_1	ratio of cross sectional area of bed particle to D^2
A_2	ratio of volume of sediment particle to D^3
A_3	ratio of exchange time for bed particle, to time required for particle to settle in fluid through distance D
A_L	ratio of bed particle step length to D
A_{LO}	value of A_L under low-transport conditions
b	exponent in sediment discharge equation $Q_{ss} = AU^b$
C_1	low-transport sorting coefficient, $= d_g/D_g\sigma_g$
C_2	low-transport sorting coefficient, $= s_g/\sigma_g$
$C(y)$	concentration of suspended sediment of given size, shape, and density, at reference level y
$C(y, d_s)$	concentration of suspended sediment in size fraction d_s, at reference level y
d_g	geometric mean sieve size of load
d_s	geometric mean sieve size of size fraction
D	characteristic particle diameter
D_s	mean sieve size of sediment
D_g	geometric mean sieve size of bed material
D_{65}	particle size for which 65 percent by weight are finer

f	Darcy-Weisbach friction factor for channel, $= 8(U_*/U)^2$
f_b	friction factor of bed, $= 8(U_{*b}/U)^2$
$f(x)$	longitudinal bed profile
$f(x_i)$	digitized bed profile
F	Froude number of stream, $= U/\sqrt{gH}$
g	gravitational constant
g_s	sediment discharge per unit width
g_B	bed-load discharge per unit width
H	stream depth
$\bar{h}$	mean height of bed waves
i	indexing parameter
i_b	bed material fraction by weight, of size D
i_B	bed-load discharge fraction by weight, of size D
k	bed wave number, $= 2\pi/\lambda$
k_{max}	maximum wave number considered in spectral computation, $= \pi/\Delta x$
K	von Karman's universal constant
K_s	bed material roughness size
L	bed profile length
m	indexing parameter
M	number of lag intervals considered in autocovariance computation
N	number of samples in digitized bed profile
$( )_N$	normalized parameter

p_s load density

P time fraction during which bed particle exchange occurs per unit area

P_s probability of bed particle of diameter D being eroded during a second

q_{sb} volumetric bed-load discharge per unit width

q_{*b} dimensionless volumetric bed-load discharge per unit length, $= q_{sb}/U_{*b}D_g$

Q stream discharge

Q_{ss} suspended sediment discharge of stream

r hydraulic radius of channel, equal to the flow cross sectional area divided by the wetted perimeter

r_b hydraulic radius of bed

R stream Reynolds number, $= 4Ur/\nu$

R_* boundary Reynolds number of section, $= U_*D_s/\nu$

R_{*b} boundary Reynolds number of bed, $= U_{*b}D_g/\nu$

R'_{*b} boundary Reynolds number of bed based on grain roughness shear stress, $= U'_{*b}D_g/\nu$

R_μ bed grain Reynolds number, $= \frac{D_g^{3/2}}{\nu}\sqrt{\left(\frac{\gamma_s-\gamma}{\gamma}\right)g}$

$R(\tau)$ autocovariance function defined in Eq. (5.15)

s_g load geometric standard deviation of sizes

s_b bed slope

S_f friction slope, $= S_b$ for uniform flow

$S(k)$ spectral distribution function defined in Eq. (5.15)

S. F. shape factor of bed particles

S. G.$_w$ specific gravity of sediment determined by buoyant-weight analysis

$S.G._v$	specific gravity of sediment determined by volumetric analysis
t_l	exchange time of bed particles of size D
T	water temperature
u	velocity used by Einstein to compute lift on bed particles
$\sqrt{\overline{u'^2}}$	root-mean-square longitudinal turbulence intensity
U	mean stream velocity
U_*	shear velocity of section, $= \sqrt{\tau_{ob}/\rho}$
U_{*b}	shear velocity of bed, $= \sqrt{\tau_{ob}/\rho}$
U'_{*b}	bed shear velocity based on grain roughness shear stress, $= \sqrt{\tau'_{ob}/\rho}$
U_{*cl}	bed shear velocity along centerline of channel, $= \sqrt{gHS_f}$
W_{sa}	weight of sediment in air, in grams
W_{sw}	weight of sediment submerged in water, in grams
x	longitudinal coordinate along bed profile
X	reference level above bed defined in Eq. (2.7)
y	distance above stream bed
y_*	dimensionless elevation above bed, $= U_{*b}y/\nu$
Y	lift correction factor for bed mixtures
Z	exponent in suspended sediment distribution equation, $= \omega/\beta K U_{*b}$
β	ϵ_s/ϵ_m
γ	specific weight of fluid, $= \rho g$

γ_s specific weight of sediment, $= \rho_s g$

$(\gamma_s - \gamma)$ buoyant specific weight of sediment

δ' thickness of hypothetical viscous sublayer, $= 11.6\nu/U_{*b}$

Δk wave number interval, $= k_{max}/M$

Δv change in volume

Δx internal between digitized bed profile data points, $= x_{i+1} - x_i$

ϵ_m turbulent diffusion coefficient for momentum

ϵ_s turbulent diffusion coefficient for sand particles

λ bed wavelength

$\overline{\lambda}$ mean bed wavelength

$\overline{\lambda}_o$ mean distance between alternate zero crossings in bed profile

μ dynamic fluid viscosity

ν kinematic fluid viscosity

ξ sheltering correction factor defined in Einsteins bed-load function

ρ density of fluid

ρ_s density of bed sediment

$\overline{\sigma}$ mean standard deviation of bed profiles, $= \sqrt{\overline{\sigma^2}}$

σ^2 variance of bed profile defined in Eq. (5.14)

$\overline{\sigma^2}$ mean variance of bed profiles

σ_g geometric standard deviation of bed material sizes

τ lag interval in autocovariance function

τ_o mean shear stress of section

τ_{ob} mean bed shear stress

τ'_{ob} mean bed shear stress based on grain roughness

χ emperical factor in velocity distribution equation used by Einstein

ω particle fall velocity in turbulent shear flow

ω_s still-water particle fall velocity

APPENDIX B

FALL-VELOCITY SAND SEPARATION

In order to obtain uniform, naturally-worn bed materials for the experiments of Series G 7000 lbs of clean, well-graded silica sand (Nevada #60) was separated into eight well-sorted size fractions by a fall-velocity process. The apparatus that was used is described in Section B. 1; and the separation procedure is outlined in Section B. 2.

B. 1 APPARATUS

The separation was accomplished in a 130-ft recirculating flume located in the W. M. Keck Laboratory. The flume is 43 in. wide, 24 in. deep, and has a working length of 130 ft. Flume discharge is recirculated from an outlet basin to an inlet box by one of two variable-speed, axial-flow pumps located in separate return lines. The two 30 in. girders that support the flume are supported by a central hinge, and electrically-driven, screw-type jacks can be used to adjust the flume slope. Discharge is measured with a venturi tube in the return line which is connected to a water-mercury vertical differential manometer.

The flume bed is stainless steel, and the side walls are of glass (see Fig. B. 1) except for short sections at the upstream and downstream ends which are of stainless steel.

Fine-mesh screens can be positioned laterally in the flume just below the inlet to damp large scale turbulence present in the inlet box.

A wedge-shaped hopper 40 in. long and 29 in. deep constructed of 0.0938 in. steel plate was suspended laterally on the top of the flume side walls (see Fig. B.1). The hopper has a narrow opening at the bottom where the two side walls converge. The width of this opening can be changed by raising or lowering a narrow plate bolted through slotted holes to the bottom of one of the side plates. To insure steady and uniform sand discharge a variable-speed, pneumatic vibrator was clamped to the upstream side of the hopper.

The hopper was located approximately 60 ft downstream from the flume inlet to avoid the residual turbulence from the inlet screens. Also in order to avoid the turbulent boundary layers that developed along the flume side walls 10 in. at either end of the opening in the bottom of the hopper were closed off with masking tape.

Slot dividers were positioned along the flume bed downstream from the hopper (see Fig. B.1). The slots were positioned by trial and error so as to obtain eight well-sorted size fractions whose geometric mean sizes were uniformly distributed over the range 0.1 mm to 0.4 mm.

After separation the material in each bed slot was removed by siphoning a sand-water mixture through a 1 in. I.D. reinforced rubber hose to one of eight large cylindrical containers placed along side of the flume. The discharged sand settled to the bottom of the container and the water overflowed into a nearby floor drain.

Fig. B. 1 Upstream View of 130-ft Flume With Metal Hopper Mounted on Side Walls, And Metal Slot Dividers Positioned on Flume Bed. Note metal sheets which provided smooth transition from tops of end slots to flume bed. (Photo No. 11216)

The separated material was dried by placing it on a fine-mesh screen supported above a gas burner by an open-top-and-bottom rectangular box. The box and gas burner were positioned approximately two feet above the laboratory floor. As the wet sand dried it fell through the screen and box and accumulated on the floor where it was collected and stored in reinforced paper sacks.

B.2 SEPARATION PROCEDURE

The fall-velocity separation took several days. Each day after uniform flow conditions ($U \sim 12$ cm/sec, $H \sim 56$ cm, $T \sim 21^{\circ}C$) were established in the flume sand was added to the hopper, and the pneumatic vibrator was adjusted to maintain a hopper discharge of approximately 60 lbs of sand per hour. At higher discharges the sand particles interacted during their fall and the size separation was not as efficient. Fig. B.2 shows the sand plume which obtained for a hopper discharge near 60 lbs per hour.

After approximately 200 lbs of sand had been discharged through the hopper, separation was discontinued long enough to remove the material that had accumulated in the bed slots.

The characteristics of the eight size fractions obtained in the fall-velocity separation are given in Table B.1.

Fig. B.2 Sand Plume Which Obtained For Hopper Discharge of Approximately 60 lbs of Sand per hour; U ~ 12 cm/sec, H ~ 56 cm, T ~ 21°C.
(Photo No. 11217)

Table B. 1 Eight Size Fractions of Silica Sand Obtained in Fall-Velocity Separation.

Geom. Mean of Size Fraction (mm)	Geom. Std. Deviation of Size Fraction	Approximate Amount of Material Obtained (lbs)
0.112	1.25	100
0.138	1.25	370
0.158	1.21	940
0.191	1.26	1180
0.248	1.27	1220
0.319	1.20	940
0.357	1.23	800
0.397	1.14	920

APPENDIX C

TABULATION OF POINT VELOCITY AND POINT CONCENTRATIONS FOR HIGH-TRANSPORT, FLAT-BED EXPERIMENTS

Table C. 1. Point Velocity, and Point Sediment Concentrations Measured in Experiment-Pairs F-23, F-24; F-27, F-28; and G-9, G-10

Run No.	y Distance Above Bed (cm)	U(y) Point Velocity (cm/sec)	Point Sediment Concentration (ppm)	C(y, d_s) Point Sediment Concentrations For Different Size Fractions (ppm)								
				d_s = 0.081 (mm)	0.096	0.114	0.135	0.160	0.191	0.226	0.269	0.322
F-23	0.60	57.3										
	0.85	61.9	2580.	47.8	39.2	206.	393.	853.	373.	427.		
	1.85	70.1	581.	26.2	23.8	87.9	105.	203.	59.8	45.0		
	2.85	75.3	313.	30.0	24.6	63.4	65.3	83.5	17.5	8.61		
	3.85	77.1	209.	21.7	16.7	50.6	33.2	58.3	9.42	4.54		
	4.85	79.6	134.	19.4	14.4	30.4	23.7	25.0	6.25	-		
	5.85	82.0	88.6	13.8	7.08	20.2	15.3	14.3	2.66	2.48		
	6.85	82.9	60.2	7.52	5.27	9.66	10.9	12.5	1.32	-		
F-24	0.45	53.0										
	0.70	58.2	3610.	220.	217.	743.	804.	877.	255.	237.		
	1.70	67.7	923.	118.	80.3	227.	166.	164.	22.3	12.1		
	2.70	69.5	658.	125.	60.5	151.	80.6	58.0	6.37	2.23		
	3.70	74.4	409.	76.7	43.3	87.2	45.6	30.2	4.59	3.94		
	4.70	75.3	325.	69.5	31.4	56.2	24.2	14.2	4.20	-		
	5.70	76.5	266.	27.7	25.4	47.2	15.8	7.99	-	-		
	6.70	79.2	186.	32.9	14.6	17.9	7.0	3.73	-	-		
F-27	0.71	65.2										
	0.96	68.3										
	1.46	72.5	2.17	27.1	34.9	236.	428.	827.	277.	240.	68.1	15.7
	2.46	79.6	0.935	14.3	16.3	115.	212.	363.	110.	76.0	20.0	3.02
	4.46	88.4	0.436	13.6	13.6	76.6	155.	106.	32.5	23.0	3.30	0.64
	8.46	96.6	0.123	6.17	6.08	25.4	34.3	36.7	5.96	3.44	0.27	0.09
F-28	0.33	58.5										
	0.58	66.8										
	1.08	73.2	3.42	65.2	97.9	510.	715.	1290.	352.	299.	72.8	16.0
	2.08	80.5	1.24	63.6	71.6	258.	283.	374.	80.5	59.4	9.87	1.45
	4.08	89.9	0.490	46.2	46.4	112.	99.3	101.	15.5	8.27	0.73	0.38
	8.08	99.1	0.148	21.5	16.4	35.3	23.7	18.4	2.06	0.97	0.25	0.25
G-9	0.20	46.0	9930.									
	0.50	53.0	2160.									
	1.20	60.0	471.									
	3.00	68.6	78.5									
	5.00	73.2										
	6.50	73.5										
G-10	0.20	47.5	7300.									
	0.50	53.0	2660.									
	1.20	61.0	763.									
	3.00	69.2	161.									
	5.00	75.0										
	6.50	75.0										

APPENDIX D

Discussion by the author and Professor Vito A. Vanoni of "Effects of Water Temperature on Bed-Load Movement", by John J. Franco; published in the Proceedings of American Society of Civil Engineers, Journal of Waterways and Harbors Division, 2, May, 1969, pp. 247-255.

The notation used in the discussion follows the notation used in the rest of this thesis with the following exceptions:

d = depth

S = friction slope

$\overline{u}$ = mean stream velocity

ΔT = change in water temperature

EFFECTS OF WATER TEMPERATURE ON BED-LOAD MOVEMENT[a]

Discussion by Brent D. Taylor and Vito A. Vanoni

BRENT D. TAYLOR,[3] AND VITO A. VANONI,[4] F. ASCE.—The problem of temperature effects in an alluvial stream being studied by the author is both interesting and quite important practically, but as he has mentioned it is not an easy one to untangle.

In laboratory experimentation it is difficult to isolate the temperature effect on each of the several flow parameters, for when a perturbation (temperature, ΔT, etc.) is introduced into an alluvial stream that is flowing in a state of equilibrium several stream parameters (velocity, slope, etc.) change simultaneously to bring the stream to a new position of equilibrium. Thus, in interpreting the data, it is difficult and perhaps impossible to segregate the direct effect of the temperature perturbation on a given parameter and one is led to think in terms of the change in equilibrium position which can be defined in terms of several variables. This makes it necessary in alluvial stream studies to keep track of the changes in each of the explicit flow parameters (mean stream velocity, $\bar{u}$, depth, d, sediment discharge q_s, energy slope, S, and temperature T, in order to follow the changes from one point of equilibrium to another. In the author's data presentation this process has not

[3] Grad. Research Assist., Calif. Instit. of Tech., Pasadena, Calif.
[4] Prof. of Hydr., Calif. Instit. of Tech., Pasadena, Calif.
[a] August, 1968, by John J. Franco (Proc. Paper 6083).

been carried through. Thus, it is difficult to interpret the results and easy to reach misleading or incorrect conclusions.

It has been found both in laboratory flumes (11) and in natural streams (1) that for a given water temperature and bed material there is good correlation between sediment discharge and mean stream velocity for a constant stream slope, depth, or discharge Q. In view of this correlation and because of the

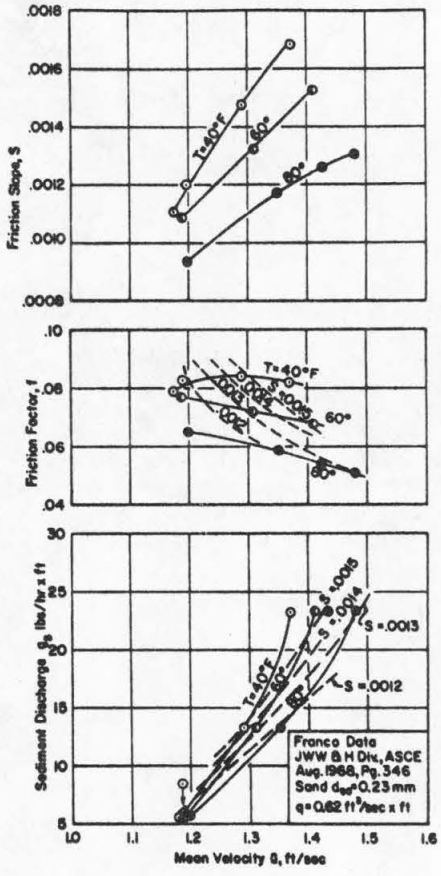

FIG. 10.—PLOT OF SLOPE (S), FRICTION FACTOR (f) AND SEDIMENT DISCHARGE (q_s) VERSUS MEAN STREAM VELOCITY ($\bar{u}$) FROM THE AUTHOR'S EXPERIMENTS WITH FINE SAND AND A CONSTANT DISCHARGE

significant velocity variations among the different runs of the author's study, it is more enlightening to plot his data on graphs of slope, S, Darcy-Weisbach friction factor, f, and the sediment discharge, g_s, versus mean stream velocity for each of the three water temperatures as shown in Fig. 10, than to present the results as in Fig. 3. In this figure, several constant slope contours have been located by data interpolation. The Darcy-Weisbach friction

factor f is defined by $\bar{u} = \sqrt{8/f}\sqrt{g\,r\,S}$ in which r is the hydraulic radius of the cross section, g is the gravitational constant, S is the friction slope of the flow and $\bar{u}$ is the mean stream velocity. From the graphs of the author's data in Fig. 10 it is seen that all relations between variables are single valued. For example, for any given slope and temperature, only one value of velocity and sediment discharge is shown. However, as will be seen later, this is not true over the whole range of possible stream velocities.

Fig. 10 suggests three important results of changing the water temperature in a stream of constant discharge with a rippled bed of fine sand. They are:

1. At a given velocity a decrease in water temperature is accompanied by an increase in sediment discharge, slope, and friction factor.
2. For a constant total sediment discharge, a decrease in water temperature results in a decrease in flow velocity, but the slope and friction factor increase.
3. Along an iso-slope contour, as the water temperature is reduced and the discharge held constant, the total sediment discharge and the mean stream velocity decrease, but the friction factor increases.

The increase in sediment discharge outlined in result one may be explained, in part, in terms of the temperature effect on particle fall velocity, w. A moderate decrease in water temperature causes a relatively large reduction in the still-water fall velocities of particles in the size range of fine sand (see Fig. 2-B. 9, p. 95, Journal of Hydraulics Division, ASCE, July, 1962) and thus tends to make the sediment concentration profile more nearly uniform over the stream depth. This tendency towards profile uniformity produces an increase in mean concentration and in the suspended sediment discharge. The effect of water temperature on bed load discharge is not understood and therefore cannot be explained even qualitatively.

One fact outlined in the first result is that in a stream of a given velocity and depth, the slope and friction factor increase as the temperature is lowered. This indicates what might be called a "cold-water roughening" of the bed. This "roughening" is believed to be caused by a change in the character of the bed configuration with temperature. The author makes the observation that the mean ripple heights of the cold water runs were greater than those of the warmer runs, which indicates a change in bed configuration. However, in each of the three sets of runs with constant sediment discharge, the stream velocity changes as temperature changes so that the temperature effect on ripple height for a given velocity cannot be deduced.

The tendency of the slope to increase as the temperature is reduced and the velocity is kept constant has the same kind of effect on the distribution of suspended load as a reduction in temperature and may be considered as an indirect effect on the suspension mechanism. This may be seen by observing that the exponent in the relation for the distribution of suspended sediment is directly proportional to the particle fall velocity and inversely proportional to the square root of the friction slope. (See p. 57, Journal of Hydraulics Division, ASCE, Sept., 1963.)

The second result is, in part, just another way of looking at the first. One significant difference is that in this case particular data can be used as evidence. This approach indicates that at each of the three specified sediment

discharges, as the temperature was raised, the equilibrium velocity necessary to carry the given sediment discharge increased. Result two may be restated to read that for a given discharge to carry sediment at a given rate as the water temperature is raised, requires an increase in velocity. The fact that in this case slope and friction factor decrease as the temperature and velocity increase is a manifestation of the temperature effect on friction factor through altering of the bed form. Except for the case of $T = 40°$ F, if the same increase in velocity had occurred at a constant temperature the friction factor would have tended to decrease only slightly instead of appreciably.

The apparent convergence of the data points at the lower sediment discharges indicates, by extrapolation, that the variation with temperature of the critical stream velocity for initiation of motion is small.

The third result qualifies the author's findings (Fig. 1) of temperature effect on sediment discharge. In Fig. 10, as the temperature is raised along a constant slope contour, both the sediment discharge and the stream velocity

TABLE 3.—DATA FROM CIT STUDY OF TEMPERATURE EFFECTS IN FLUME 10-1/2 IN. WIDE BY 40 FT LONG

Bed Sediment: D_g = 0.215 mm, σ_g = 1.39								
Run number (1)	Water temperature, in degrees Farenheit (2)	Discharge, in cubic feet per second per foot (3)	Mean velocity, in feet per second (4)	Depth, in feet (5)	Slope (6)	Sediment discharge, in pounds per hour (7)	Bed friction factor[a] (8)	Bed form (9)
1	70	0.181	0.92	0.196	0.00320	21.20	0.181	Ripple
2	97	0.188	0.98	0.192	0.00257	6.72	0.124	Ripple
3	69	0.226	1.17	0.193	0.00364	31.00	0.133	Ripple
4	98	0.218	1.13	0.193	0.00255	14.33	0.090	Ripple
5	71	0.370	2.01	0.184	0.00307	133.10	0.029	Flat
6	96	0.397	2.21	0.179	0.00400	148.70	0.031	Flat
7	70	0.413	2.19	0.188	0.00372	156.80	0.030	Flat
8	96	0.413	2.10	0.197	0.00309	119.40	0.032	Flat

[a] See Ref. 1 for detailed definition of bed friction factor.

increase. Thus, in view of the first two, results, it is apparent that the qualitative nature of the temperature effect on sediment discharge cannot be expressed without also indicating its effect on other stream properties such as velocity, depth and slope. The increase in velocity and sediment discharge with increase in temperature at a given slope is basically the result of two phenomena: (a) The cold-water roughening or conversely the "hot-water smoothing"; and (b) the fact, established experimentally (11), that an increase in the velocity of an alluvial stream, maintained at conditions of uniform flow, with constant temperature and rippled bed, will result in an increase in slope over a certain range of velocity, which range covered the experiments made by the author. Further discussion of this point will be presented later.

At the California Institute of Technology (CIT), during the spring of 1968, a series of eight runs was made by the writers in a recirculating flume 10.5 in. wide and 40-ft long [see Brooks (11) for a complete description of this flume] with an alluvial bed of fine sand (geometric mean size, D_g = 0.215 mm, and geometric standard deviation, σ_g = 1.39) for the purpose of studying tem-

perature effects on bed friction and sediment discharge. The steady-state, uniform-flow runs were made at two different water temperatures, ~ 70° F and ~ 97° F. Table 3 gives the complete set of data observed in these runs. The qualitative results of the CIT study are in basic agreement with the corresponding results drawn from the author's data.

Fig. 11 is a plot of data from the CIT study listed in Table 3 in which the flow depth was held very nearly constant and the slope, velocity, and discharge were allowed to vary. The lower-velocity, ripple-bed data support results drawn from Franco's data: for a given velocity and depth (and hence discharge) as the temperature is reduced the sediment discharge, slope, and bed friction factor (f_b) increase significantly. The bed friction factor f_b is

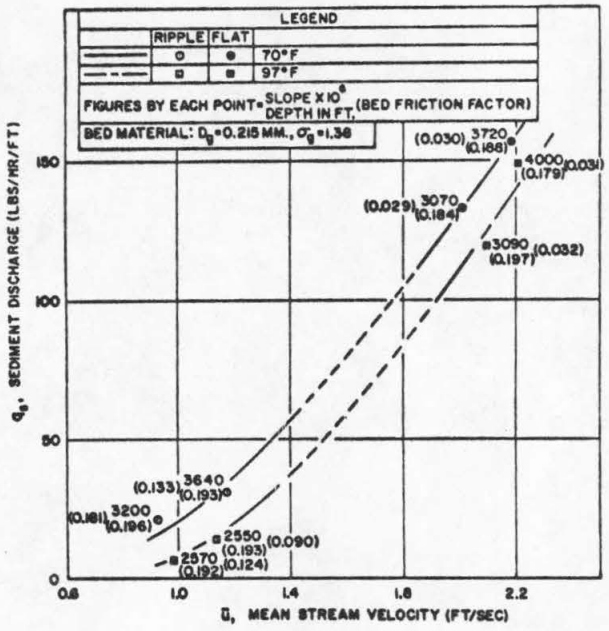

FIG. 11.—CIT DATA GIVING THE VARIATION OF SEDIMENT DISCHARGE (q_s) WITH MEAN STREAM VELOCITY ($\bar{u}$) FOR A VERY SMALL DEPTH RANGE AND A BED OF FINE SAND

obtained by correcting for the effect of the friction on the flume walls by a method developed by Johnson (12). The higher-velocity data points in Fig. 11 illustrate that the qualitative difference in sediment discharge with temperature at a given velocity, is the same in the flat bed regime as in the lower-velocity, ripple-bed regime. Also, there is some indication that in this regime a cold water flow at a given velocity and depth has a slightly lower slope and bed friction factor than does a corresponding warm flow. This indication agrees with results of a study by Vanoni and Nomicos (15) wherein it was found that for a solidified ripple-bed configuration a flow with a given sediment discharge has a lower slope and bed friction than one with the same temperature, velocity, and depth but with a lower sediment discharge.

By drawing on the results of flume studies by several workers, including those of the author and the present writers, it seems possible to outline, at least qualitatively, the general relation between sediment discharge, mean velocity, stream slope, and water temperature for the case of constant discharge. With this aim in view Fig. 12 has been constructed. The curves for the intermediate temperature are based qualitatively on results of a study by Kennedy and Brooks (13). In this study, a series of ripple and flat bed runs was made at a constant discharge (0.50 cfs per ft) over an alluvial bed of fine sand (D_g = 0.142 mm, σ_g = 1.38). The curves for the other two temperatures, labeled low and high temperature, were sketched in, using for a guide the author's results for the low velocity region and the CIT data for the high ve-

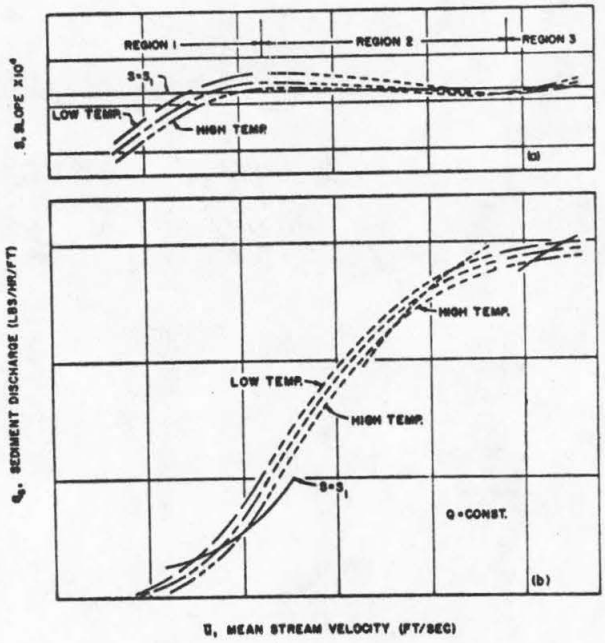

FIG. 12.—SCHEMATIC VARIATION OF SLOPE (S) AND SEDIMENT DISCHARGE (q_S) WITH MEAN STREAM VELOCITY ($\bar{u}$) FOR A CONSTANT DISCHARGE AND A BED OF FINE SAND

locity, flat-bed region. The dashed portions of the temperature contours in Fig. 12 (a,b) represent the transition zone where, as observed by Kennedy and Brooks, for a given discharge and water temperature there are two simultaneous flow solutions for $\bar{u}$, d, S, q_S, and f_b, one of which is in the low velocity ripple zone and the other in the high velocity flat-bed zone.

The constant-slope contour drawn in these plots illustrates that the response of a constant-slope stream to a change in water temperature depends on which of the regions 1, 2, or 3 indicated in the plots, the stream flow lies in. In region 1, an increase in water temperature in a stream of constant slope and discharge results in an increase in stream velocity and sediment

discharge. In region 2, an increase in temperature produces the opposite effects, that is, as the stream temperature increases along an iso-slope contour the velocity and sediment discharge are reduced and the friction factor increases. However, as indicated in Fig. 12, the only flows which may appear in region 2 in laboratory flumes occur at the lower velocities of the region. This difference in temperature effects for a constant slope is the result of the shape of the slope-versus-velocity function, and in particular the change in the sign of the first derivative of this function which occurs between regions 1 and 2 as illustrated in Fig. 12(*a*). Whereas in region 1 in order to maintain a constant stream slope as the water temperature increases the stream velocity must also increase with a consequent increase in sediment discharge, in region 2, when iso-slope flows are possible, they require that the stream velocity decrease as the water temperature increases, with a consequent decrease in sediment discharge.

In region 3 the velocity range of the flat-bed regime, there exists the same qualitative temperature effects along an iso-slope contour as those identified in region 2. This is because of the intersection of the constant temperature contours near the entry into region 3 and the reversal in the slope of the slope-versus-stream velocity function from region 2 to 3.

Available field data seem to indicate that natural streams lie in regions 2 and 3, and that in this case unique solutions exist at the higher velocities of region 2. If this is true, then the above analysis and Fig. 12 explain the general nature of temperature effects in a natural stream, and also the basic difference between temperature effects in natural streams and those observed in laboratory flumes according to the available data. In several natural streams (1,14), it has been observed that for a given discharge a drop in water temperature causes the mean stream velocity and sediment discharge to increase, particularly for that part of the load in the size range of fine sand (0.05 mm $\leq d_s \leq$ 0.35 mm), with a consequent decrease in friction factor. This is precisely what Fig. 12 predicts for streams in regions 2 and 3. On the other hand, the author's data, which are for flows in region 1, indicate that for a stream of constant discharge and slope a reduction in temperature causes a decrease in velocity and sediment discharge with a consequent increase in friction factor; this also agrees with Fig. 12.

As pointed out by Colby (1), there are several important differences between natural streams and experimental flows in laboratory flumes. These differences make the natural stream a more complex system than the flume and thus it can not be expected that the above analysis will provide the key to the temperature effects in all natural streams. It is not offered here in this way but rather as an hypothesis which can be used as a conceptual tool for further work in this area.

Other laboratory investigations of temperature effects in alluvial channels include one made by Straub et al. (5) and another by Hubbel and Ali (3). In Straub's study, essentially six flat-bed runs were made at constant discharge and six different water temperatures ranging from 35° to 86° F with a bed material of fine sand from the Missouri River. Since there was only one run at each temperature, the interrelationships brought out so well by the author's systematic data could not be deduced. The published results of Hubbel and Ali include only the sediment discharge concentration and friction factor for pairs of runs made at the same discharge but different temperatures. In order to make a meaningful interpretation of the results, and to determine whether

they are consistent with Fig. 12 the velocities and slopes of the experimental runs are needed.

It has been the purpose of this discussion to present the author's data in an elucidative way and to present a model which illustrates how the results of this study and the CIT study on temperature effects can be reconciled with natural stream data that heretofore have seemed to indicate contradictory results. This has been done essentially by assuming primary correlation between stream velocity and sediment discharge for a given bed material, temperature and discharge; and by dividing the velocity range into three flow regions which have different temperature-effect characteristics particularly with respect to a stream of constant slope.

The significant results of the discussion can be summarized as follows: (a) At any given velocity above the critical value for sediment movement with discharge held constant, a cool water flow over an alluvial bed of fine sand will transport a larger sediment discharge than a corresponding warmer flow; (b) for any given velocity in the ripple bed regime, with discharge constant, there is a change in the character of the bed configuration with temperature, which is instrumental in effecting a significant increase in the bed friction factor as water temperature decreases; (c) a reduction in the temperature of a stream with rippled bed and constant discharge and slope may cause the sediment discharge and velocity either to decrease or increase depending on sign of the derivative $\partial S/\partial \bar{u}$ of the curve of slope S against mean velocity $\bar{u}$ for the given discharge and constant water temperature in the range of velocity of interest. If the derivative is positive a reduction of water temperature keeping slope and discharge constant will cause the velocity and sediment discharge to decrease. Conversely, if the derivative is negative a reduction in temperature results in an increase in velocity and sediment discharge; (d) there is some indication that a decrease in water temperature in the flat-bed regime for a given velocity and depth causes the friction factor also to decrease. If this is true a reduction in temperature of a flat-bed stream of constant discharge and slope causes the sediment discharge and stream velocity to increase, and the friction factor to decrease, thus giving the same qualitative temperature effects as indicated in the ripple regime where $(\partial S/\partial \bar{u})$ is negative.

These results apply specifically to alluvial flows such as occur in laboratory flumes. Though they may be used as a model in studying natural streams, the significant differences that exist between natural streams and flume flows preclude their direct use in predicting temperature effects therein.

The author's data for the coal-bed runs do not show a consistent behavior on plots of sediment discharge, slope and friction factor against velocity and thus the analytical tools used for the sand bed data yield no meaningful results in this case. Perhaps the problem lies in the inherent difficulty of measuring the very small slope in these runs. The author's data also indicate that in all of his experimental runs the slopes of the bed, water surface, and energy grade-line each had a significantly different value. Based on the author's technique (least-squares fit) of computing these slopes, the differences indicate that non-uniform flow (backwater profile) existed over at least part of the flume length. This flow non-uniformity may explain part of the scatter in the author's fine-sand duplication runs. It is suggested that the results could be improved and this uncertainty removed by establishing uniform flow in future studies.

Acknowledgments.—The preparation of this discussion was supported partially by National Science Foundation Grant K3910.

Appendix.—References.

11. Brooks, N. H., "Mechanics of Streams with Movable Beds of Fine Sands," *Transactions*, ASCE, Vol. 123, 1958, p. 526.
12. Johnson, J. W., "The Importance of Side-Wall Friction on Bed-Load Investigations," *Civil Engineering*, Vol. 12, June, 1942, p. 329.
13. Kennedy, J. F., and Brooks, N. H., "Laboratory Study of an Alluvial Stream at Constant Discharge," *Proceedings*, Inter-Agency Sedimentation Conference, 1963, Misc. Publication No. 970, Agricultural Research Service.
14. Missouri River Channel Regime Studies, *MRD Sediment Series No. 13A*, U.S. Army Engineer District, Omaha, Nebraska, November, 1968.
15. Vanoni, V. A., and Nomicos, G. W., "Resistance Properties of Sediment-Laden Streams," *Transactions*, ASCE, Vol. 125, Part I, 1960, p. 1140.

APPENDIX E

Discussion of "Indeterminate Hydraulics of Alluvial Channels", by Thomas Maddock, Jr.; published in the Proceedings of American Society of Civil Engineers, Journal of Hydraulics Division, 5, May, 1971, pp. 756-760.

The notation used in the discussion follows the notation used in this thesis with the following exceptions:

B_f, B_{fs}, B_{fv} = dimensionless bed-form factors

C = sediment discharge concentration

d = characteristic diameter of bed sediment

D = stream depth

q = unit stream discharge

S = friction slope

V = mean stream velocity

$\Delta\gamma$ = buoyant specific weight of bed sediment

INDETERMINATE HYDRAULICS OF ALLUVIAL CHANNELS[a]

Discussion by Brent D. Taylor

BRENT D. TAYLOR.[2]—The purpose of this discussion is to consider (1) The author's initial thesis; (2) his method of functional expression; and (3) the general and particular solutions that are developed in the paper.

1. The author's thesis that "to establish determinate relations for the solution of the dual problems of resistance to flow and sediment transport in allu-

[a] November, 1970, by Thomas Maddock, Jr. (Proc. Paper 7696).

[2] Grad. Research Asst., W. M. Keck Lab. of Hydraulics and Water Resources, California Institute of Technology, Pasadena, Calif.

vial channels . . . is an impossible task" is a bold statement, and one not justified by the arguments or data presented.

Natural alluvial regimes are extremely complex—unsteady and nonuniform from the smallest scale hydraulic processes to the largest scale flow patterns and boundary geometry; and with our present knowledge it is not possible to accurately predict sediment discharge and channel roughness. However there are no empirical data currently available which indicate that precise solutions for these parameters are not possible.

Thus the writer feels that the author's thesis should be qualified as follows: "it is not possible with our present knowledge to establish precise determinate relations for the solution of the dual problems of resistance to flow and sediment transport in alluvial channels."

2. The author's expression of general functional relationships is awkward and in some cases may lead to incorrect concepts. The author states that, "For a given sediment mixture (and water temperature in a flume of constant width) according to Brooks

$$q_s \neq \phi \ (q, S) \quad (17)$$

Therefore as a general statement

$$\phi \ (S, q, q_s) \neq 0 \quad (18)$$

$$\phi \ (V, D, S) \neq 0 \quad (19)$$

$$\phi \ (C, D, S) \neq 0. \text{"} \quad (20)$$

These statements are interpreted to mean that the functions ϕ don't exist. In this context Eqs. 17, 18, 19 and 20 do not correctly express Brooks' experimental observations which showed that these functions exist but are multivalued under some conditions. Experimental data which support Brooks' conclusions are presented in papers by Kennedy and Brooks (18), and by Brooks (2).

Kennedy and Brooks (18) found that in a laboratory flume with a bed of fine sand and constant discharge, sediment discharge could not be expressed as a single-valued function [For a clear explanation of a single-valued function see Brooks (2)] of discharge and slope. This does not mean that q_s is not a function of q and S as implied by Eqs. 17 and 18, but rather that there are multiple solutions to

$$q_s = \phi \ (q, S) \quad (21)$$

The fact that there are multiple solutions of Eq. 20 precludes its use in predicting q_s, for in the range where multiple solutions exist there are two or more possible values of q_s for each set of values for q and S and thus without additional constraints a unique solution for q_s is not possible.

Similarly Brooks (2) found that in a laboratory flume with a bed of fine sand and constant depth, mean velocity and sediment concentration could not be expressed as single-valued functions of depth and slope. Again this does not imply Eqs. 19 and 20, but rather that there are multiple solutions to

$$V = \phi \ (D, S) \quad (22)$$

and $$C = \phi \ (D, S) \quad (23)$$

and thus these equations cannot be used to predict mean velocity and sediment concentration without additional constraints.

Eqs. 21, 22 and 23 can be made single-valued by adding to each equation parameters which uniquely describe the bed configuration. However in a natural stream or laboratory flume the bed configuration is a dependent variable and cannot be predicted in advance. Also it would be extremely difficult to quantify the geometric characteristics of any but the simplest of bed configurations. For these reasons it is impractical if not impossible to make Eqs. 21, 22 and 23 single-valued by incorporting the bed configuration into each. Nevertheless the author proposes Eqs. 1 through 6 wherein dimensionless bed factors have been introduced to produce single-valued functions. If in fact the bed configuration can be uniquely described by one parameter these equations are single-valued, but they are without exception awkward. Their format does not reflect the author's concern for particular functional relationships. In Eq. 1 he is attempting to make Eq. 21 single-valued. But Eq. 1 does not express this objective. Eq. 1 can also be interpreted as

$$S = \phi\,(q, q_s, B_{fs}) \quad \ldots\ldots\ldots\ldots\ldots\ldots\ldots\ldots \quad (24)$$

in which case B_{fs} is a redundant variable since if q and q_s are known S in uniquely determined along with all other flow parameters such as velocity, depth, friction factor and bed form. This ambiguity is present in each of the six equations and it weakens the author's development for it is not clear particularly in Eqs. 5 and 6 which quantities are considered to be dependent and which ones are to be independent.

3. The primary purpose of the author's paper was to rectify some seeming inconsistencies that have appeared in the literature. This is a commendable objective and one which must be continually pursued. The author's success in realizing this objective was limited, however, by the approach he chose.

In developing functions which can be used to predict sediment discharge or resistance to flow it is necessary to incorporate hydraulic parameters which (1) Uniquely determine sediment discharge or resistance to flow, respectively; (2) can themselves be evaluated in the alluvial regime. Also, to correctly express the solution and avoid redundancies; (3) the minimum number of variables in accord with 1 and 2 must be included in the function.

The author's functional development is not consistent with the preceeding rules, and consequently his proposed relations cannot correctly express the phenomena involved.

Eqs. 5, 10 and 11 all contain redundant variables, and each includes a bed form parameter which would be extremely difficult to evaluate in an alluvial regime.

In Eq. 5 regardless of which variables are taken to be independent there is at least one and sometimes two redundant variables. This redundancy is illustrated by solving Eq. 5 for velocity and concentration, respectively. In a flume of constant width for a given bed material and water temperature the velocity is a unique function of depth, slope, and bed configuration. Thus with this interpretation of Eq. 5 concentration which is also a unique function of depth, slope and bed configuration is an extraneous variable. Considering the same type of alluvial system and Eq. 5, the concentration is a unique function of velocity and depth therefore with this interpretation slope and bed configuration, each of which are also unique functions of velocity and depth, are extraneous variables.

Similarly in Eqs. 10 and 11 the bed factors are extraneous variables for in

a flume of constant width with a given bed material and water temperature velocity and slope are each unique functions of discharge and sediment discharge.

The inclusion of extraneous variables in a function is conceptually incorrect for it implies that all but one of the variables in the function are independent. It also complicates the functional solution, for unless the interdependence of the variables is recognized the solution is indeterminate.

The author has attempted to make

$$q_s = \phi\ (q, S) \quad \ldots\ldots\ldots\ldots\ldots\ldots\ldots\ldots\ldots\ldots\ldots\ldots\ (25)$$

$$V = \phi\ (q, S) \quad \ldots\ldots\ldots\ldots\ldots\ldots\ldots\ldots\ldots\ldots\ldots\ldots\ (26)$$

single-valued by introducing a bed factor into each of these equations. In evaluating the bed factors for

$$q_s = \phi\ (q, S, B_{fs}) \quad \ldots\ldots\ldots\ldots\ldots\ldots\ldots\ldots\ldots\ldots\ (27)$$

$$V = \phi\ (q, S, B_{fv}), \quad \ldots\ldots\ldots\ldots\ldots\ldots\ldots\ldots\ldots\ldots\ (28)$$

the author states that "Equations giving the characteristics of bed forms, without exception, are inadequate. Consequently, the intent of the analysis is to describe the bed form factors and to associate the factors with some observable characteristic of stream behavior." This statement and the general complexity of measuring a bed-form factor raises the question—why not use "observable characteristics of stream behavior" to make Eqs. 25 and 26 single-valued? By replacing slope with depth in these equations both are single-valued. Eq. 25 becomes

$$q_s = \phi\ (q, D) \quad \ldots\ldots\ldots\ldots\ldots\ldots\ldots\ldots\ldots\ldots\ldots\ldots\ (29)$$

and Eq. 26 becomes the continuity equation. Flow depth is in general as easily measured as slope thus with this simple transformation the functions are made to satisfy each of the three rules previously stated.

The author's solution of Eq. 28 illustrates the fallacy of his approach. In order to measure the bed factor in this function he must solve for it as the dependent variable, after assuming a particular form of the equation. He does this by fitting

$$V = B_f\ \frac{(g^{1/2}\ \gamma^{1/2}\ q\ S)^{1/2}}{(\Delta\gamma d)^{1/4}} \left(\frac{\rho\omega^2}{\Delta\gamma d}\right)^{1/8} \quad \ldots\ldots\ldots\ldots\ldots\ (30)$$

to data compiled by Gilbert, and concludes that $B_f = 4.7$ as shown in Eq. 7. With the bed factor defined in this way Eq. 7 expresses the velocity as a function of discharge and slope for a given sediment and water temperature. But as previously indicated this function is not single-valued; thus the author has fallen into the difficulty he intended to avoid. The author may argue that Gilbert's data characterize alluvial flows in a sand-feed flume for a particular range of velocities, and that with these flows Eq. 7 is single-valued. If this is true Eq. 26 is also single-valued for these flows and B_f is a redundant variable. However it can be shown experimentally that under certain conditions Eq. 7 is in fact a multivalued function and therefore cannot be a universally useful relation.

Guy, Rathbun and Richardson (17) have shown that there are no characteristic differences between the solutions obtained in a sand-feed flume and those

obtained in a recirculating flume, therefore the data taken by Kennedy and Brooks (18) in a recirculating flume can be used to check Eq. 7. In Kennedy and Brooks' (18) runs 3-7 and 3-6a the bed material (fine sand), water temperature, discharge, and slope were the same but the velocity in run 3-7 was 1.45 fps and in run 3-6a the velocity was 2.13 fps. Thus for these two runs there is a double solution to Eq. 7. Both of these runs are in the velocity range of Gilbert's data.

The author has classified alluvial regimes according to velocity—low velocity, midvelocity, and high velocity. This classification is a personal artifice which apparently helps the author to clarify his thinking. In Fig. 2 the author distinguishes between low velocity and midvelocity flows by fitting a straight line of one slope through the lower velocity data, and a straight line of another slope through the higher velocity data. This curve-fitting may be useful as an approximation, but it is only an approximation and must be identified as such. For it has been shown both in laboratory studies [Brooks (2)] and in field studies [Colby (16)] that sediment discharge is a smooth continuous function of velocity over a wide range of velocities.

In conclusion the writer would like to emphasize that by incorporating the bed configuration into a function in order to remove the possibility of multiple solutions one complicates the solution unnecessarily for other more tractable parameters can be used to accomplish the same objective. The fact that the bed configuration is in general extremely complex and not amenable to mathematical description, and that it is actually part of the solution and strictly speaking cannot be determined in advance make it an awkward choice both practically and conceptually.

Acknowledgement.—This discussion was prepared with the support of the National Science Foundation Grant No. GK 3910.

Appendix.—References.

16. Colby, B. R., "Discharge of Sands and Mean-Velocity Relationships in Sand-Bed Streams," U.S. *Geological Survey Professional Paper 462*-A, 1964.
17. Guy, H. P., Rathbun, R. E., and Richardson, E. V., "Recirculation and Sand-Feed Type Flume Experiments," *Journal of the Hydraulics Division*, ASCE, Vol. 93, No. HY5, Proc. Paper 5428, September, 1967, pp. 97-114.
18. Kennedy, J. F., and Brooks, N. H., "Laboratory Study of an Alluvial Stream at Constant Discharge," Proceedings of the Federal Inter-Agency Sedimentation Conference 1963, *Miscellaneous Publication No. 970*, Agricultural Research Service.

APPENDIX F

Discussion of "Initiation of Ripples on Flat Beds", by Philip B. Williams and Patrick H. Kemp; accepted for publication in the Proceedings of American Society of Civil Engineers, Journal of Hydraulics Division.

The notation used in the discussion follows the notation used in the rest of this thesis with the following exceptions:

t = time required for flat bed to exhibit visual instability

$\overline{t}$ = mean value of t for a given set of flow conditions

U_* = bed shear velocity, = $\sqrt{\tau_o/\rho}$

τ_o = mean bed shear stress

τ_* = bed Shields stress, = $\tau_o/(\gamma_s-\gamma)D_g$

R_* = boundary Reynolds number of bed, = U_*D_g/ν

INITIATION OF RIPPLES ON FLAT SEDIMENT BEDS [a]

Discussion by Brent D. Taylor

BRENT D. TAYLOR [3] -The purpose of this discussion is: 1) to develop a bed instability hypothesis which may be used to correlate experimental observations, and define critical conditions for flat-bed instability; 2) to present data from experiments made by the writer which indicate that flat-bed instability can occur at mean bed shear stresses smaller than those given by the authors' curve for critical flat-bed instability; and 3) to present data which suggest that the phenomena of bed instability and sediment discharge are not closely related in a low-transport, flat-bed flow.

1) The complex phenomenon of alluvial, flat-bed instability is not at present amenable to analytic treatment. To study this phenomenon heavy reliance must be placed on experimental observations. It is therefore most important that experimental observations be carefully interpreted. This interpretation can be facilitated by considering only those parameters which are of primary importance in the instability process, and then further reducing the number of independent variables through a dimensional analysis.

---

[a] April, 1971 by Philip B. Williams and Patrick H. Kemp (Proc. Paper 8042.)

[3] Graduate Research Assistant, W. M. Keck Laboratory of Hydraulics and Water Resources, California Institute of Technology, Pasadena, California 91109.

In a wide, flat-bed alluvial channel wherein the flow is steady and uniform, the dynamic flow conditions are uniquely specified by the following parameters: mean bed shear stress (τ_o), bed slope (S_b), dynamic viscosity of the water (μ), density of the water (ρ), geometric mean size of the bed material (D_g), geometric standard deviation of bed material sizes (σ_g); and particle shape factor (S. F.), particle density (ρ_s), and buoyant specific weight (γ_s-γ). The phenomenon of flat-bed instability then may be expressed as a function of these nine variables. To quantify this expression a measurable parameter(s) must be introduced to characterize the bed instability. The instability parameter which is perhaps most easily measured experimentally is the time (t) required after flow begins for a flat-bed to exhibit instability. As noted by the authors, inherent bed instability is first revealed by the growth of a small disturbance which produces flow separation. Once initiated this disturbance grows fairly rapidly; and thus the time when it is first visually discernable closely approximates the time when the flat bed becomes unstable.

If an alluvial, flat bed is inherently unstable the flow time (t) required for this instability to produce a bed disturbance may vary due to the statistical nature of the contributing factors (fluid turbulence, flat bed uniformity, etc.). Therefore the characteristic time used to describe bed instability for a given set of flow conditions should be the ensemble mean ($\bar{t}$).

If alluvial, flat-bed instability is quantified by the mean time ($\bar{t}$) required after flow begins for a flat bed to exhibit visual instability, the instability function can be expressed as

$$\bar{t} = \varphi(\tau_o, S_b, \mu, \rho, D_g, \sigma_g, \text{S. F.}, \rho_s, \gamma_s-\gamma). \quad (5)$$

In flow regimes where $S_b << 1$ the effect of bed slope on bed instability may be assumed small; and S_b can be eliminated from Eq. (5). This condition ($S_b << 1$) obtains in most flat-bed flows, and thus

$$\bar{t} = \varphi(\tau_o, \mu, \rho, D_g, \sigma_g, \text{S. F.}, \rho_s, \gamma_s-\gamma). \quad (6)$$

Using the Buckingham-Pi Theorem Eq. (6) can be non-dimensionalized as follows,

$$\frac{\bar{t}U_*}{D_g} = \varphi(\tau_*, R_*, \frac{\rho_s}{\rho}, \sigma_g, \text{S. F.}) \quad (7)$$

in which $U_* = \sqrt{\tau_o/\rho}$

$$\tau_* = \frac{\tau_o}{(\gamma_s-\gamma)D_g}$$

$$R_* = \frac{U_* D_g}{\nu}$$

and $\nu = \mu/\rho$.

Eq. (7) suggests that for a naturally-worn, silica bed material of given σ_g the flat-bed instability can be expressed in terms of three dimensionless parameters,

$$\frac{\bar{t}U_*}{D_g} = \varphi(\tau_*, R_*) \ . \quad (8)$$

According to Eq. (8) flat-bed instability contours ($\bar{t}U_*/D_g$ = constant) for naturally-worn, silica bed materials of given σ_g can be plotted on a graph of τ_* versus R_*. On such a plot the flow conditions for inherent flat-bed stability would be defined asymtotically by the instability contours as $\bar{t}U_*/D_g$ approaches infinity.

This method of defining the flow conditions for inherent flat-bed stability has considerable experimental advantage. In laboratory experiments the duration of flow is finite. Thus from such experiments flow conditions for critical flat-bed stability ($\bar{t} \rightarrow \infty$) probably cannot be precisely defined. However, the data from these experiments can be used to define instability contours on a plot of τ_* versus R_*; and from such contours the shape and approximate location of the critical flat-bed instability contour may be deduced.

2) The authors' data have suggested that the critical bed instability contour ($\bar{t}\, U_*/D_g \rightarrow \infty$) lies above Shields' incipient transport data and approximately parallel to the curve defined by these data. Results from a series of experiments by the writer do not agree with these conclusions.

Six low-transport, flat-bed experiments were made by the writer in a flume $10\frac{1}{2}$ in. wide by 40-ft long with a bed material of fine, naturally-worn, silica sand ($D_g = 0.215$ mm, $\sigma_g = 1.42$, $\rho_s = 2.65$ gms/cm^3). The pertinent data from these experiments are given in Table 1. The depth in all six experiments was 6.10 cm. The experiments were made in pairs. In each experiment-pair the mean velocity was the same, but the water temperature in one of the experiments was approximately 21°C (cold water experiment) and approximately 36°C in the other (warm water experiment). The odd-numbered experiments are cold water experiments and the even-numbered ones are warm water experiments.

Table 1 - Data from CIT study in flume $10\frac{1}{2}$ in. wide by 40-ft long.

Bed Sediment: D_g = 0.215 mm, σ_g = 1.42, ρ_s = 2.65 gm/cm^3; Flow Depth: 6.10 cm

Run No.	Mean Velocity U (cm/sec)	$\frac{\tau_*}{\frac{\tau_o}{(\gamma_s-\gamma)D_g}}$	$\frac{R_*}{\frac{U_* D_g}{\nu}}$	Sediment Discharge $g_s \times 10^5$ (gm/cm/sec)	$\frac{q_s \times 10^5}{U_* D_g}$	Instability Time $\bar{t}$ (sec)	$\frac{\bar{t} U_* \times 10^3}{D_g}$	dg (mm)
B-1	22.9	0.0405	2.61	2.57	37.9	>245,000	135.	0.301
B-2	22.9	0.0366	3.43	10.3	159.	5620	2.95	0.295
B-3	21.3	0.0374	2.48	0.642	9.86	- *	-	0.353
B-4	21.3	0.0335	3.34	1.86	30.1	24,400	12.3	0.330
B-5	19.8	0.0319	2.29	0.033	0.55	-	-	- **
B-6	19.8	0.0286	3.04	0.124	2.17	-	-	0.365

* - not measured.

** - sample too small to be analyzed.

In experiment B-1 the flume was operated continuously for 68 hours, and while the flat bed did become streaked similar to the author's description of the bed condition illustrated in Fig. 4(c) bed ripples never appeared. The sediment discharge during this experiment was approximately constant thus indicating that the bed did not armour. This conclusion is supported by the fact that the geometric mean size of the load was significantly larger than that of the bed material (see Table 1).

In the corresponding warm water experiment B-2 after two hours of flume operation small ripples appeared on the bed. At this time the flume was shut off, the bed was scarified to provide new surface material, and then releveled; and the warm water experiment was started again. Small ripples reappeared on the bed after $1\frac{1}{2}$ hours of flume operation. The experiment was repeated two more times. Bed ripples appeared after $1\frac{1}{2}$ hours (see Fig. 11(a)) and $1\frac{1}{4}$ hours respectively in these two trials. In each of the four trials the appearance and geometric characteristics of the spontaneous bed ripples agreed with the authors' observations. The ripples appeared in random fashion along the bed; and the first discernable characteristic of the instabilities was a small, narrow ripple-front which produced flow separation. In each case the disturbances developed after the flat bed became streaked in appearance; and when the experiment was continued after the small bed ripples appeared ripple trains propagated downstream from the initial disturbances, leaving little doubt but that the bed would eventually be covered with ripples (see Fig. 11(b)).

(a) Spontaneous Ripples Near Flume Station 8.0 (8.0 meters below inlet) Formed After 1-1/2 hours. (Photo No. 11218)

(b) Spontaneous Ripple Train at Flume Station 9.0 Formed in Approximately 2 hours. (Photo No. 11219)

Fig. 11 Spontaneous Bed Ripples in Third Trial of Experiment B-2.

(Scales are in cm: flow is from right to left.)

In experiment B-3 the flume was run for 17 hours and though the bed exhibited characteristic streaks toward the end of this time, ripples did not appear anywhere along the bed. With the corresponding warm water experiment B-4 spontaneous ripples appeared after 6 hours and 43 minutes. The experiment was repeated and this time ripples appeared after 6 hours and 50 minutes.

Experiments B-5 and B-6 were each run for 66 hours and in neither experiment did spontaneous ripples form on the bed. After 66 hours of flume operation in these two experiments a small artificial wave was introduced on the bed. An example of these artificial bed waves is shown in Fig. 12(a). The bed waves were created by inserting a spatula approximately 1.5 cm wide vertically into the sand bed and then lifting it out of the bed and at the same time moving it in the downstream direction. The flume was operated for 12 additional hours in each experiment after the artificial bed waves were introduced. The resultant bed deformation in each experiment is shown in Fig. 12.

In experiment B-6 the artificial bed perturbation clearly grew and produced a ripple train downstream similar to that produced by the spontaneous bed perturbations in experiments B-2 and B-4. The artifical bed perturbation in experiment B-5 elongated as shown in Fig. 12(a), but did not cause additional bed waves to form downstream.

The data from experiments B-1 through B-6 have been plotted in Fig. 13 along with the authors' data and proposed critical bed instability curve; and Shields incipient transport curve as modified by the authors.

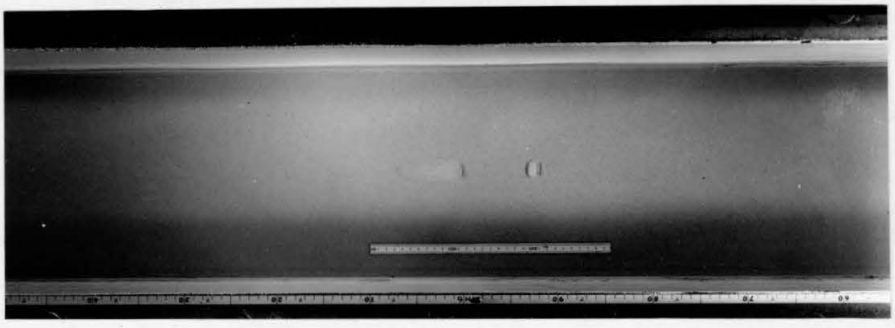

(a) Artificial Perturbation Growth in Experiment B-5. (Note: Perburbation furthest right is an example of initial shape of artificial bed perturbations.) (Photo No. 11220)

(b) Artificial Perturbation Growth in Experiment B-6. (Photo No. 11221)

Fig. 12 Growth of Artificial Bed Perturbations in Experiments B-5 and B-6 After 12 Hours of Flume Operation.

(Scales are in cm; flow is from right to left.)

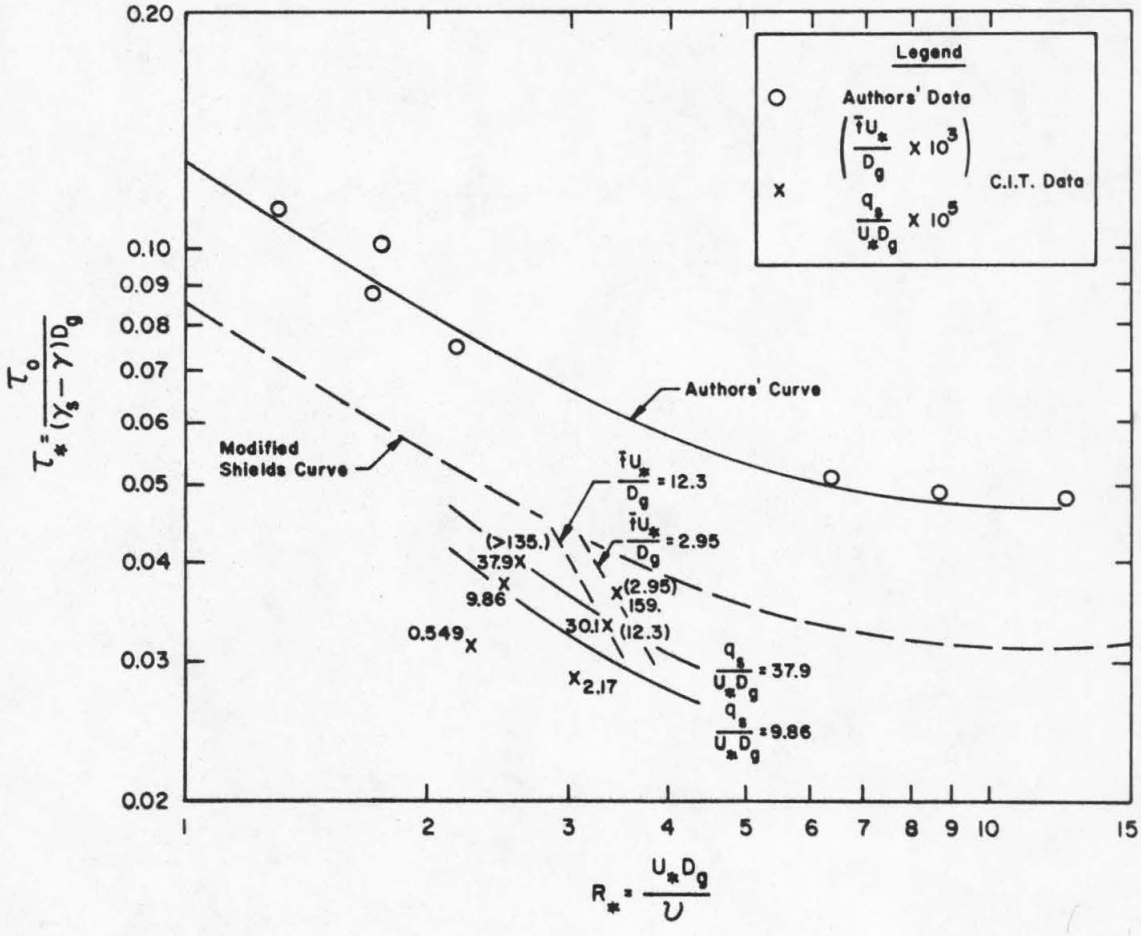

Fig. 13. Authors Data and Proposed Stability Curve, Modified Shields Incipient Transport Curve; and CIT Data with Dimensionless Stability Contours and Dimensionless Sediment Discharge Contours

The numbers in parenthesis beside the writers data points are dimensionless instability times ($\bar{t}U_*/D_g$); and the open numbers are the corresponding dimensionless sediment discharge values (q_s/U_*D_g) as explained in part 3 of this discussion. The values of mean bed shear stress for experiments B-1 through B-6 were computed according to the side-wall correction procedure proposed by Johnson (11).

In all six of the writers' experiments the computed values of τ_o were considerably less than the critical values given by the authors' curve. However in experiments B-2 and B-4 a flat-bed condition was clearly unstable; and the perturbation growth observed in B-6 indicates that for the flow conditions of this experiment a flat-bed condition may be inherently unstable.

Using the instability data from experiments B-1, B-2, and B-4 as a guide two dimensionless instability contours ($\bar{t}U_*/D_g$ = 2.95, 12.3) have been sketched in Fig. 13. These instability contours indicate that there is a discrepancy between the authors' results and those obtained by the writer in the slope of the critical bed instability contour, as well as in its location. They suggest that the critical bed instability contour lies below the authors' curve and has a steeper negative slope.

The experimental flow times indicated in Fig. 3 suggest that a primary source of the discrepancy between the authors results and those of the writers are the relatively short flow times of the authors' experiments–the authors may not have run all of their experiments long enough for inherent bed instability to manifest itself. In experiment B-2 it took 5000 to 7000 seconds before bed instability became visually

discernable; and in B-4 approximately 25,000 seconds. These times are considerably larger than those shown in Fig. 3. Thus it is felt that if the authors would have run their experiments for longer times their conclusions may have been significantly different.

3) Experimental results obtained in experiments B-1 through B-6 indicate that sediment discharge and bed instability as defined in Eq. (7) are not closely related in a low-transport, flat-bed regime.

With arguments similar to those used in deriving Eq. (7) it can be shown that in a low-transport, flat-bed regime

$$\frac{q_s}{U_* D_g} = \varphi(\tau_*, R_*, \frac{\rho_s}{\rho}, \sigma_g, \text{S. F.}) \tag{9}$$

in which q_s = sediment discharge per cm of channel width in cm^2/sec. Then for a naturally-worn, silica bed material of given σ_g,

$$\frac{q_s}{U_* D_g} = \varphi(\tau_*, R_*) \tag{10}$$

Using Eqs. (8) and (10) dimensionless bed instability contours and dimensionless sediment discharge contours can both be located on a plot of τ_* versus R_*, for a given bed material.

In Fig. 13 this double plot has been sketched using the data from experiments B-1 through B-6 as a guide. The slopes of these two contour sets are significantly different thus indicating that matching dimensionless sediment discharge in two different experiments does not necessarily match bed instability conditions. This conclusion is supported directly by the bed instability and sediment discharge data from experiments B-1, B-2 and B-4. The dimensionless sediment

discharge measured in experiment B-1 lies between those measured in B-2 and B-4, however the data indicate that the bed instability time is at least an order of magnitude larger for the flow conditions of experiment B-1 than the bed instability times observed in B-2 or B-4.

Acknowledgments:- This discussion was prepared with the support of the National Science Foundation Grant No. GK-3910.

References

11. Johnson, J. W., "The Importance of Side-Wall Friction on Bed-Load Investigations", Civil Engineering, Vol. 12, June 1942, p. 329.